

Alma Mater Studiorum – Università di Bologna

**DOTTORATO DI RICERCA IN
SCIENZE E TECNOLOGIE DELLA SALUTE**

Ciclo 34

Settore Concorsuale: 06/H1 – GINECOLOGIA E OSTETRICIA

Settore Scientifico Disciplinare: MED/40 – GINECOLOGIA E OSTETRICIA

**CHEMO-PHYSICAL AND BIOLOGICAL MECHANISMS BEHIND THE
ANTICANCER ACTIVITY OF PLASMA ACTIVATED RINGER'S LACTATE
SOLUTION FOR THE TREATMENT OF PERITONEAL CARCINOSIS FROM
PRIMITIVE EPITHELIAL OVARIAN/TUBULAR TUMOR**

Presentata da: Sara Coluccelli

Coordinatore Dottorato

Prof. Marco Viceconti

Supervisore

Prof. Dr. Pierandrea De Iaco

Co-supervisor

Prof. Vittorio Colombo

Prof. Giuseppe Gasparre

Prof. Matteo Gherardi

Dr. Romolo Laurita

Esame finale anno 2022

1. TABLE OF CONTENTS

FRONTESPIZIO	1
1. TABLE OF CONTENTS	2
2. ABSTRACT	4
3. INTRODUCTION	6
3.1 OVARIAN CANCER.....	6
3.1.1 <i>High grade serous ovarian cancer: genetical and pathological features</i>	7
3.1.2 <i>Therapeutic approach of EOC</i>	13
3.2 PRECLINICAL MODELS IN OVARIAN CANCER RESEARCH.....	16
3.2.1 <i>Preclinical cancer models: from past to present</i>	16
3.2.2 <i>Ovarian cancer organotypic models</i>	18
3.3 PLASMA MEDICINE.....	19
3.3.1 <i>Plasma: the fourth state of matter</i>	19
3.3.2 <i>Application of CAP on cancer treatment</i>	21
3.3.3 <i>Mechanism of CAP-cancer cells interaction and response</i>	22
3.3.4 <i>PALs generation and their biological effects</i>	24
3.3.5 <i>PALs suitable for clinical applications</i>	26
4. AIM	27
5. MATERIALS AND METHODS	28
5.1 PLASMA DEVICE AND CHEMICAL CHARACTERIZATION OF PA-RL SOLUTION.....	28
5.2 PA-RL AND SYNTHETIC SOLUTIONS PRODUCTION.....	29
5.3 LOW-SPEED AND HIGH-SPEED FILTER IMAGING.....	30
5.4 PATIENT SAMPLES AND TISSUE PREPARATION.....	31
5.5 CELL CULTURE CONDITIONS.....	31
5.6 CELL TREATMENT AND VIABILITY ASSAY.....	32
5.7 ROS PRODUCTION AND APOPTOSIS ASSAYS.....	33
5.8 WESTERN BLOT ANALYSIS.....	33
5.9 <i>EX-VIVO</i> 3D CULTURES.....	34
5.1 SANGER SEQUENCING AND NEXT GENERATION SEQUENCING ANALYSIS.....	37
5.2 HEMATOXYLIN AND EOSIN AND IMMUNOFLOURESCENCE STAINING.....	38
5.3 STATISTICAL ANALYSIS.....	39
6. RESULTS	40
6.1 ELECTRICAL CHARACTERIZATION OF THE MULTIWIRES PLASMA SOURCE AND CHEMICAL FEATURES OF PA-RL.....	40

6.2	EVALUATION OF PLASMA DISCHARGE BEHAVIOR AND EMISSION BY MEANS OF LOW-SPEED AND HIGH-SPEED FILTER IMAGING	43
6.3	PA-RL DISPLAYS A CYTOTOXIC EFFECT ON EOC CELL LINES THAT DOES NOT DEPEND EXCLUSIVELY ON HYDROGEN PEROXIDE OR NITRITES.....	44
6.4	PA-RL IS SELECTIVE FOR EOC CELLS.....	47
6.5	DIFFERENTIALLY ACTIVATED ANTIOXIDANT DEFENSE MECHANISMS MAY UNDERLIE DIVERSE SENSITIVITY TO PA-RL.....	49
6.6	CREATION OF AN OVARIAN CANCER SAMPLES COLLECTION.....	52
6.7	PRIMARY EOC CELLS FROM ASCITES GROWN IN 3D MAINTAIN THE <i>TP53</i> DRIVER MUTATION, UNLIKE ASCITES IN 2D CULTURES	52
6.8	SET UP OF A REPRODUCIBLE PERFUSED-EOC <i>EX VIVO</i> MODEL	60
6.9	PERFUSED FRESH AND SLOW-FROZEN EOC 3Ds RECAPITULATE THE ORIGINAL TME	71
6.10	EOC PERFUSED-3Ds MIMIC THE ORIGINAL TUMORS FROM A MOLECULAR POINT OF VIEW	76
6.11	PA-RL EFFECTS ON A PERFUSION-BASED 3D HGSOC <i>EX VIVO</i> MODEL.....	79
7.	DISCUSSION AND CONCLUSIONS	84
8.	REFERENCES.....	96

2. ABSTRACT

What do lightnings, neon lights and the ionosphere have in common? The answer dates back to the 1920s, when the chemist Irving Langmuir first described and named the fourth state of matter: plasma, an ionized gas full of charged particles like reactive oxygen and nitrogen species (RONS), electrons, but also ultraviolet, and electromagnetic fields. Well-known for its uses in industry and technology, its application in medicine is the subject of a relatively young discipline called Plasma Medicine, whose most important research field is the potential use of plasma in oncology.

Plasma-activated liquids (PALs) are produced by exposing a liquid to high voltage electrical discharges, leading to the production of RONS, of which the most important are nitrites (NO_2^-) and hydrogen peroxide (H_2O_2). They can trigger anticancer effects as assessed both *in vitro* and *in vivo* biological contexts.

This thesis aimed at studying PALs effectiveness against Epithelial Ovarian Cancer (EOC) serous histotype (HGSOC), one of the most lethal diseases in women due to its high aggressiveness (75% of patients diagnosed at FIGO III-IV state) and poor prognosis (less of 50% in 5 years), whose therapy often fails as chemoresistance sets in. In this context, PALs treatments seem a promising new therapeutic strategy to be used in combination with standard therapies given their ability to act locally against cancer cells, preserving healthy tissue and thus reducing common chemotherapy side effects.

The biggest challenge in transferring this potential anti-cancer agent to clinics is to test it on a research model capable of mimicking the complex nature of the EOC. The failure rate of standardized treatment approaches for EOC has led to the urgent need to fine-tune more sophisticated and faithful preclinical models able to recapitulate the features of the primary tumor, with the final aim to shed light on new potential therapeutic targets. In this regard, the ascitic fluid, typically associated with advanced disease and poor prognosis has been proposed as a valuable source of tumour material and information on tumour biology, from which it is possible to establish primary cell cultures.

However, the recently emerging 3D culture models might be more advantageous than 2D tumour models to reproduce both histological and genomic features of the original tumour. In detail, perfusion-based cell cultures have demonstrated a unique ability to promote generation of tissue constructs displaying biological and structural characteristics comparable with those of primary tissues, in addition to the maintenance of tumour and tumor microenvironment (TME) viability. The novel perfusion-based bioreactor U-CUP, providing direct perfusion throughout the tumor tissue, was used

to obtain an EOC 3D *ex vivo* model able to mimic the original tumor' TME and cellular heterogeneity. Moreover, we optimized this approach so that it can be successfully applied to slow-frozen tumoral tissues, further extending the usefulness of this tool. We also investigated the effectiveness of Plasma Activated Ringer's Lactate (PA-RL) solution against HGSOC in both 2D and 3D cultures using *ex vivo* specimens. We propose PA-RL as a novel therapy with local intraperitoneal administration, which could act on primary or metastatic ovarian tumors inducing a specific cancer cell death with reduced damage on the surrounding healthy tissues.

3. INTRODUCTION

3.1 Ovarian cancer

When all types of cancer are considered, ovarian cancer (OC) is the eleventh most common type in women, the fifth largest cause of their cancer-related death, and the most lethal gynecologic cancer¹. White women have the highest prevalence, with an annual incidence of 11.3 out of every 100.000 being affected^{1,2}. The OC average age of onset is 65 years, but hereditary cases (5-10%) could occur early, at the age of 30-35 years³. Genetic predisposition and nulliparity are the two major risk factors in addition to the obesity, factors interrupting ovulation such as contraceptive use, pregnancy, and breastfeeding correlate with a reduced risk. Considering the lack of effective screening alternatives for detecting OC at an early stage, as well as a lack of early, specific warning signs or symptoms that contribute to a diagnosis delay, prevention should be emphasized especially through the education of general public regarding the risk factors of OC⁴.

OC has three main types⁵:

- ⌚ *Epithelial ovarian cancer (EOC)*: arises from cells located on the surface of the ovary. This is the most common OC type. It occurs with a frequency of 90%, mainly in old women.
- ⌚ *Germ cell cancer*: arises from cells involved in the production of oocytes. It occurs with a frequency of 5%.
- ⌚ *Sex-cord stromal*: is often involved in the production of steroidal hormones. It occurs with a frequency of 5%.

EOC histopathology consists of four primary subtypes, of which: serous, endometrioid, mucinous and clear cell^{5,6}. Serous subtype could be high-grade serous ovarian cancer (HGSOC) or low-grade serous ovarian cancer (LGSOC), respectively accounting for 70-80% of all EOC subtypes and less than 5%. The other subtypes occur in the 10%, 3% and 10%, respectively⁶.

Distinct OC histotypes differ in epidemiology, genetic changes, gene expression, tumor markers and response to therapy⁷. As in other solid tumors, 90% of EOCs are clonal: they develop from the progeny of single cells that have accumulated a number of genetic changes in oncogenes and oncosuppressors involved in ovarian oncogenesis. The genetic changes induce proliferation, inhibition

of apoptosis, blockade of anoikis, increased motility, adhesion, invasion and attraction of stromal components, including mesenchymal stem cells. This acquisition of malignant potential likely determines three different main origins for EOCs is the reason why EOCs often have three origin locations: ovarian, tubal or epithelial sites in the pelvis^{5,8}.

Based on malignancy and growth rate, EOCs can be divided into two groups:

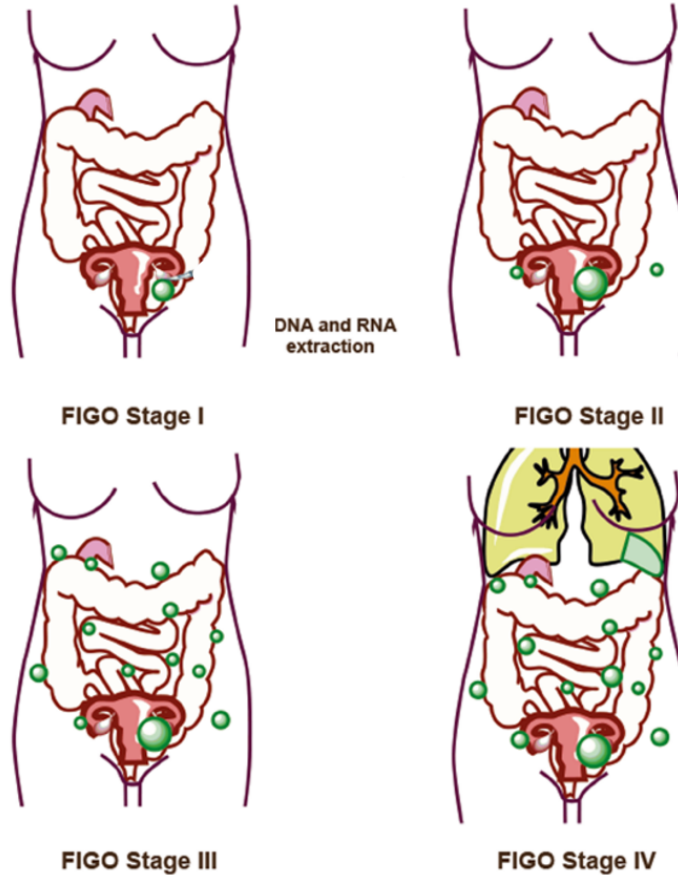
- Type I tumors include low-grade serous, endometrioid, clear cell, mucinous and transitional cell carcinomas. They often occur at an early stage, may arise from borderline ovarian tumors or endometriosis and they usually have a more favorable outcome⁹.

- Type II tumors include high-grade serous carcinoma, undifferentiated carcinomas and mixed mesodermal tumors. They account for about 75% of the EOCs and are commonly associated with deadly prognosis⁶. These malignancies are generally diagnosed later and connected to *BRCA* gene mutations and *TP53* alterations, another tumor suppressor gene. This type of tumors may have migrated from the fallopian tubes, where they originated¹⁰.

Each histological group has distinct molecular pathways that influence chemosensitivity, pattern of metastasis and probability of survival¹¹.

3.1.1 High grade serous ovarian cancer: genetical and pathological features

HGSOC is the most common subtype accounting for 75% of all EOCs¹², characterized by rapid and early metastatization in the peritoneal cavity and more specifically to the omentum, which corresponds to FIGO stages (International Federation of Gynecology and Obstetrics) III and IV¹³.



Stage I	Tumor limited to the ovaries
Stage IA	Tumor limited to one ovary, no ascites
Stage IB	Tumor limited to both ovaries, no ascites
Stage IC	Stage IA or IB with ascites
Stage II	Tumor involves one or both ovaries with pelvic involvement
Stage IIA	Extension or implants to the uterus or fallopian tubes, no ascites
Stage IIB	Extension to other pelvic tissues, no ascites
Stage IIC	Stage IIA or IIB with ascites
Stage III	Tumor involves one or both ovaries with peritoneal metastases outside the pelvis or retroperitoneal lymphadenopathy
Stage IIIA	Tumor grossly limited to pelvis
Stage IIIB	Peritoneal metastases beyond the pelvis (<2 cm)
Stage IIIC	Abdominal implants (>2 cm) and/or retroperitoneal lymphadenopathy
Stage IV	Distant metastasis including liver parenchyma

Figure 1. Schematic representation of EOC FIGO stages (modified from Bischof et al.¹⁴)

This malignancy is generally diagnosed at an elderly age (patients median age: 56 years¹¹) due to the lack of manifest symptoms in early stages, leading to the poor survival rate of 29% within 5 years from diagnosis¹⁵.

Similarly, to other advanced intra-abdominal tumors, HGSOC first symptoms are in general unspecific such as nausea, vomiting, abdominal pain and bloating. The usefulness of medical imaging techniques such as ultrasound, magnetic resonance imaging (MRI) and computed tomography (CT) in preoperative tumor staging is still limited¹⁶. Laparoscopic surgical assessment using the Fagotti scoring system and peritoneal cancer index (PCI) are used to determine the disease severity in terms of carcinomatosis spread pattern, thus determining the feasibility of the primary cytoreductive surgery (PCS), used for disease staging¹⁷.

From the histopathologic point of view, HGSOC tumors are heterogeneous showing two histological types: classic and Solid, pseudo Endometrioid and Transitional (SET) variants¹⁸. Classic HGSOC tumors (HGSOCs) feature masses of cancer cells characterized by fenestrations and/or a papillary and glandular architecture similar to the fallopian tube surface epithelium¹⁹. Solid growth is typically accompanied by widespread necrosis. Common cytological features of tumor cells include nuclear pleomorphism, large eosinophilic nucleoli and strong mitotic activity. Psammoma bodies, calcified regions linked with papillary tumors, are also common⁸. Micropapillae and odd large cells are visible (Figure 2). Also, these tumors have a high number of tumor-infiltrating lymphocytes and geographical necrosis²⁰.

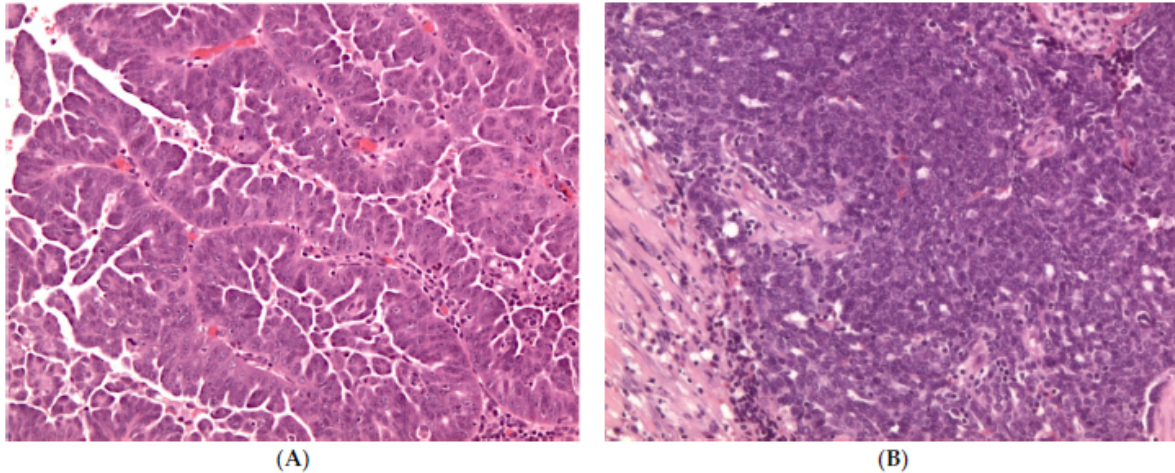


Figure 2. (A) Histologic appearance of classic HGSOc (hematoxylin and eosin, H&E, $\times 100$); (B) Solid, pseudoendometrioid, transitional cell carcinoma-like (SET) variant of HGSOc (hematoxylin and eosin, H&E, $100\times$)¹⁶.

Around 80% of the HGSOcs arise from the distal fimbrial end of the fallopian tube from the serous tubal intraepithelial carcinoma (STIC) which is often considered to be the lesion of origin⁸. On the contrary, primary peritoneal HGSOcs is extremely rare and thus, the peritoneal origin should be evaluated only when the existence of tubal STIC or HGSOc has been ruled out, as well as the absence of ovarian involvement. Precursor STIC lesions showed molecular characteristics superimposable to those observed in the fimbrial end of the fallopian tubes demonstrating that most, if not all, HGSOcs have a clonal link and a direct evolutionary ancestry from these cells^{8,21}.

The majority of HGSOcs are sporadic, however 15-20% of EOC patients exhibit a hereditary propensity, with mutations in the homologous recombination (HR) genes *BRCA1* and *BRCA2* or less prevalent genetic alterations in other HR genes^{22,23}. A 2011 study conducted by the cancer genome atlas (TCGA) network revealed the HGSOc genomic landscape using microarrays and exome sequencing of samples from 316 patients. Somatic mutations in *TP53* oncosuppressor gene were detected in almost all HGSOcs (96%)²⁴, suggesting its likely role as driver for disease initiation as well as contributing to patients' prognosis²⁵. Retrospective analyses revealed that the limited number of *TP53* wild type samples from the TCGA analysis came from patients whose condition was most likely misdiagnosed as HGSOc²⁶. Further in-depth studies about *TP53* genetic status and function in HGSOc patients reported that about 70% of mutations were missense, mostly affecting the DNA-

binding domain of the p53 protein. Missense mutations result in three phenotypes based on their effects on p53 protein function: loss of function (LOF), dominant-negative and gain of function (GOF). A much smaller contribution is given by frameshift (12%), nonsense (8.67%) and splice mutations (5.1%) encoding for truncated proteins or causing protein misfolding defects^{26,27} Therefore, the TCGA findings support a model of HGSOCs carcinogenesis where early p53 loss is followed by extensive DNA copy-number alterations. The TCGA study also reported that *BRCA1* and *BRCA2* genes were mutated in 12.5% and 11.5% of patients, respectively, as well as other mutations in genes responsible for the HR pathway in DNA repair characterize 51% of cases. HGSOCs genomic landscape consists also of somatic copy-number alterations (CNAs), among which the most common is *CCNE1* amplification and epigenetic modifications such as altered promoter methylation of 168 genes²⁴.

In terms of metastatic potential, HGSOC does not require blood circulation to colonize distant sites since it spreads directly to surrounding organs within the peritoneal cavity. Cancer cells growing on the surface of the ovary are not limited to spread in the peritoneal cavity: once cells detached from the primary tumor site, either singly or as aggregates, they are resuspended in the peritoneal fluid and passively spread following the psychological movement of this fluid around the peritoneal cavity. In this way, cancer cells can colonize distant organs and tissues, rapidly developing in metastases²¹ (Figure 3).

The secondary dissemination can affect any organ within the peritoneal cavity, with a preference for the omentum, which is colonized in 80% of HGSOC patients²⁸. This predilection has been proposed to originate from a cellular metabolic demand for fatty-acid based catabolism (β -oxidation)²⁹. Although spread outside the peritoneal cavity is unusual, some pelvic and/or para-aortic lymph nodes may be affected. However, there is a risk of spreading to the liver, and in the HGSOC FIGO stage III-IV, tumor cells may overcome the diaphragmatic barrier and enter the pleural space, where they can induce pleural effusions or potentially implant in the lung parenchyma^{30,30}.

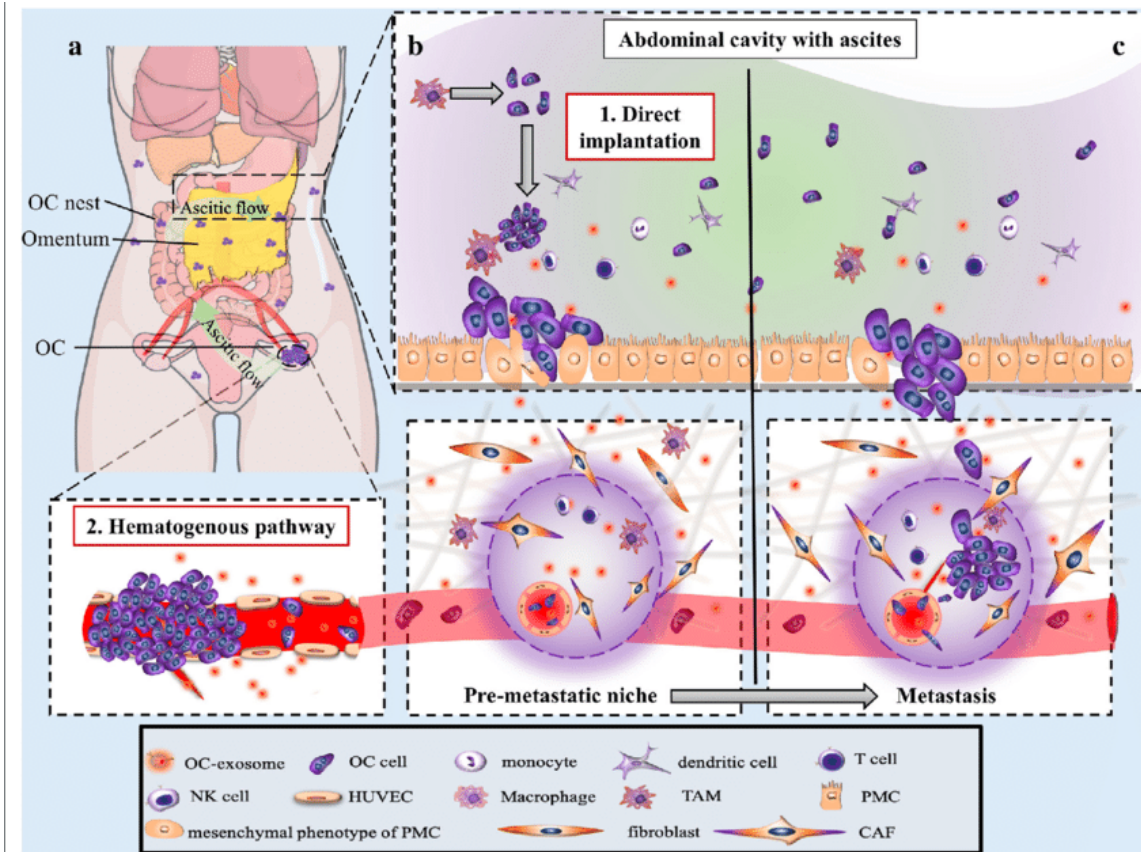


Figure 3. Natural evolution of OC. Metastatic paths of OC are presented, the local spread using peritoneal fluid/ascites as a vehicle is the most frequent mode of spread. (adapted from Feng et al.³¹).

Late-stage patients typically develop ascites with a substantial cellular component including host cells, soluble factors, vesicles, immune cells and tumor-associated macrophages (TAMs) responsible for tumor progression, immune evasion and therapy resistance³². HGSOC cells may contribute to the formation of ascites by either obstructing lymphatic outflow or secreting vasoactive and angiogenic substances that increase vascular permeability³⁰. Ascites is characterized by multicellular structures taking the shape of spheroids or aggregates of tumor cells in suspension. These have been postulated to be a key unit of metastatic dissemination, as well as a chemo-resistant niche that allows HGSOC cancer cells to survive therapy. Importantly, multicellular structures could allow cells to survive in anchorage-free environments by inhibiting anoikis³⁰ (Figure 4).

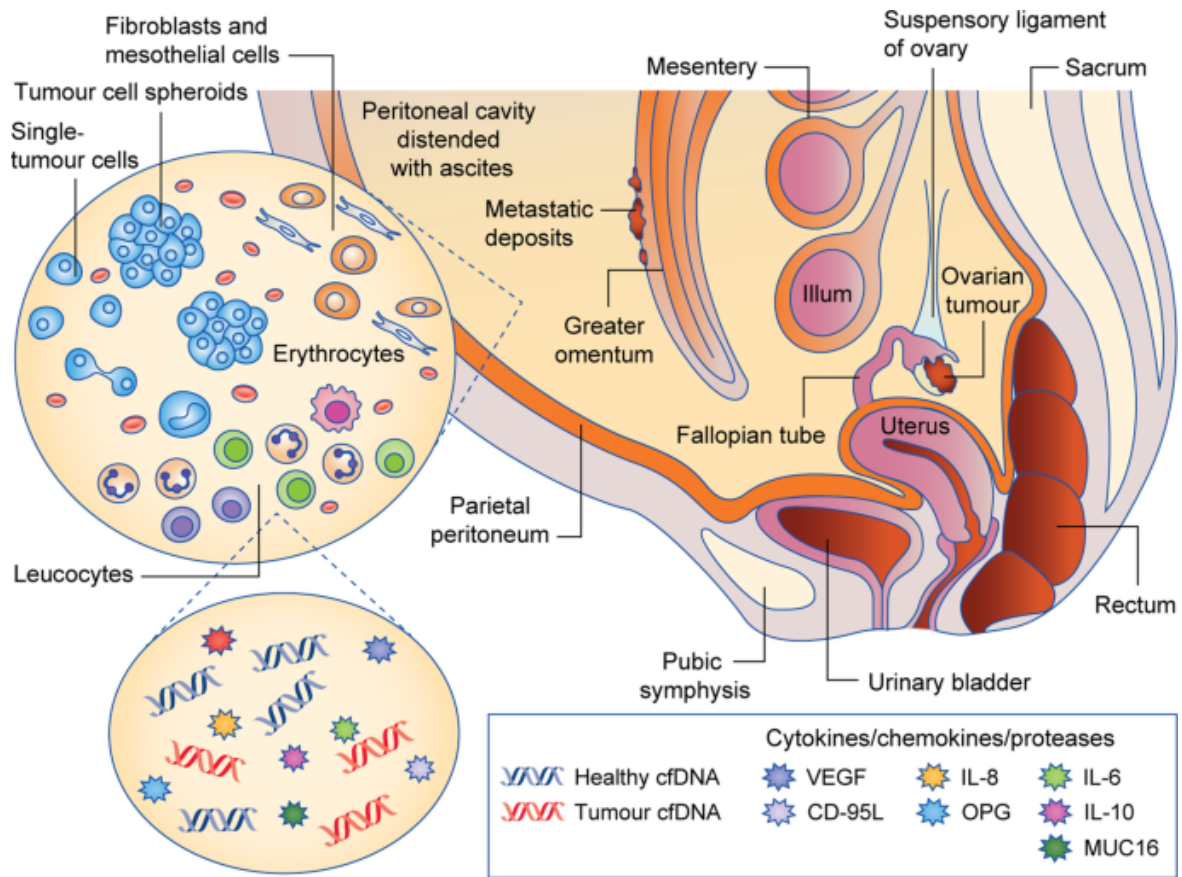


Figure 4. The contents of ascitic fluid in OC patients (modified from Ford et al.³³)

3.1.2 Therapeutic approach of EOC

In EOC, therapeutic management is accomplished using multidisciplinary approaches such as debulking surgery, chemotherapy, and radiotherapy (rarely)^{34,35}. Women with suspected HGSOc are evaluated to determine their eligibility to PCS, consisting of oophorectomy, hysterectomy, omentectomy and resection of other afflicted tissues that can be removed. The surgery envisions to reduce tumor burden and residual disease with the aim of increasing patients survival³⁶. Indeed, smaller residual lesions (less than 2cm) have been linked to a better prognosis than larger ones. Another advantage of debulking surgery is the possibility to accurately determine the disease's histologic subtype, which is critical for diagnosis³⁷.

Even though surgery is the cornerstone of OC treatment, it is rarely curative on its own for individuals with advanced disease, necessitating the addition of chemotherapy³⁸. Chemotherapeutic

agents administration methods are intravenously (IV), intraperitoneally (IP) or by IV/IP combination. Chemotherapeutic agents supplied via IP revealed to be most effective to treat peritoneal spread^{39,40}. Two phase III clinical trials combining cisplatin (CDDP) and paclitaxel (PTX) as adjuvant treatment for advanced stage EOC were conducted in the late 1990s. Since then, the combination of taxane and platinum derivatives, such as CDDP and carboplatin (CBT), has been employed as a standard therapy method for EOC patients, resulting in a 60–80% response rate and complete clinical remission^{41,42}. The mechanism of action of CDDP and CBT is the direct insertion of platinum into DNA to form crosslinks. The resulting structural DNA distortion is either repaired by specialized DNA repair enzymes or starts a signaling cascade that causes apoptosis. Platinum monotherapy is rarely utilized in HGSOC treatment and only infrequently in elderly patients who do not tolerate combination chemotherapy⁴³.

Neoadjuvant chemotherapy (3 to 4 cycles of carboplatin and paclitaxel) is preferred for patients with bulky stage IV disease whose tumors are unlikely to be totally cytoreduced to less than 1 cm (no macroscopic disease)^{44,45}. On the contrary, up-front PCS followed by six cycles of platinum-based chemotherapy favors stage IIC patients, with tumors smaller than 4.5cm⁴⁶, for whom the perioperative morbidity and mortality risk is ruled-out. However, when surgery is performed the main goal is the optimal cytoreduction of all the macroscopic disease inside the abdomen and pelvis⁴⁷. Indeed, one of the most powerful indicators of survival for patients with HGSOC is the amount of residual disease remaining after PCS⁴⁸.

Initially, HGSOC is chemo-sensitive but as the tumor grows and develops, it eventually becomes resistant to drug therapy and results in disease recurrence⁴⁹ in around 75% of cases within 5 years⁵⁰. Chemosensitivity in HGSOC is based on the platinum-free interval (PFI) intended as the time passed between the last platinum chemotherapy and recurrence. According to the Gynecologic Cancer InterGroup (GCOG) consensus statement, platinum-sensitive patients have a PFI longer than 6 months, while platinum-resistant patients PFI is less than 6 months⁵¹. Practically all HGSOC patients develop platinum resistance at the end and they die due to disease recurrence⁵². There are two types of platinum resistance: limited development of platinum-DNA adducts and cell death following adducts

formation⁵³. The first could be due to the increased export or to the decreased drug influx^{54,55}; the latter is ascribable to the DNA repair mechanisms activated when platinum-DNA adducts are mature.

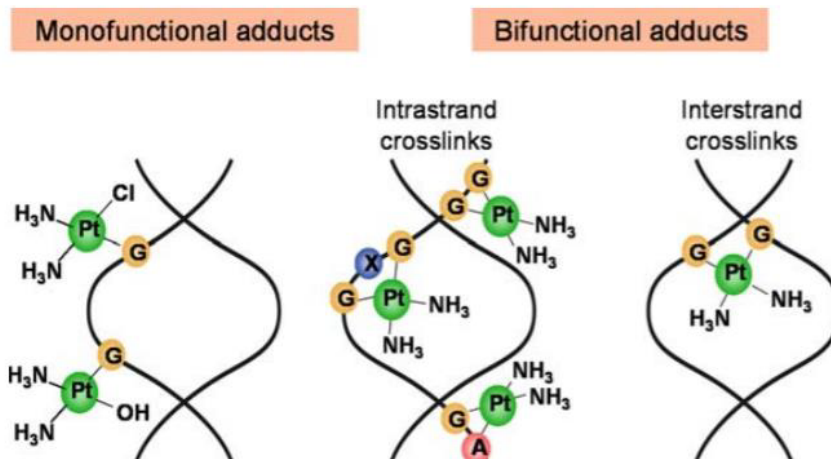


Figure 5. Formation of intra-strand e inter-strand platinum-DNA adducts⁵⁶

Improving survival for HGSOC patients is dependent on optimizing therapies to overcome or minimize drug resistance onset⁵⁷. Over the last few years, a greater knowledge about EOC biology and chemoresistance mechanisms aided the development of molecular targeted therapies, which aimed to improve survival and quality life in platinum-refractory patients³⁸. One of the most studied agents is the recombinant humanized monoclonal antibody Bevacizumab (Avastin®, Genentech, Inc.) targeting the vascular endothelial growth factor (VEGF), thus blocking angiogenesis⁵⁸. It has been shown to restore tumor vascularization and reduce tumor interstitial pressure, improving the efficacy of standard therapy and from 2018, it has been proposed in combination with platinum and taxane, as a maintenance single-agent for HGSOC patients (stage III or IV)^{20,58}. In general, bevacizumab has been demonstrated to improve PFS for 2–4 months and also OS in some cases, albeit it is associated with higher degree of side effects^{59,60}.

Also, poly (ADP-ribose) polymerase inhibitors (PARPi) are noteworthy; in 2014 they obtained approval from both FDA and EMA as maintenance treatments for *BRCA*-mutated patients diagnosed with a fresh or relapsed platinum-sensitive HGSOC⁶¹. Also, in the case of PARPi there are still matters

of debate, such as the optimal duration of administration. Indeed, some trials showed that PARPi efficacy tended to decrease with increasing lines of chemotherapy⁶¹. Because the only accepted predictors of response to PARPi are cisplatin sensitivity and presence of BRCA1/2 mutations, the selection of the right patients for maintenance treatment is also a challenge^{62,63}.

Despite the modest improvements in survival rates, innovative therapies cannot completely eradicate the disease^{64,65}. However, advances in surgery are paving the way for this type of neoplastic invasion to be treated. One innovative surgical approach aimed to eradicate ovarian disease diffusion inside the peritoneal cavity is based on the standard chemotherapy IP administration; indeed, this way of administration was proven to increase the drug's dose delivered to the tumor site and thus the median survival with respect to the IV administration⁶⁶⁻⁶⁸. This could be performed by immediately pumping chemotherapy into the peritoneal cavity during surgery, as with Hyperthermic Intraperitoneal Chemotherapy (HIPEC)⁶⁹. This method allows for the cleansing of the abdominal cavity by injecting a chemotherapeutic solution locally. Despite the good results of intraperitoneal chemotherapy delivery, the discovery of effective ways to reduce severe drug side effects and combat chemoresistance remains a pressing concern.

3.2 Preclinical models in ovarian cancer research

3.2.1 Preclinical cancer models: from past to present

Cancer research and development of targeted agents in this field was based on robust studies using preclinical models. Due to the failure rate of traditional treatment techniques for various solid tumors there is an urgent need to refine more sophisticated and faithful preclinical models able to replicate cancer properties of *in vivo* human tumors, in order to shed light on novel possible therapeutic targets⁷⁰.

One of the conventional approaches is the two-dimensional (2D) cell culture system that, although it allows to study cancer cell autonomous processes in a straightforward, relatively low cost and reproducible way, is not representative of the complex architecture of the tissue *in vivo*. As a consequence, 2D immortalized models not accurately predict a response to treatments, while the establishment of primary 2D cell cultures suffers of a very low success rate⁷¹.

More reliable preclinical models are represented by mouse xenografts, generated upon injection of cell lines in immunodeficient mice. More sophisticated and advanced models, even more suitable for translational cancer research, are patient-derived tumor xenografts (PDXs), derived by injecting primary tumor cells or small pieces of human-derived tumor samples subcutaneously or in mice. PDXs have significant limitations which impede them from being readily available, indeed their establishment is inefficient due to the sample quality and tumor type, with engraftment rates ranging between 20 and 80%^{70,72}. Lack of human stroma, including immune cells, is ascribable to their rapid loss followed by the replacement by murine stroma, which compromise the utility of PDX models in human microenvironment-targeted therapeutic research (Figure 6). Moreover, PDXs establishment is time-consuming, expensive and requires specialized facilities and trained personnel⁷³.

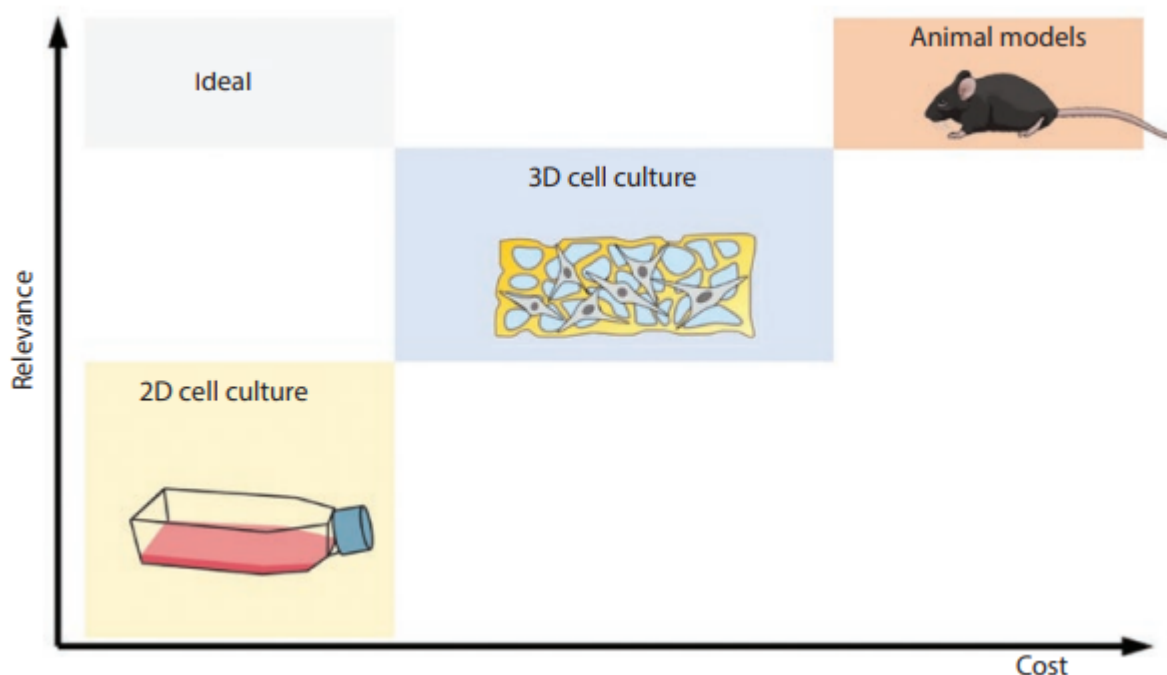


Figure 6. Schematic representation of relevance vs costs of pre-clinical models in cancer research ⁷⁴

Increasing evidence suggests that human three-dimensional (3D) cancer cell cultures represent the best model to bridge the gap between cancer cell lines *in vitro* and *in vivo* models^{70,75}. They are proposed as the best approach to reduce the amount of animals needed for testing, thus overcoming cost and ethics issues. In general, 3D cultivation better replicates the physiologic environment that

cells encounter in the body, so cells react to external signals in a more physiologic manner than in 2D cultures. Therefore, this approach is of enormous interest in the field of drug development for the high-throughput screening of several substances or conditions^{71,76}.

There are different types of 3D cell cultures, each of them having different advantages as well as drawbacks. Multicellular tumor spheroids (MCSs) appear as spherical aggregates of malignant cells, bigger than 1mm and mimicking *in vivo* cells behaviors and organization in terms of morphology and physiology. Their spherical form can be sustained by a forced-floating method, mechanical rotation or by other methods such as hanging droplets⁷². The MCSs improvement by using organ-specific stem and/or progenitor cells allowed for the development of more advanced 3D constructs known as organoids. These cells are embedded in a scaffold made of a porous biomimetic hydrogel that creates an artificial niche. Therefore, due to their complex cellular morphology and heterogeneity as well as cell-environment crosstalk, organoids allow a more accurate simulation of the native cancer tissue⁷⁷. Unfortunately, this method presents some noticeable drawbacks, out of which the imperfect resemblance to the original tissue due to the lack of surrounding fibroblasts and endothelial cells in the culture, which fail to recreate the TME that includes also immune cells and the extracellular matrix (ECM)⁷⁸. Then, they are not fully mature and cannot be expanded for long term. The TME deficiency may impair the 3D cancer cell cultures application to predict clinical outcome.

3.2.2 Ovarian cancer organotypic models

The lack of prototypes able to accurately reproduce the high biological complexity of EOC and its heterogeneous nature contributes to the failure of current pharmacological approaches^{77,79}. This can be mainly attributed to the inadequacy of existing 2D ovarian cancer cell lines to model pathophysiological aspects of the disease. In the same way, even though EOC PDXs models showed the potential to be used as a platform for translational EOC research, the biggest drawback is represented by the long latency in generating them which would translate in a delayed treatment initiation⁸⁰.

With respect to the ovarian cancer research based on alternative pre-clinical models, different 3D models have been fine-tuned. Studies using spheroid derived from ovarian cancers patients have been conducted predominantly with HGSOC samples obtained from ascitic fluid. Different isolation protocols were tested, among which the forced-floating method⁸¹, plating in low-adhesion 96 well

plate V bottom⁸² and laser isolation of tumor spheroids prepared on a coated glass slide⁸³. In general, these spheroids contained fewer stromal cells. Furthermore, the success rate of spheroid culture from ovarian HGSOE tissues was only 13%⁷⁹. More recently, a high success rate (80–90%) of organoid cultures was reported for ovarian HGSOE, most of all obtained through embedding in matrixes such as the basement membrane extract (BME) and supplementation with mediums added of compounds reported to support EOC growth in 3D culture conditions⁸⁴. In spite of the organoids ability to maintain histological and genomic features of the original tumor and especially its heterogeneity, as well as being genetically modified, used for drug testing and xenografting, they were not proven to tackle the complexity of the different ovarian cancer TMEs. Furthermore, these models present no vasculature or cell-ECM communication.

Organotypic models of ovarian cancer made it possible to overcome many of the limitations relating to 3D cultures. In particular, 3D models including primary stromal population together with OC cells in an ECM background allowed to study adhesion and invasion mechanisms in a more reproducible and accurate way^{85,86}. These models also have their limits such as the lack of vasculature, adipocytes and host immune cells. A further upgrade of the ovarian organotypic models is given by experiments performed under flow conditions. In this way, one can simulate the transcoelomic spread that cannot be reproduced in standard static cultures, as well as other factors such as increased adhesion under flow conditions and the continuous release of growth factors or nutrients⁸⁷. The application of perfusion flow on *ex-vivo* patients derived tissues, so the maximum TME reproduction, still remains only an idea, especially in the context of ovarian cancer research.

Another big limitation in cancer research is the availability of viable fresh human tissue to generate 3D models; indeed, it often depends on the proximity of surgical rooms and equipped research laboratories. Therefore, there is an urgent need to optimize protocols to obtain viable EOC 3D models from banked slow-frozen tissues, in time-independent manner⁸⁸.

3.3 Plasma medicine

3.3.1 Plasma: the fourth state of matter

In 1920s, the chemist Irving Langmuir first described and named the fourth state of matter: Plasma, an ionized gas full of charged particles like reactive oxygen and nitrogen species, electrons, but also

ultraviolet, and electromagnetic fields; globally, it can be considered neutral given its total electrical charge equal to zero. The minting of plasma word is due to the resemblance of a fluid carrying high-speed electrons and ions to the way in which blood plasma carries several corpuscles in the blood. "Ionized" means that a significantly large fraction of electrons has been torn off from the atoms. The free electrical charges make the plasma a good conductor of electricity, able to strongly respond to electromagnetic fields.

The simplest way to produce plasma artificially is by igniting it at low or atmospheric pressure adding energy to a gas, such as air, argon, or helium. An important parameter to characterize plasma is the background gas temperature; thus, plasmas are classified as "thermal/hot" or "non-thermal/cold"⁸⁹. Thermal plasma is virtually entirely ionized, whereas non-thermal plasma (NTP) is just partially ionized and characterized by temperatures varying between the atmospheric one and around 1000K and by electrons with a temperature around 10^4 K. This situation is defined "nonequilibrium plasma". NTP is used in a wide range of applications, among which technology and industry, e.g. in metallurgy or sterilization. In detail, the NTP generated at atmospheric pressure found application as well in medicine and biology, known as Cold Atmospheric Plasma (CAP). Plasma application to the medicine is the subject of a relatively young discipline called "Plasma Medicine", combining plasma physics with medicine and life science^{90,91}.

Plasma has found applications in microbial cleaning, wound healing, blood coagulation applications, dental applications and cancer treatment because it may cause cell death as well as encourage cell multiplication^{7,91-94}. CAP inactivation of bacteria and fungus, as well as similar cytotoxic effects on eukaryotic cells, is thought to be due to the oxidative damage to the cells' membrane and intracellular components, including DNA, caused by many reactive oxygen species (ROS) and reactive nitrogen species (RNS)⁹⁵. ROS are represented by H_2O_2 , superoxide (O_2^-), hydroxyl radicals ($\cdot OH$), singlet oxygen ($\cdot O_2$), and ozone (O_3). RNS include nitric oxide (NO), nitrogen dioxide (NO_2), nitrous oxide (N_2O), nitrogen trioxide (NO_3), and dinitrogen tetroxide (N_2O_4)⁹⁶.

3.3.2 Application of CAP on cancer treatment

In recent years, cancer therapy has become one of the major areas of interest in plasma medicine. CAP has been investigated as a potential cancer treatment method, so the interest in using it to treat cancer has been growing⁹⁷.

The main purpose in this context is to induce cell death of cancer cells and tissue by implementing two main approaches: direct CAP discharge to the target area, that is an active part of the discharge, or indirect CAP discharge where active plasma species are moved by a gas flow⁹⁸. Two CAP devices frequently employed in plasma medicine are used to generate direct and indirect discharges, respectively: the plasma jet⁹⁸ and the dielectric barrier discharge (DBD). In both systems a violet plasma is generated in the space between the anode and the cathode of the plasma source, where the latter is the pouter ground electrode. To retain CAP creation, the plasma jet device requires a carrying gas such as helium or argon, whereas the DBD device generates plasma directly in the air. These operating principles generate a thin CAP jet and a short but a wide plasma, respectively. Based on these characteristics and properties, the plasma jet device may be more suited for gently treating a tiny area of a sample. The DBD, on the other hand, may be better suited for a more intensive treatment on a larger area of sample⁹⁹.

In both cases, the intracellular release of reactive oxygen and nitrogen species (RONS) would contribute to cellular senescence and apoptosis¹⁰⁰. Recent *in vitro* studies identified CAP as a selective therapeutic with a high propensity for causing cancer cell death while leaving normal cells intact, and with no specificity for any kind of cancer¹⁰¹. CAP has been successfully used to treat roughly 20 cancer types *in vitro*, including neuroblastoma, pancreatic carcinoma, melanoma, cervical carcinoma, lung carcinoma, head and neck carcinoma, and breast cancer, while in animal models CAP treatment induced tumor burden reduction in and increased survival^{102–105}.

There are two ways to apply plasma: direct treatment and indirect treatment with cell culture media or other fluids, previously exposed to gas flows dense of plasma species, named PALs. The first way involves directly applying the CAP on cells *in vitro*, models *in vivo* or human *ex vivo* tissues. The second approach entails generating PALs and then put cell cultures or tumors in contact with them. PALs are mostly produced by vertically treating the medium or other liquids surface with a CAP jet or DBD; alternatively, they can be produced via direct discharge in the medium. Moreover, direct CAP treatment has several downsides such as the hazardous manner of distribution in the body and the storage capacity. Therefore, PALs have recently piqued interest as cancer treatment option because they can be delivered through the body without using a CAP device besides providing the advantages of off-site production and storability^{106,107}.

The hypothesis to employ PALs in clinics, to wash the peritoneal cavities of patients affected by metastasizing cancers, necessitates a plasma prototype capable of treating considerable volumes of liquid¹⁰⁸. In this context, one of the conceivable configurations satisfying this need is the multiwire to plate configuration^{109–112}, which has the added benefit of employ environmental air as a working gas. A recently reported multiwire prototype was capable of treating up to 200 mL of liquid solution by working in two discharge regimens (DBD and corona discharges)¹¹³. However, more efforts are needed to improve the design of such plasma sources so they can treat all the liquid volume required for intraperitoneal administration.

3.3.3 Mechanism of CAP-cancer cells interaction and response

It is remarkable that molecules containing RONS do play important roles in biological systems¹¹⁴. PALs include a wide range of biologically reactive species which may have biological effects on living cells and tissues. These species may enter the intracellular space and interact with cells to cause diverse effects correlated with plasma dose, ranging from altered metabolism and apoptosis to specific DNA damages affecting a variety of cellular responses such as stem cell differentiation or inhibition of proliferation of cancer cells¹¹⁵. Moreover, ROS are thought to play a key role in cell lipid peroxidation¹¹⁶. Actually, the apoptotic cell death induced by plasma irradiation has been reported to target both normal cells and various cancer cells¹¹⁷. To understand why plasma affects cell proliferation the focus has to be moved on various electrons, ions and radicals generated in the air interface between plasma source and liquid, by interacting with oxygen, nitrogen and water. Molecules such as H₂O₂, NO₂⁻ and NO₃⁻, are thus moved in the solution where they interact with the liquid cellular environment. H₂O₂ acts as a key intermediate in killing cells, while NO₂⁻ has not damaging effects against mammalian cells^{102,106,114,118}.

Inhibition of cell proliferation and the subsequent death are ascribable to the impairment of redox equilibrium of cells caused by RONS¹⁰². Cancer cells react to oxidative stress through gene mutations, increase in growth and resistance to apoptosis, as features of their treatment resistance. However, when the oxidative stress to which they are exposed exceeds a specific threshold, cancer cells endure oxidative damage and thus arrest of proliferation and induction of apoptosis (

Figure 7). So, it is considered that cancer cells sensitivity to plasma effect depends on their higher basal ROS concentration compared to normal cells¹¹⁹. The explanation about the RONS-mediated mechanism of selective cancer cells damage is in the different states of cancer and normal cells in the PAM environment in terms of basal RONS concentration. If healthy cells have higher intrinsic levels of antioxidants useful to counteract additional RONS released from plasma, cancer cells metabolic rate makes them unable to tolerate any increase in oxidative stress¹²⁰; indeed, cancer cells with a high rate of RONS synthesis are more sensitive to intracellular RONS accumulation. A series of studies focused on clarifying the tumor cell selectivity of plasma compared with that for healthy cells concluded that, although normal cells are similarly harmed by high-energy plasma irradiation, there is a specific treatment range (treatment window) that exists between normal and malignant cells¹⁰².

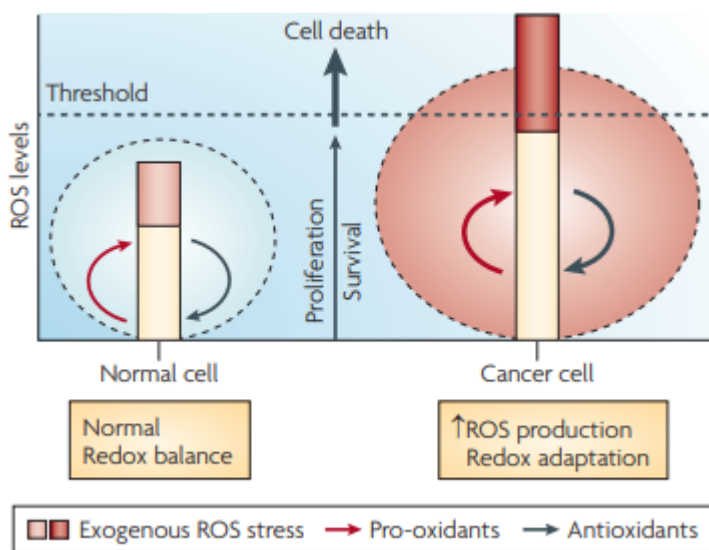


Figure 7. ROS levels homeostasis in normal and cancer cells. ¹²¹

Furthermore, also differences in their proliferation activity and apoptosis-inhibitory control system determine differences in plasma sensitivity¹²². Plasma-induced apoptosis has been proven as mediated also by different molecular mechanisms. Among these, Tanaka et al. reported that PAM downregulates the AKT, ERK and mTOR pathways, thus promoting apoptotic death¹²³. Other signal transduction pathways such as ATM/p53¹²⁴, TNF/ASK1¹²⁵ and the endoplasmatic reticulum stress pathways¹²⁶ mediate apoptosis in a series of solid tumors. The 4-hydroxy-2-nonenal (4-HNE), generated by lipid peroxidation, was reported to induce selective apoptosis in cancer cells, as well as NO/peroxynitrite and HOCl pathways, followed by the mitochondrial apoptosis pathway¹²⁷. Alternative cell death forms other than apoptosis would be the autophagy¹²⁸, the ferroptosis and the immunogenic cell death mediated by macrophages¹²⁹.

3.3.4 PALs generation and their biological effects

Biological plasma activity is due to the synergistic effects of its components, whose interaction both with the liquid cellular environment and cellular structures triggers to specific biological signaling cascades in the cell¹¹⁴.

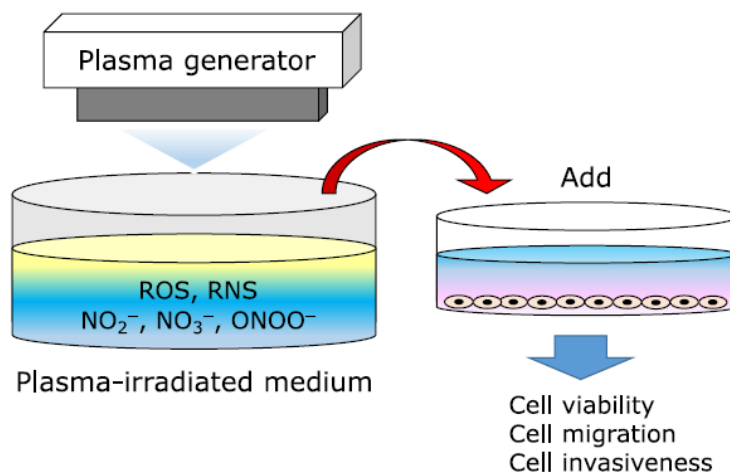


Figure 8. Indirect plasma treatment method: plasma-irradiated solution is added to the culture supernatant of separately cultured cells to expose them to RNOS without direct plasma irradiation¹²²

The chemistry of plasma-liquid interactions is extremely useful in understanding the mechanisms by which plasma interacts with biological systems. PALs are produced by exposing them to high voltage electrical discharges applied in the gas-liquid interface. When a high voltage is applied to the gas phase, plasma filaments emerge resulting in a flow of free radicals, electrons, ions, reactive species, and UV radiation. A liquid exposed to these plasma filaments is enriched of dozens of long-lived RONS, of which NO_2^- , NO_3^- , peroxy nitrates (OONO^-) ozone (O_3), $\cdot\text{O}_2$, $\cdot\text{OH}$ and H_2O_2 and is then delivered to cells or tissues⁹⁰. At low concentrations, plasma RONS were shown to drive cell proliferation or cytokine production, but at greater quantities, they can cause DNA damage, induce cell cycle arrest, and trigger apoptosis¹⁰¹. However, the activation of death by intracellular ROS formation has been proposed as a mechanism by which CAP could be a promising cancer treatment (

Figure 8). PALs generation is currently rising as a promising new technology in the field of plasma therapy given their stability (at room temperatures) and easy administration to hidden places such as body cavities.

Among liquids typically treated through plasma discharges there are cell culture media, PBS and Ringer's Lactate Solution (RL)¹¹⁹. The hugest set of publications focused on the applicability of plasma-activated media (PAM) to treat cancer cells. Tanaka et al. firstly discovered that PAM causes glioblastoma brain tumor cells death *in vitro*, causing morphological alterations compatible with apoptosis^{115,130}. This discovery paved the way for further numerous investigations contextually to the cervical tumor, melanoma, bone cancer, pancreatic cancer, gastric cancer, breast cancer, lung cancer, colorectal and bladder squamous cell carcinoma^{102,131–133}. Any anti-cancer treatment must be able to target only cancer cells with reduced damage on the surrounding healthy cells. In this regard, PALs were observed to induce a selective anticancer effect both *in vitro* and *in vivo*¹³⁰.

PAM efficacy was also widely proven against EOC cells, whose proliferative rate and metastatic ability *in vitro* were compromised¹³⁴. Its selective cytotoxicity against chemio-resistant EOC cell lines *in vitro* and *in vivo* makes it a novel combined anti-cancer therapy^{131,135}. Utsumi et al., 2013 and Nakamura et al., 2017 were pioneers in proposing PAM treatment in EOC xenografts, in order to assess the inhibition of intraperitoneal dissemination^{122,136}. In the same wake, PAM intraperitoneal administration was experimented in another disease typically disseminating in the peritoneum: gastric cancer¹³⁷. Both ovarian and gastric cancers are characterized by high rates of recurrence ascribable to the peritoneal dissemination, whose managing is critical to improve patients' outcomes. These studies

provided more information about PAM inhibitory effects on cancer cell metastasis as well as new evidence of the global impact of PAM in *in vivo* models: intraperitoneal injection of PAM can inhibit tumors growth and prevent cells metastasis in the abdominal cavity by reducing their adhesion capacity. As a consequence, mice treated with PAM showed greater chance of survival^{137,138}.

3.3.5 PALs suitable for clinical applications

The use of PAM *in vivo* murine models implied that intraperitoneal lavage with PALs has the potential to be translated as a method to prevent intraoperative peritoneal dissemination in human¹³⁹. Given the selective toxicity exerted against cancer cells and the little influence on mice body weight, PAM is envisioned as a safe and practical alternative therapy or used in combination with other chemotherapeutic agents to prevent intraperitoneal dissemination of chemoresistant EOC subclones.

In the perspective to propose PALs in clinical applications, liquids suitable to the clinical phase must be exposed to plasma, such as RL, an intravenous fluid commonly used to treat hypovolemia and metabolic acidosis¹⁴⁰. Tanaka et al. first recommended the use of RL, which has a simple composition (NaCl, KCl, CaCl₂, and lactate) that makes it suitable for the generation of PAL while minimizing the possible influence of additional organic medium components on the final biological effect¹¹⁷. *In vitro*, PA-RL solution was shown to have an anti-tumorigenic effect in lung, breast, and ovarian cancer cells, as well as in glioblastoma^{115,123}, and in pancreatic and cervical cancer *in vivo*¹⁴¹. RONS together with activation of lactate may be responsible for PA-RL effects in several investigations¹¹⁹. Indeed, the capacity of an anti-neoplastic agent to operate selectively on cancer cells is required to protect the healthy tissue counterpart. The selective targeting has become a critical issue in the context of PA-RL treatment of EOC⁹⁹. There is no available evidence regarding the safety of any type of PAL intraperitoneal administration in humans and even though PA-RL was proven to cause no side effects in mice, in support of its safety and effectiveness, further investigations are needed to support PA-RL as a good candidate to respond to the requirement for novel therapies based on the local administration of chemotherapeutics in the context of the HGSOC.

4. AIM

The intricate and multifaceted interactions between ovarian cancer cells and the TME creates a complex system which cannot be captured by classical monolayer 2D or 3D cultures with immortalized cell lines. While these models represent a helpful tool for researchers to dissect various biological mechanisms, their applicability remains limited when aiming towards the development of a personalized medicine.

The first aim of this work was to investigate the effects of PALs treatment in order to propose it as a novel approach with local intraperitoneal administration that can induce EOC cells death with reduced damage on the surrounding healthy tissues.

Furthermore, we aimed at exploring the potential of the perfusion-based bioreactor U-CUP to be used for carrying out experiments on *ex-vivo* samples from HGSOC patients' tumors, seeking to reproduce a condition more similar to the clinical setting, since the effect of PALs is unknown on TME.

In addition, we aimed at developing a reliable and reproducible method that can allow for the temporization of experiments normally performed on fresh patient *ex-vivo* samples, to overcome the problem caused by the distances between research labs and surgical rooms.

5. MATERIALS AND METHODS

5.1 Plasma Device and Chemical Characterization of PA-RL solution

PA-RL was obtained by exposing RL (Fresenius Kabi Italia S.r.l.) to a micropulsed plasma discharge (Figure 9a). The high voltage electrodes are represented by four steel wires each individually fixed on aluminum supports. The connection to the high voltage generator is made through a ballast resistor of 70 k Ω . The ground electrode consists of an aluminium sheet located on the bottom of a 5mm thick vessel which holds the liquid substrate. The electrode is connected to the ground through a resistor of 30 k Ω . In order to guarantee a controlled atmosphere during the treatment, the plasma source is encased in a polymethylmethacrylate box. The box was equipped with a fan to ensure thermal control throughout the whole process. The setup in Figure 9b was used to measure the time evolution of electrical parameters of the plasma discharge using a 5mm gap value between the high voltage electrodes and the liquid surface. The plasma device was driven by a micropulsed high voltage generator (AlmaPULSE, AlmaPlasma s.r.l., Bologna, Italy) delivering a peak voltage of 18 kV with a pulse duration FWHM (Full Width at Half Maximum) of 8 μ s and pulse repetition rate set at 1kHz. To measure the voltage, a high voltage probe (Tektronix P6015A) was used, while a Pearson 6585 probe was used to measure the current. Both probes were connected to an oscilloscope (Tektronix DPO 40034). The average power (P) over a period (T) was calculated starting from current (I) and voltage (V) measurements.

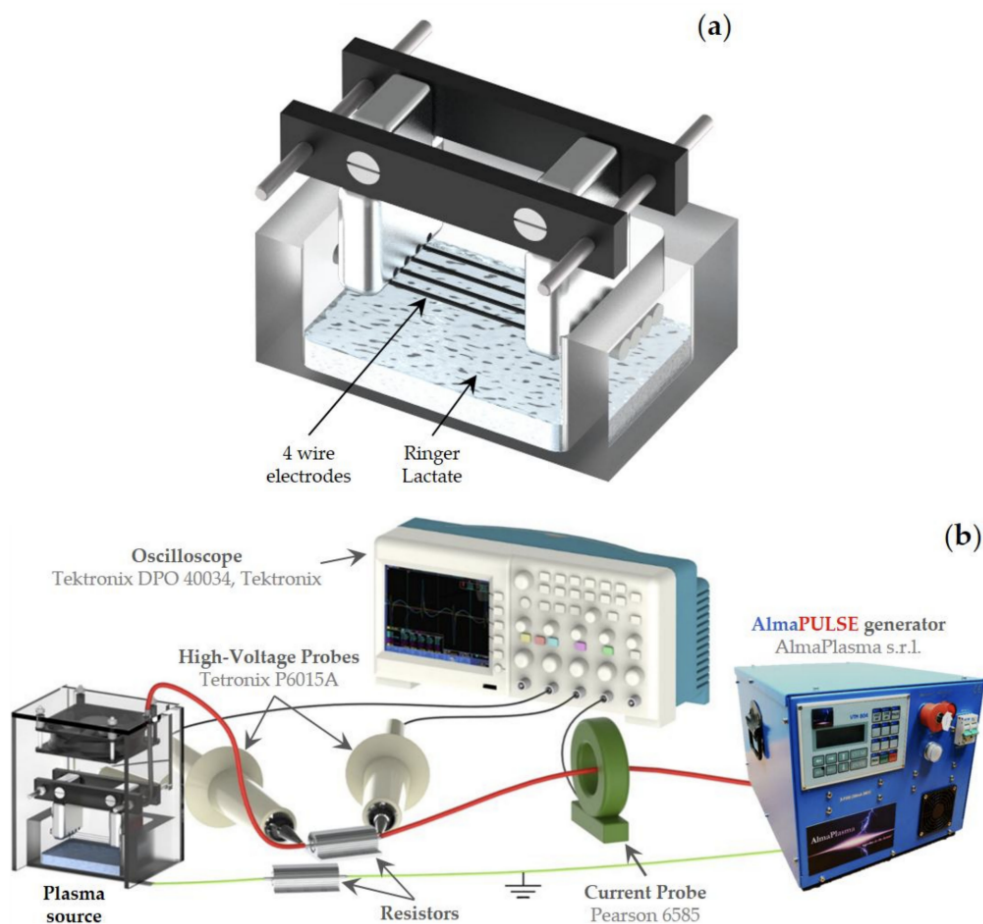


Figure 9. Device used to produce (a) and characterize (b) PA-RL solution [adapted from Bisag A, Bucci C, Coluccelli S et al., 2020¹⁴²]

5.2 PA-RL and Synthetic Solutions Production

PA-RL solution was obtained by exposing RL to the plasma discharge for 10min with a 5mm gap between the high voltage wire electrodes and liquid surface. Amplex® Red Hydrogen Peroxide Assay Kit (Thermo Fisher Scientific #A22188, Waltham, MA, USA) and Nitrite/Nitrate colorimetric assay (ROCHE #11746081001, Basel, Switzerland) were used to measure the quantity of H₂O₂ and NO₂⁻ in the obtained solution. Moreover, before and after the exposure of RL to plasma, pH and conductivity were evaluated using inoLab® pH 7110 and Oakton Instrument Con 6+ Meter, respectively. PA-RL was diluted by serial dilution (1:4, 1:8 and 1:16 dilutions) in RL and their effect was tested on our cell

models. Synthetic solutions were also prepared to serve as positive controls. Namely, two different RL solutions were supplemented with 226 μ M of H₂O₂ (Sigma-Aldrich, #216763, St. Louis, MO, USA) and 65 μ M of NO₂⁻ (Alfa Aesar by Thermo Fisher Scientific (Kandel) GmbH, #43015, Karlsruhe, Germany). These values were chosen as they are the same concentrations generated by plasma treatment of PA-RL. An additional synthetic solution was prepared by adjusting the pH of RL to 5.36 with a solution of 0.01M HCl, according to the pH-value gauged in PA-RL. The above mixtures were also diluted in RL as mentioned before. EOC cell lines were treated with the synthetic solutions at a 1:16 dilution.

5.3 Low-Speed and High-Speed Filter Imaging

A low-speed camera (Nikon D800, Shinjuku, Tokyo, Japan) was operated at 30fps for the evaluation of the behavior of the plasma discharge, as presented in

Figure 10. The high-speed filter imaging setup, used for the characterization of the plasma source, was composed of a high-speed camera (Memrecam GX-3 NAC image technology) operated at 100fps and 1/200 shutter time. Additionally, a camera lens (SIGMA 180MM 1:3.5 APO macro DC HSM) and a 402nm filter (CHROMA ET402/15x, #327585, Bellows Falls, VT, USA) were used to evaluate the emission of N₂(C³Π_u → B³Π_g) second positive system near 400nm. During HS-filter imaging, the focus of the acquisitions was set in correspondence to the electrode closer to the filter.

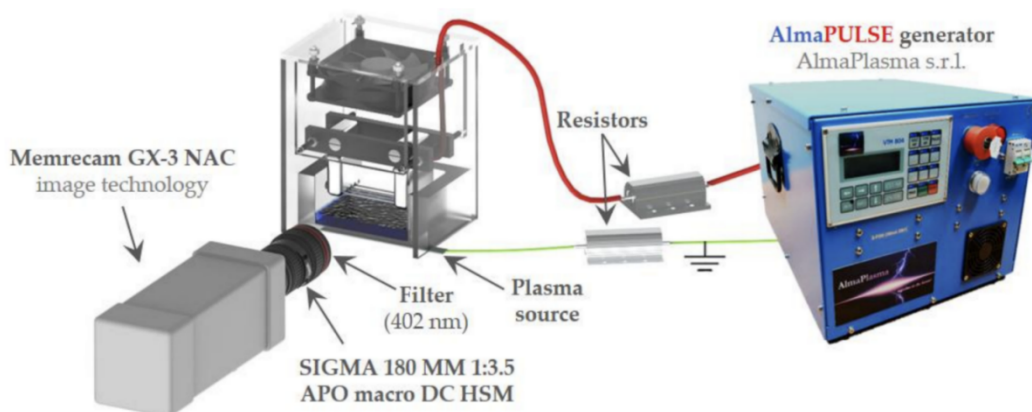


Figure 10. High-speed filter imaging setup used to evaluate the behaviour of the plasma discharges. [adapted from Bisag A, Bucci C, Coluccelli S et al., 2020¹⁴²]

5.4 Patient samples and tissue preparation

The MiPEO project (Mitochondria in the Progression of Endometrial and Ovarian Cancer) was approved by the local ethics committee in 2011 (No. 107/2011/U/Tess of 11.10.21). Written informed consent was obtained from OC patients prior to their enrollment at the S. Orsola-Malpighi Hospital in Bologna. The collected tissues were then assigned an alphanumeric code to ensure the patient's anonymity. Samples were processed immediately after surgery to avoid compromising the specimen. Tumor pieces were chopped with a sterile scalpel and used directly for fresh U-CUP experiments or frozen for later use in the case of slow-frozen experiments. Ascitic fluid samples (25mL) were placed in cell culture flasks mixed at a 1:1 ratio with cell culture media and left in the incubator for 3 days allowing the cells to attach¹⁴³.

5.5 Cell culture conditions

SKOV-3 and OV-90 human EOC cell lines were purchased from ATCC® (Manassas, VA, USA) while the HOSE cell line was purchased from ScienCell Research Laboratories, Inc. (Carlsbad, CA, USA). Non-cancer cell lines used in this work were represented by two lines of immortalized fibroblasts (F1 and F2) obtained from skin biopsies of two patients, in the context of a study approved by the Independent Ethics Committee of the S. Orsola-Malpighi Hospital, Bologna, Italy (107/2011/U/Tess). EOC cell lines, HOSE and fibroblasts were grown in Roswell Park Memorial Institute 1640 medium (RPMI, EuroClone, Milan, Italy), Ovarian Epithelial Cell Medium (OEpiCM, ScienCell Research Laboratories, Inc., Carlsbad, CA, USA) and Dulbecco's modified Eagle's medium (DMEM High glucose, EuroClone), respectively. All media were supplemented with 10% heat-inactivated fetal bovine serum (FBS), 2mM L-glutamine, 100U/mL penicillin and 100µg/mL streptomycin (EuroClone). Cells were maintained in an incubator at 37°C with a 5% CO₂ humidified atmosphere.

5.6 Cell treatment and viability assay

SKOV-3, OV-90, HOSE, F1 and F2 were seeded in 96-well plates in complete medium at the following concentrations:

Cell line	No. of cells/well
SKOV-3	2×10^3
OV-90	4×10^3
HOSE	7×10^3
F1	9×10^3
F2	1×10^4

After 24h, cells were treated with 100 μ L of freshly produced PA-RL at different dilutions (1:4, 1:8 and 1:16) and RL serving as a control. Treatment was left for 2h after which cells were washed with phosphate buffered solution (PBS) and the cultured in complete medium at 37°C and 5% CO₂ (Figure 11).

Sulforhodamine B (SRB; Sigma-Aldrich, #S1402, St. Louis, MO, USA) assay was used to measure cell proliferation at the following timepoints: 2, 24, 48 and 72h after treatment. Trichloroacetic acid (TCA) was used to fix the cells for 1h after which the wells were washed 5 times with distilled water to eliminate TCA and stained with 0.4% SRB for 30min.

After washing the unbound excess dye with 1% acetic acid, the protein-bound dye was dissolved in 10mM pH 10.5 Tris base solution.

Cell density was determined indirectly based on the measurement of cell protein content. Absorbance values were measured at 570nm using a 96-well Multilabel Plate Reader VICTOR3 (1420) Multilabel Counter-PerkinElmer, Turku, Finland). The percentage of viability was calculated considering RL-treated cells as the control (CTR-RL).

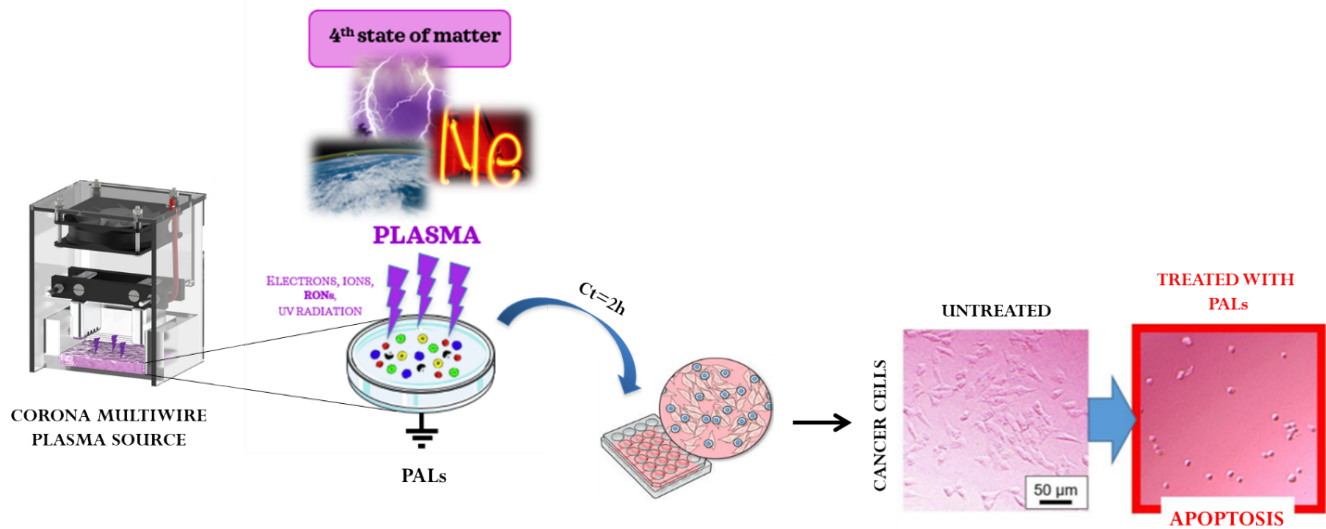


Figure 11. Workflow of PA-RL treatments on 2D cell models.

5.7 ROS production and apoptosis assays

ROS production measurement and cytotoxicity levels was performed with the incubation of cells with Cell-ROX probe (Thermo Fisher Scientific, #C10422) and Incucyte® Caspase-3/7 Dye for Apoptosis (Sartorius, #4440) respectively by using IncuCyte S3 Live-Cell Analysis System. Cells were seeded 40×10^3 in a 96-wells plate and 24 hours after were incubated with the fluorescent probes and placed in the dedicated Incucyte slot. The set acquisition protocol was set for the acquisition of 3 images/well at time 0 and after 1h. At the end of the experiment, a specific mask was applied to all the wells of the 96-wells plate, capable of recognizing the fluorescent signals. Raw data were exported from the instrument and represented in GraphPad.

5.8 Western Blot analysis

Seeded cells were treated after 24h with RL solution and freshly produced PA-RL 1:16 dilution. At this point, an untreated (UT) sample was collected for each cell line. Treatments were left for two hours after which cells were washed in PBS and cultured in complete medium at 37°C and 5% CO₂. Cells were harvested after 72h. Total lysate was obtained by using RIPA buffer (50mM Tris-HCl pH

7.4, 150mM NaCl, 1% SDS, 1% Triton X-100 and 1 mM EDTA pH 7.6) supplemented with protease and phosphatase inhibitors (Thermo Fisher Scientific #A32955, Waltham, MA, USA). The protein concentration was determined using Lowry protein assay (Bio-Rad #5000116, Hercules, CA, USA). Proteins (30 µg) were separated by using SDS-PAGE on a 12% polyacrylamide gel and then transferred onto a Trans-Blot Turbo Midi Nitrocellulose membrane (Bio-Rad #1704159). Membranes were blocked with 5% TBS-Tween/milk (0.1% Tween 20 (Sigma-Aldrich #P9416, St. Louis, MO, USA) and incubated with the anti-SOD-1 1:1000 (Santa Cruz Biotechnology #sc-11407, Dallas, TX, USA) overnight at 4°C and subsequently with anti-β-actin 1:10000 (Sigma-Aldrich #A5316) for 1h at room temperature (RT). Membranes were washed four times for 5min using TBS-Tween and then incubated with secondary antibodies (Jackson ImmunoResearch Laboratories #111035144 and #111035146, West Grove, PA, USA), diluted 1:20000 (anti-rabbit) and 1:10000 (anti-mouse) in TBS-Tween for 30min at RT. Clarity Western ECL Substrate (Bio-Rad #1705061) was used to develop the membranes and the signal was captured with ChemiDoc XRS+ (Bio-Rad). Protein levels were determined by densitometric analysis using ImageJ software (Version 1.53m, Bethesda, MD, USA). Each protein of interest was normalized using β-actin as housekeeping.

5.9 *Ex-vivo* 3D cultures

Upon arrival, freshly excised tissues were cut into small pieces of around 2x2x2 mm. Two random pieces were fixed in formalin for structural characterization through histopathological analysis and immunofluorescence (IF); a series of four pieces clusters were slow-frozen in the cryopreservative medium, in order to repeat the same experiment on slow-frozen tumors; four random pieces were placed in a flask for culture in static conditions; other four random pieces were placed between two commercial collagen sponge discs (Avitene™ Ultrafoam™, BD #1050050, Franklin Lakes, NJ, USA) in a sandwich-like configuration to perform *ex-vivo* 3D static cultures.

The sandwich was assembled within a ring-shaped plastic holder closed on top and bottom by two EFTE nylon meshes. The scaffold assembly was then placed into the perfusion chamber of a the perfusion-based bioreactor U-CUP (Cellec® Biotek AG, #9018.9084, Basel, Switzerland) for culture under perfusion flow rate set at 0.47mL/min, corresponding to a superficial velocity of 100µm/s, as previously shown for the generation of normal and tumor tissue-like constructs (Figure 12). U-CUP bioreactors were maintained in an incubator at 37°C with a 5% CO₂ humidified atmosphere.

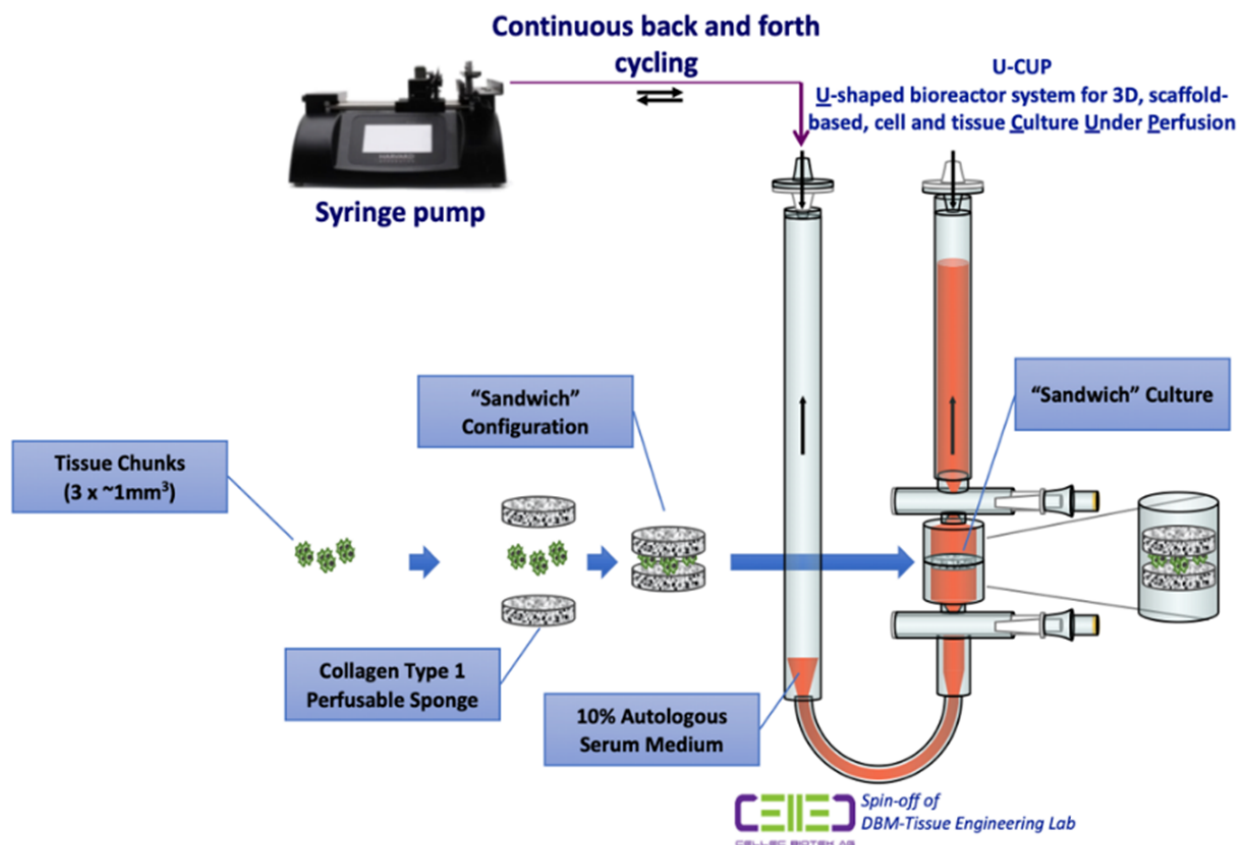


Figure 12. Schematic view of primary tissue culture assembled in a “sandwich” configuration inside U-CUP bioreactor ¹⁴⁴

Different culture media (Table 1) were tested to improve survival and preservation of tissues, as well as different time points (3, 5 and 7 days) to establish the preservation benefit provided by the perfusion system. The same procedure was carried out for banked slow-frozen primary ovarian tumors and HGSOc metastases, with the final aim to evaluate the ability of both fresh and frozen tissues to develop viable perfused-3D models.

Following culture in U-CUP, sandwich scaffold constructs containing EOC tissues were cut in two halves. One half was fixed in formalin 4% for at least 24h and embedded in paraffin; the other half was disassembled, and tumor pieces inside it were used for DNA extraction.

Tumors obtained from 5 patients, out of which both primary tumors and metastases, were used for Next Generation Sequencing (NGS).

Table 1. Culture media used for the ex-vivo 3D cultures.

Dulbecco's Modified Eagle's Medium/Nutrient Mixture F-12 Ham	# D8437	Sigma-Aldrich	w/w 10% FBS, 2mM L-glutamine, 100U/mL penicillin and 100µg/mL streptomycin.
RPMI-1640 Medium	# R8758	Sigma-Aldrich	w/w 10% FBS, 2mM L-glutamine, 100U/mL penicillin and 100µg/mL streptomycin.
Medium 199	# M4530	Sigma-Aldrich	w/w 10% FBS, 2mM L-glutamine, 100U/mL penicillin and 100µg/mL streptomycin.
Keratinocyte SFM (1X)	# 17005042	Thermo Fisher Scientific	w/w 10% FBS, 2mM L-glutamine, 100U/mL penicillin and 100µg/mL streptomycin.
Ovarian TumorMACS™ Medium	# 130-119-483	Miltenyi Biotec	w/o supplements
Advanced DMEM/F12 1X (AdvDMEM/F12)	# 12634-010	Gibco (Thermo Fisher Scientific)	w/w 1X GlutaMAX™, 10mM HEPES, 100µg/mL Primocin, 100U/mL penicillin and 100µg/mL streptomycin.
AdvDMEM/F12+++++	# 12634-010	Gibco (Thermo Fisher Scientific)	AdvDMEM/F12 supplemented w/w: - 25ng Human EGF - 10mM Nicotinamide - 1,25mM N-Acetylcysteine - 1X B27

Three metastatic tumors derived from HGSOCs were used to be treated with the afore mentioned concentrations of PA-RL, compared to a NT culture. For each patient three bioreactors were assembled: control in RL (CTRL RL), PA-RL 1:4 and PA-RL 1:16 produced according to previously established methods, so diluting PA-RL in RL by preparing two-fold serial dilutions (1:2,1:4; 1:16).

5.1 Sanger sequencing and Next Generation Sequencing analysis

DNA extraction was performed using GenElute™ Mammalian Genomic DNA Miniprep Kits following the manufacturer's instructions. DNA was eluted using a pre-warmed AE buffer to maximize DNA final yield and quantified using the NanoDrop2000. For Sanger sequencing of TP53, all 10 coding exons of TP53 and exon-intron boundaries of the gene were amplified using Fast Start Taq DNA Polymerase (Roche Diagnostics). PCR amplification was performed in a final volume of 25ul in a 9700 thermal cycler (Life Technologies), and PCR products were purified with Multiscreen PCR clean-up Filter Plates (Millipore). Primer sequences and PCR conditions for all reactions are available on request. Sequencing was performed with BigDye™ Terminator v1.1 Cycle Sequencing Kit (#4337458, Thermo Fisher Scientific) on both strands according to manufacturer's instructions. Briefly, 0.32 mM of primer was used in 10ul final reaction, together with 0.5ul of BigDye v1.1 and 2ul of Buffer. Upon cycling (4-min elongation) the amplicons were precipitated and run in an ABI3730 Genetic Analyzer automated sequencing machine (Life Technologies). Electropherograms were analyzed using Chromas Lite v.2.01 (Technelysium, South Brisbane, QLD, Australia).

For NGS analysis, an “extended version” of a previously published NGS lab-developed multi-gene panel¹⁴⁵ was used. The panel includes the following genomic regions (human reference sequence hg19/GRCh37, total of 343 amplicons, 21.77 kb) (Table 2).

Briefly, about 50ng of input DNA were used for NGS libraries preparation with the AmpliSeq Plus Library Kit 2.0 (Thermo Fisher Scientific). Templates were then sequenced using an Ion 530 chip and the results were analyzed with the IonReporter tools (version 5.16, Thermo Fisher Scientific) and IGV software (Integrative Genome Viewer version 2.9.2 - <https://software.broadinstitute.org/software/igv/>). According to the previously reported validation¹⁴⁵, only mutations present in at least 5% of the total number of reads analyzed and observed in both strands

were considered for mutational calls. The significance of alterations was checked using the Varsome database (<https://varsome.com/>) and “IARC TP53 Database” (<http://p53.iarc.fr/>).

Table 2. Genes included in the extended version NGS panel

<i>BRAF</i>	exons 11, 15	<i>c-Kit</i>	exons 8, 9, 11, 13, 14, 17	
<i>MED12</i>	exons 1, 2	<i>KRAS</i>	exons 2-4	
<i>MET</i>	exons 2, 14	<i>IDH2</i>	exon 4	
<i>NRAS</i>	exons 2-4	<i>IDH1</i>	exon 4	
<i>PDGFRα</i>	exons 12, 14, 18	<i>HRAS</i>	exons 2-4	
<i>PIK3CA</i>	exons 8, 10, 21	<i>H3F3A</i>	exon 1	
<i>PTEN</i>	exon 5	<i>GNAS</i>	exons 8, 9	
<i>RET</i>	exons 5, 8, 10, 11, 13, 15, 16	<i>GNAQ</i>	exons 4, 5	
<i>RNF43</i>	exons 2-10	<i>GNA11</i>	exons 4, 5	
<i>SMAD4</i>	exons 2-12	<i>EIF1AX</i>	exons 1, 2, and chrX intronic region g.20148634–20148745	
<i>TERT</i>	promoter region, g.1295141-1295471	Chr5	<i>EGFR</i>	exons 18, 19, 20, 21
<i>TP53</i>	CDS		<i>DPYD</i>	exons 11, 13, 22, chr1 intronic regions: g.98187018- 98187098, g.98045419- 98045499, g.97915570-97915789
<i>TSHR</i>	CDS		<i>DICER1</i>	exons 10, 21, 26, 27, 29
<i>VHL</i>	CDS		<i>CTNNB1</i>	exons 3, 7, 8

5.2 Hematoxylin and eosin and Immunofluorescence staining

Freshly resected tumor chunks and fragments maintained in static or perfusion-based cultures were formalin fixed following standard protocols and then embedded in paraffin. Sections of 4 μ m were deparaffinized in xylene, rehydrated and used for hematoxylin and eosin (H&E) coloration and IF staining.

Heat-induced epitope retrieval was performed in the microwave at 800W for 10min using the Citrate Buffer, pH 6.0, 1X (#C9999, Sigma-Aldrich) as antigen retriever. Permeabilization step was done using a 0.25% solution of TritonX100 in PBS for 5min. Slides were blocked in a freshly made blocking solution (5%FBS, 1%BSA and 0.1% TritonX100 in PBS) at room temperature for 1h. Primary and secondary antibodies were diluted in an antibody dilution solution containing 1%BSA and 0.1% TritonX100 in PBS and slides were incubated at 4°C overnight with primary antibodies and at room temperature for 3h with secondary antibodies. After washes in PBS 0.1% Tween20, slides were mounted using the ProLong™ Gold Antifade Mountant (#P10144, Thermo Fisher Scientific), containing DAPI to counterstain nuclei.

A trained gynecological pathologist used H&E staining to analyze the quantity of epithelial and stromal components of cancer tissues. In IF studies, epithelial and stromal compartments were identified upon staining with anti-E-cadherin rabbit antibody (#3195S, Cell Signaling, 1:200), followed by Alexa Fluor 555-labeled goat anti-rabbit polyclonal antibody (#4413S, Cell Signaling, 1:500), and anti-vimentin mouse antibody (#MA5-11883, Invitrogen, 1:200), followed by Alexa Fluor 647-labeled goat anti-mouse polyclonal antibody (#4410S, Cell Signaling, 1:500), respectively. Immune cells were identified by staining with anti-CD45 rat antibody FITC-conjugated (#34399, Cell Signaling, 1:1000) and endothelial cells were labelled by using the anti-CD31 rabbit antibody (#PA5-32321, Thermo Fisher Scientific, 1:200), followed by Alexa Fluor 647-labeled goat anti-rabbit polyclonal antibody (#4414S, Cell Signaling, 1:500). Proliferating and apoptotic cells were identified by staining with anti-Ki67 mouse antibody (#9449, Cell Signaling, 1:800) and anti-cleaved Caspase 3 (cC3) rabbit antibody (#9661, Cell Signaling, 1:200), followed by Alexa Fluor 647-labeled goat anti-mouse polyclonal antibody and Alexa Fluor 555-labeled goat anti-rabbit polyclonal antibody, respectively. Images were taken by using the inverted wide-field microscope Nikon Ti2.

5.3 Statistical Analysis

Statistical was performed using GraphPad Prism version 8. Continuous variables were expressed as mean \pm standard error of the mean (SEM). To compare groups, Students t test was used. A p-value ≤ 0.05 was considered significant.

6. RESULTS

6.1 Electrical Characterization of the Multiwire Plasma Source and Chemical Features of PA-RL

Applying plasma on cancer cells revealed its ability to induce strong cytotoxic effects¹⁰¹. While direct plasma delivery can be used in the case of *in vitro* experiments, this approach is unfeasible in a clinical setting, especially in the case of multiple microscopic metastases like those present in the case of OC patients. Thus, recent studies focused on the indirect effects of plasma, obtained by irradiating liquids which can be further administered to patients¹³⁹. In this setting, RL solution has been proposed since it is a type of isotonic, crystalloid fluid widely used in medical contexts for fluid replacement. Moreover, since it is a standard solution, it represents a suitable medium for the study of mechanisms associated with the action of plasma⁹¹.

In this thesis, RL solution was exposed to plasma generated by a multiwire plasma source developed at the Alma Mater Studiorum – University of Bologna by the Research Group for Industrial Application of Plasmas and used for the first time to produce PA-RL. Before using generated PA-RL for any type of treatment, electrical chemical and physical characterization of the plasma discharge followed by the chemical characterization of the treated liquid in terms of RONS concentrations, pH and conductivity were required. This step is important as it not only assures the optimization of the parameters, but also allows the standardization of the procedure to produce all PA-RL solutions used in this study.

With regard to the results shown from the chapter 6.1 to 6.5, the experiments on cancer cells were performed in the Golgi BioPlasma Cell laboratory (DIN), while experiments on primary fibroblasts were carried out in Genetica Medica Laboratory (DIMEC); my contribution in these experiments dealt with cell culturing and biological analysis and were performed in collaboration with Dr. Cristiana Bucci, while PA-RL production was performed by Dr. Alina Bisag.

Thus, the plasma discharge characterization in terms of average power was performed evaluating the dynamic behavior of voltage and current waveforms during the treatment of RL solution (Figure 13a). Voltage data was recorded and used to calculate the average power as a function of the applied voltage, according to the previous established equation by B. Dong et al. In this case, an increase in

the applied voltage in a range from 15kV to 18kV corresponds to growing power values from a minimum of 5.2W to a maximum of 12.4W (Figure 13b).

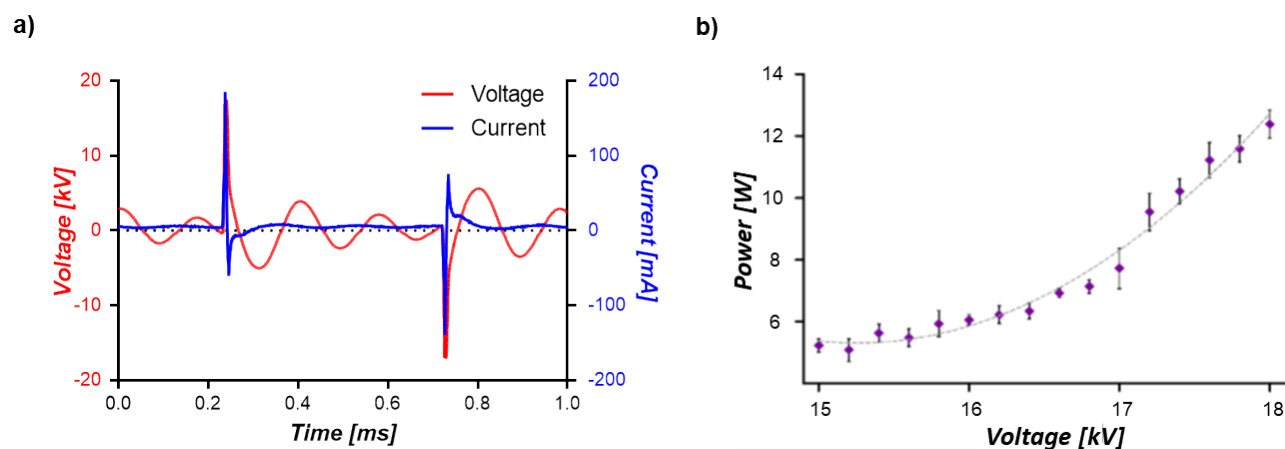


Figure 13. Electrical characterization of plasma source during treatment of Ringer's Lactate (RL) solution: (a) representative voltage (red) and current (blue) waveforms at 18 kV and 1 kHz and (b) power values as a function of the applied voltage. Data are presented as mean \pm SEM ($n = 3$).

As previously descanted on phenomena induced by plasma discharges-liquids interaction, RONS generation in the liquid was described to be the prevalent event, therefore they are regarded as key factors in PA-RL induced apoptosis^{99,117}. Given their enormous impact, it is fundamental to measure their concentrations in the liquid substrate following plasma treatment, by also evaluating the correlation with the treatment time and the applied voltage intensities. In this case, RONS concentrations in PA-RL were directly proportional to the plasma discharge time through the plasma source. H₂O₂ is another compound arising from the plasma discharges which is thought to be responsible for the majority of PALs-induced cell damage. NO₂⁻ potentiates the killing ability of H₂O₂ through the production of nitric oxide (NO•), which can inhibit tumor growth or even causes apoptosis^{146,147}. Measurements showed that both H₂O₂ and NO₂⁻ formation do not depend on the average power in the range of 7.85-12.54 W (Figure 14a), but on the length of plasma-PA-RL contact, peaking at 226 \pm 12.46 μ M and 659 \pm 15.19 μ M, respectively, after 10 minutes of treatment (Figure 14b). Thus, the ratio NO₂⁻/H₂O₂ in the RL resulted to be 2.91.

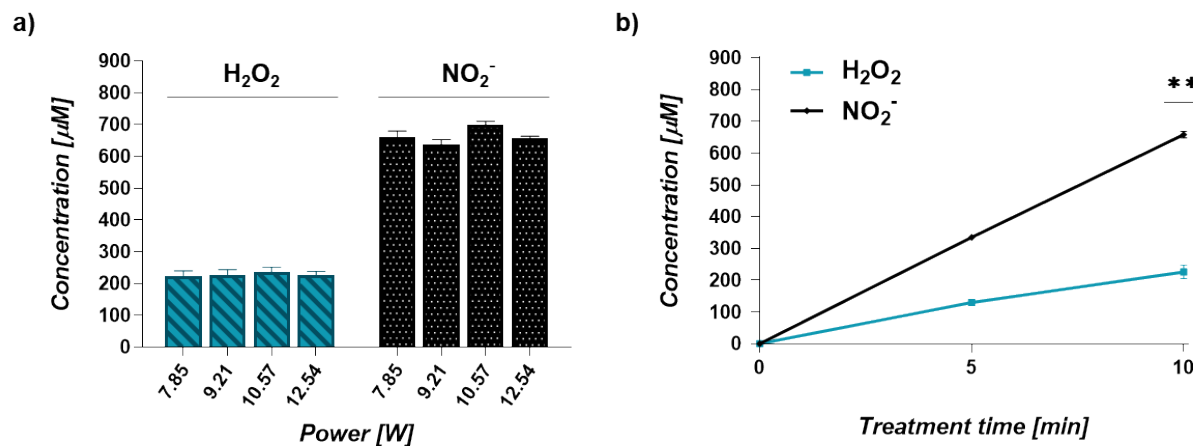


Figure 14. Plasma treatment of RL solution leads to the formation of H_2O_2 and NO_2^- (a) Reactive oxygen and nitrogen species (RONS) concentration as a function of the average power after 10 min of plasma treatment. Data are presented as mean \pm SEM ($n = 3$). (b) H_2O_2 and NO_2^- concentrations as a function of treatment time. Data are presented as mean \pm SEM ($n = 3$) and statistical significance is specified with asterisks (** $p \leq 0.001$ as determined by a paired Student's t-test, versus the 5 min treatment).

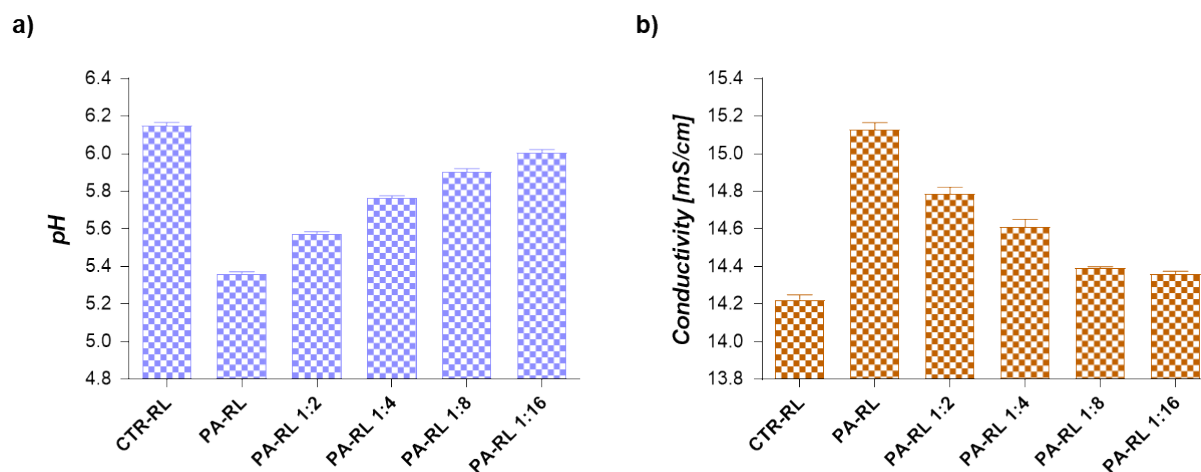


Figure 15. Chemical characterization of plasma-activated RL (PA-RL) and its dilutions after 10 min of plasma treatment at 18 kV. (a) pH and (b) conductivity as a function of serial dilutions. Data are presented as mean \pm SEM ($n = 3$).

With the final aim to assess the efficacy of PA-RL solutions with different concentration of RONS, serial dilutions of pure PA-RL (from 1:2 to 1:16) were obtained. For all of them, H_2O_2 and NO_2^- concentrations, pH and conductivity were measured after 10 minutes of plasma treatment at 18 kV. While the pH decreased to 5.36 (PA-RL) (Figure 15a), the conductivity increased to up 15.13 mS/cm (Figure 15b). These results led us to choose the PA-RL dilutions in the range between 1:4 and 1:16 for the subsequent cell treatments as they seemed to offer the best compromise between the concentration of the active components while being in proximity of the physiological pH.

6.2 Evaluation of plasma discharge behavior and emission by means of low-speed and high-speed filter imaging

To examine the global behavior of plasma filaments generated during the treatment with the plasma source, low-speed imaging was performed. Random streamers are formed between the high voltage wire-electrodes and hit the RL solution surface (Figure 16a). The emission of plasma was further investigated by visualizing it through a high-speed camera equipped with a 402 nm filter. This filter allowed to emphasize the emission of vibrationally excited nitrogen molecules, as precursors of RNS produced in the liquid phase. The filter imaging revealed pictures of the multiwire discharge applying different voltages: single filaments were randomly generated regardless the voltage applied (between 15 to 18 kV) (Figure 16b).

High-speed filter images confirmed the existence of vibrationally excited N_2 molecules, supporting the assumption that the reactions which result in RNS formation in the liquid phase are due to chemical species generated in the gas phase and diffusing into the liquid substrate.

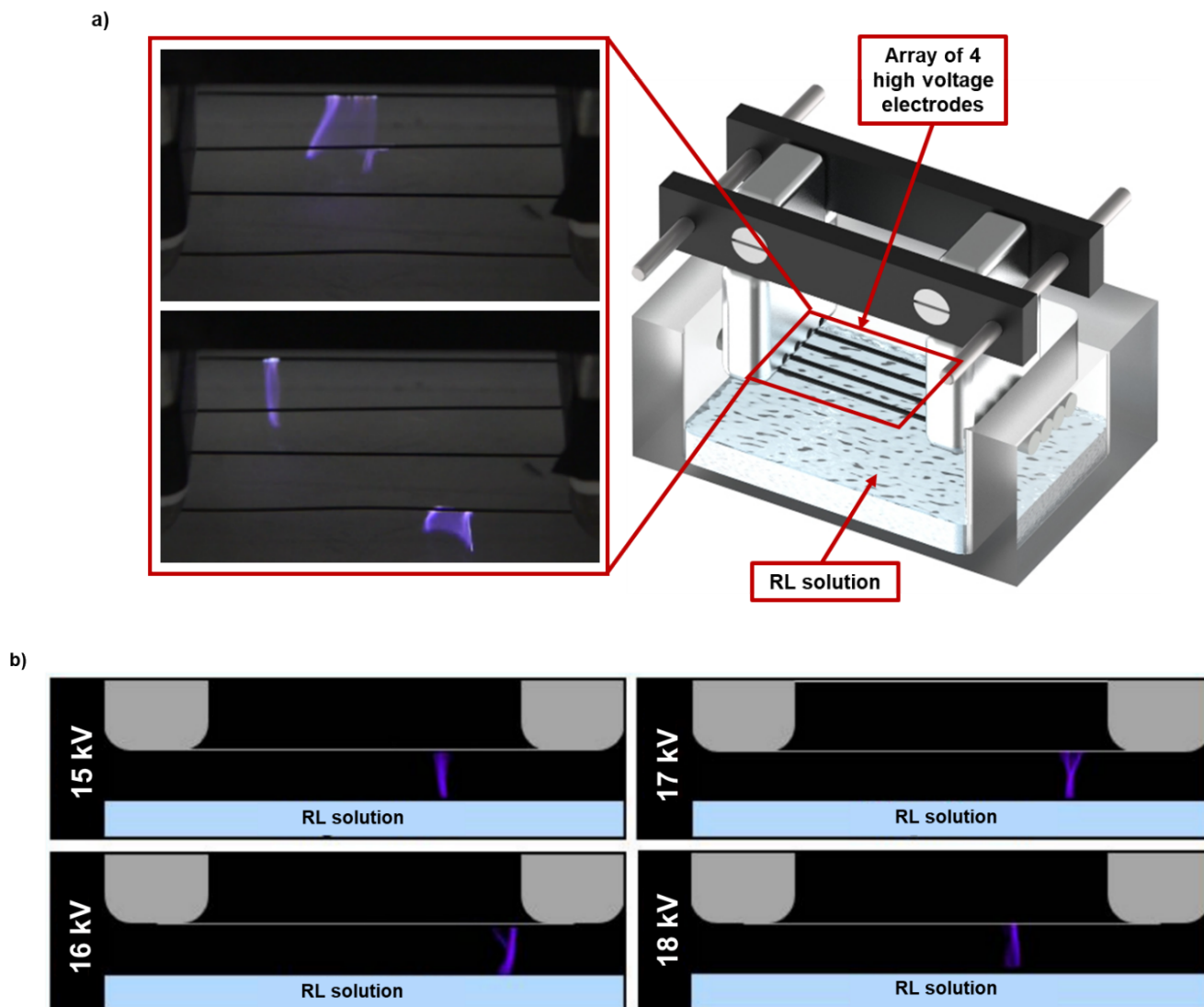


Figure 16. Low-speed images and high-speed (HS) filter images of the multiwire plasma discharge during RL solution treatment. (a) Picture of plasma generated during the treatment of PA-RL with an applied voltage of 18 kV and 30 fps. (b) HS filter images of plasma filaments for different values of applied voltage (between 15 to 18 kV) and 100 fps.

6.3 PA-RL displays a cytotoxic effect on EOC cell lines that does not depend exclusively on hydrogen peroxide or nitrites

Nowadays, PA-RL feasibility against EOC is still not well known, with only one evidence about its anti-tumor effect *in vitro* and no published data regarding consequences of its application *in vivo*¹¹⁷.

Furthermore, the capability of an anti-neoplastic drug to target selectively cancer cells is a cogent issue to preserve the healthy tissue counterpart. The assessment of PA-RL treatment effects on immortalized cancer and non-cancer cell lines is a mandatory step in view of making use of more complex organotypic EOC models.

SKOV-3 and OV-90 are two immortalized EOC cell lines, both derived from human ascites, as metastatic site of a serous cystadenocarcinoma and of a HGS adenocarcinoma, FIGO stage IIIC, respectively. As confirmed by the genetic validation, both cell lines retain a driver mutation in the *TP53* gene, of which a somatic frameshift mutation (c.267del), predicted as likely pathogenic in SKOV-3 and a somatic missense mutation (c.643 A>C) predicted as pathogenic in the case of OV-90 cell line (Figure 17). Thus, in view of their profiles faithfully mirroring the EOC histotype we are interested in, SKOV-3 and OV-90 were selected to be used for all the experiments performed to test PA-RL treatment.

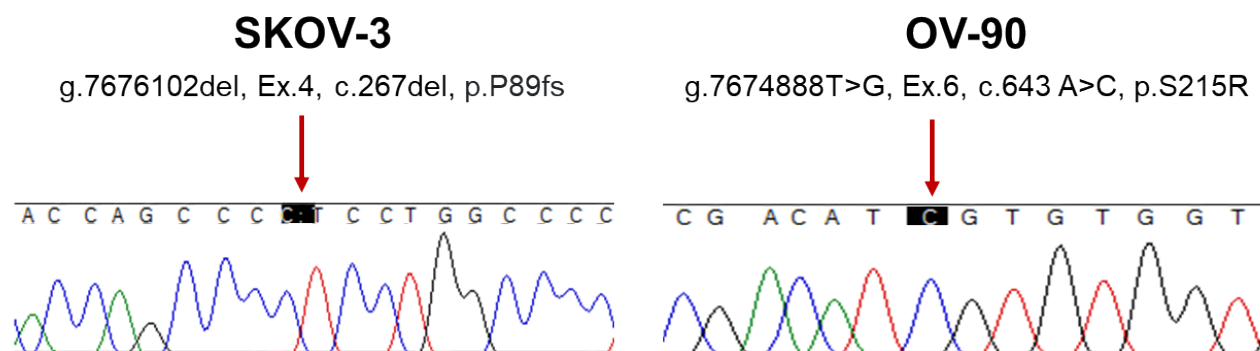


Figure 17. Sanger sequencing electropherograms of the typical SKOV-3 and OV-90 *TP53* mutations. Red arrows indicate the missense nucleotides in the FASTA sequence.

For the purpose of evaluating if PA-RL could have a cytotoxic effect on cancer cells and if this effect was dependent on its dilution, thus, indirectly to the amount of RONS to which cells were exposed, three different PA-RL dilutions (1:4, 1:8, 1:16) were tested on SKOV-3 and OV-90. Both cell lines showed a significant reduction in viability after two hours of PA-RL exposure. When the 1:4 dilution was administered, only OV-90 cell line appeared to respond to PA-RL immediately after treatment, even at larger dilutions. EOC cells were found to be similarly affected in terms of viability after 72 hours of exposure to the three PA-RL dilutions, displaying a dose-dependent response that

was more evident in the OV-90 cell line and showing a consistent decrease in viability, ranging between 80 and 95% in both cell lines. Generally, SKOV-3 cells appeared to be less sensitive to PA-RL only at first, as there was a delayed decrease in their viability than that of OV-90 cell line. The time-dependent effect of PA-RL is ascertained by cell lines viability at 24 and 48 hours (Figure 18).

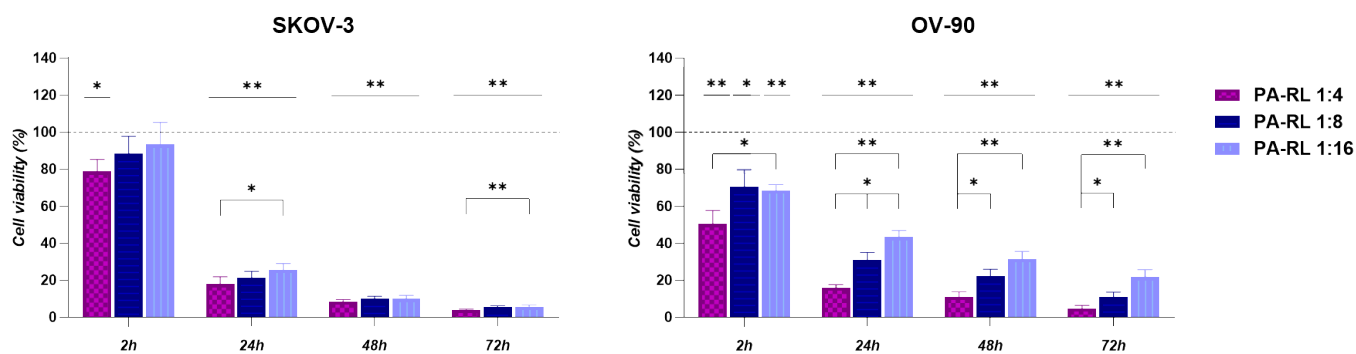


Figure 18. PA-RL displays a selective cytotoxic effect on EOC cell lines. Viability of SKOV-3 ($n = 7$) and OV-90 ($n = 9$) cell lines treated with PA-RL dilutions (1:4, 1:8 and 1:16) at 2, 24, 48 and 72 hours after treatment. Data are presented as mean \pm SEM normalized on the corresponding control in RL solution (CTR-RL). Dotted line represents the normalized CTR-RL. * p -value <0.05 ; ** p -value <0.01 ; *** p -value <0.001

The impact of our PA-RL in 2D was compared to that triggered by solutions containing H_2O_2 and/or NO_2^- in order to define their effective role in EOC cells' death. The goal of this analysis was, first of all, to verify if PA-RL efficacy on EOC cells could be due to its complexity in terms of components and, thus, if it could be replaced by a simpler solution containing, for instance, H_2O_2 , which is more widely available in the hospital or in the laboratories. We hence prepared RL solutions containing H_2O_2 and NO_2^- at the same concentrations as measured in PA-RL 1:16 dilution, since it was proven to be cytotoxic for cancer cells (SKOV-3 and OV-90 viability decrease from 93 to 5% and from 69 and 22%, respectively, from the end of the treatment up to 72 hours after the exposure). In addition, considering the effect of PA-RL on pH, we further wanted to exclude that the observed toxicity could be ascribable to a pH shift. Therefore OV-90 and SKOV-3 were exposed to RL solutions supplemented with H_2O_2 and NO_2^- with a pH of 5.91 and therefore the same pH as the 1:16 dilution; cells were treated for 2 hours before being cultured for the subsequent 72 hours in a treatment-free medium.

In these conditions, OV-90 cells were found to suffer a more immediate loss of viability of about 20%–30% after 2 hours exposure, which was consistent across all treatments, whereas SKOV-3 cells appeared to suffer a slight to no loss of viability over the same time-course. After 72 hours, nitrites had no effect on cell survival for both cancer cell lines, whereas pH and H₂O₂ suppressed proliferation in a negligible way with respect to both nitrites and control (Figure 19). Overall, PA-RL was found to be the only solution able to significantly reduce viability of both EOC cancer cell lines which suggest that the reduced viability is not due only to a putative synergistic effect of H₂O₂ and NO₂⁻ but mainly to the several RONS therein contained, that may work together to cause cytotoxicity. These findings make PA-RL complexity not replaceable by the synthetic solutions here utilized.

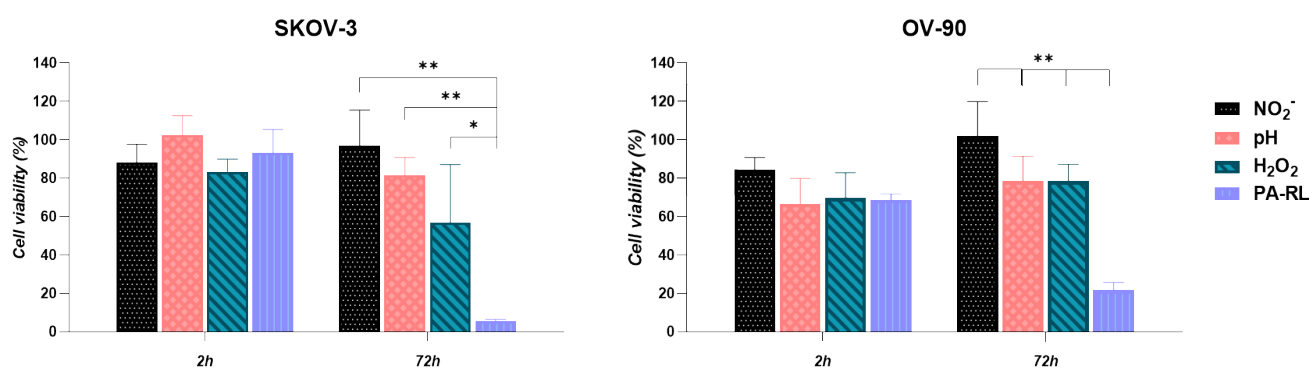


Figure 19. PA-RL displays a selective cytotoxic effect on EOC cell lines. Viability of SKOV-3 and OV-90 cell lines treated with PA-RL 1:16 and synthetic solutions at dilution 1:16. H₂O₂-supplemented RL solution, NO₂⁻-supplemented RL and pH-adjusted RL solutions were diluted in RL to obtain the final treatment solutions. Data are presented as mean ± SEM (n = 3) normalized on the corresponding CTR-RL. *p-value < 0.05; **p-value < 0.01; ***p-value < 0.001

6.4 PA-RL is selective for EOC cells

One of the primary requirements for PA-RL to be used in clinics is that its cytotoxic activity ought to be specific for cancer cells while preserving non-cancer cells, particularly those of the connective tissues, to allow for the healing of wounds within the abdominopelvic cavity. We hence wondered if PA-RL produced for these experiments may display such a selective effect. To answer our question, we performed viability tests after treatment using ovarian cancer cell lines as well as non-cancer epithelial and mesenchymal cell models. The non-cancer epithelial cell lines of ovarian origin named

HOSE were used as well as two different human immortalized fibroblast lines in order to examine the tissue mesenchymal component's response to PA-RL. Three different PA-RL dilutions were tested at the same time points as for the EOC cell lines.

The effect of PA-RL on cancer versus non-cancer cells, in terms of viability, were significantly different (Figure 20). Interestingly, both fibroblasts and HOSE cells showed a similar rate of decrease in viability, which was evident in a dose-independent manner, at the end of treatment (i.e., not observed at the 2h exposure). In detail, at 72 hours non-cancer cells viability reduced in a range between 60% and 70%, with the highest survival at the 1:16 dilution (Figure 20a). As a result, the 1:16 PA-RL dilution was chosen as the best compromise for achieving a high level of mortality in cancer cells while sparing non-cancer epithelial cells and fibroblasts. Indeed, the effect of PA-RL on SKOV-3 and OV-90 versus Fibroblasts and HOSE, in terms of viability, were significantly different, starting from 24 hours up to 72 hours after treatment (Figure 20b).

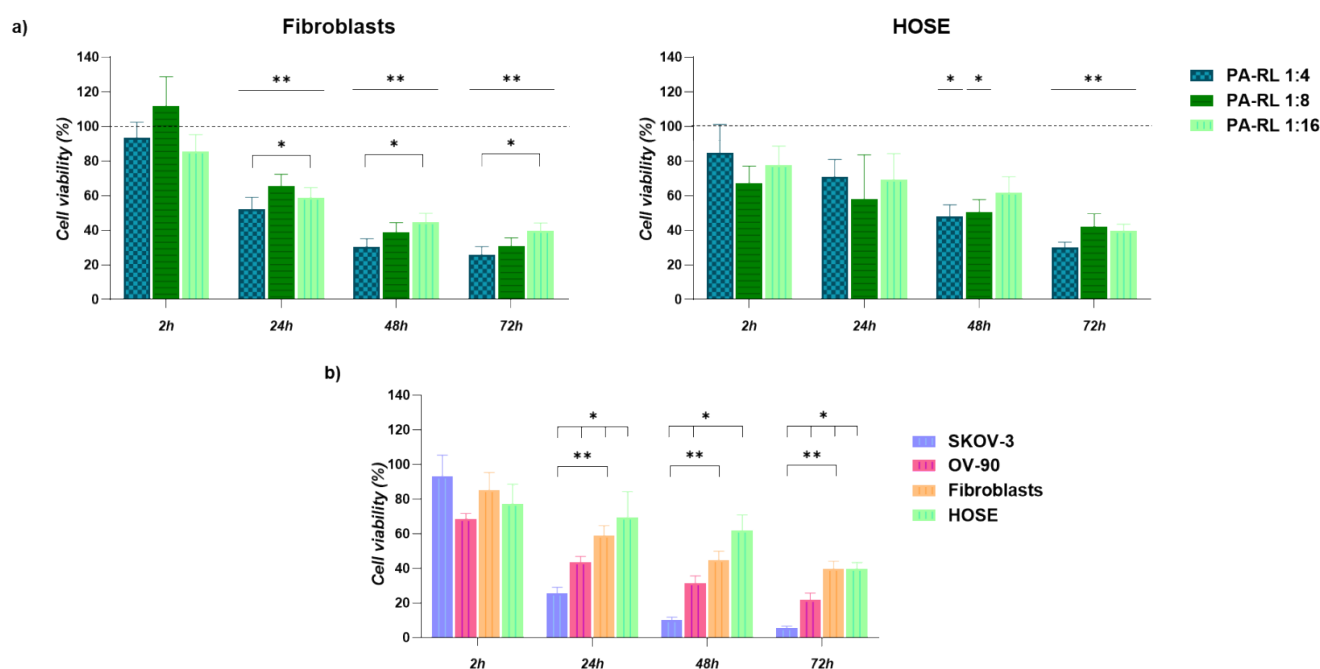


Figure 20. PA-RL displays a selective cytotoxic effect on EOC cell lines. (a) Viability of non-cancer cells, namely human fibroblasts ($n = 9$) and HOSE ($n = 4$) treated with different PA-RL dilutions (1:4, 1:8 and 1:16) at 2, 24, 48 and 72 hours after treatment. Data are presented as mean \pm SEM normalized on the corresponding CTR-RL. Dotted line represents the normalized CTR-RL (b) PA-RL 1:16 efficacy on cell viability in non-cancer and EOC cell lines at 2, 24, 48 and 72 hours after treatment. Cell viability was normalized to the CTR-RL at 2 hours and plotted as percentage relative to corresponding CTR-RL, for all time points. In each panel, data are mean \pm SEM and statistical significance is specified with asterisks (* $p \leq 0.05$, ** $p \leq 0.01$, *** $p \leq 0.001$ as determined by a paired Student's t -test). * p -value <0.05 ; ** p -value <0.01 ; *** p -value <0.001

6.5 Differentially activated antioxidant defense mechanisms may underlie diverse sensitivity to PA-RL

It is well known that cancer cells have the potential to endure a high degree of oxidative stress during their rapid proliferation, where their high ROS content is kept under control by an upregulated antioxidant system. Indeed, radical overloading in neoplastic cells might result in their oxidation-mediated collapse, thus altering the effects of ROS levels on the modulation of metabolic reactions, of signal transduction and stress response¹⁴⁸.

To evaluate whether EOC cells had higher basal antioxidant capacity with respect to non-cancer cells, we measured the expression levels of one of the most active cytosolic antioxidant enzymes involved in radical species detoxification, namely superoxide dismutase-1 (SOD-1). As envisaged, SOD-1 levels in EOC cells were significantly higher with respect to human fibroblasts (Figure 21). Regarding SKOV-3 cell line, the lower levels of ROS detected suggest that these cells might upregulate SOD-1 in order to protect them from radical overloading (Figure 22).

Because of the different basal ROS levels in cancer and non-cancer cells, we envisioned that cancer cells are unable to trigger redox adaptation under oxidative stress increase, such as the one caused after their contact with PA-RL. ROS levels were analyzed in cell lines treated with PA-RL 1:16 or RL solution alone, after 1 hour from the end of the treatment. We observed that while ROS levels remained constant in the case of fibroblasts, SKOV-3 cells were not capable of maintaining their basal redox homeostasis after the treatment (Figure 22). This is probably due to the fact that upon treating with PA-RL 1:16, fibroblasts are able to upregulate SOD-1 expression thus achieving an immediate compensation of the PA-RL induced oxidative stress, while in SKOV-3 cells this mechanism does not seem to occur (Figure 21). Moreover, ROS increasing in SKOV-3 was also correlated to a higher apoptotic death with respect to fibroblasts, 48 hours after treatment end (Figure 23).

Taken together, this information supported the fact that SKOV-3 are particularly sensitive to the oxidative stress.

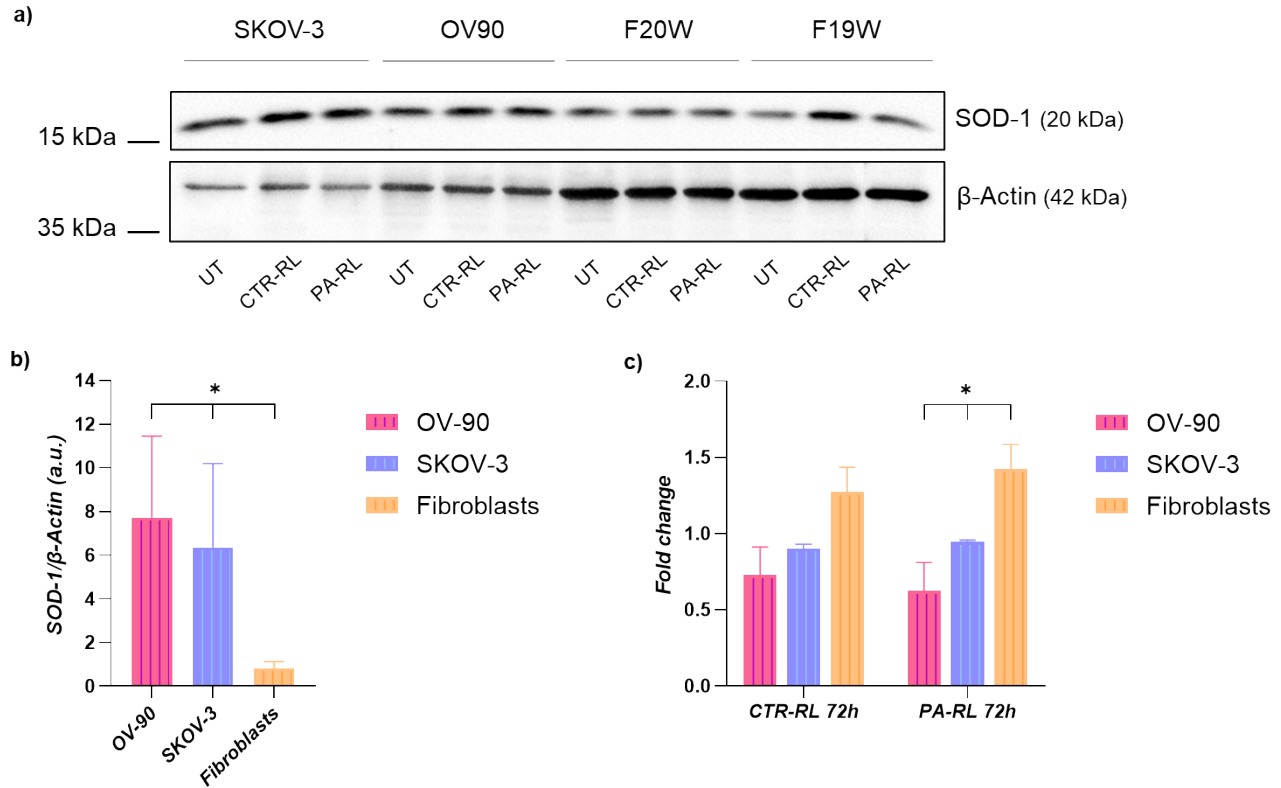


Figure 21. PA-RL solution induces an increase in Superoxide Dismutase-1 (SOD-1) expression in fibroblasts but not in EOC cell lines. (a) Western blot analysis of EOC cell lines and fibroblasts (F19W and F20W) at 72 h after treatment with PA-RL 1:16 (UT, untreated cells). A representative experiment of three is shown. (b) SOD-1 levels in untreated fibroblasts and cancer cell lines. Histograms show densitometric values of the SOD-1 protein normalized to the β -actin used as a loading control. All data are presented as mean \pm SEM of three independent experiments. (c) Relative densities of SOD-1 and β -actin were measured using densitometric analysis. SOD-1 levels of CTR-RT and PA-RL 1:16 after 72 h of treatment were normalized to β -actin and plotted as fold change relative to the untreated (UT) sample. All data are presented as mean \pm SEM of three independent experiments. Statistical significance is specified with asterisks * $p \leq 0.05$.

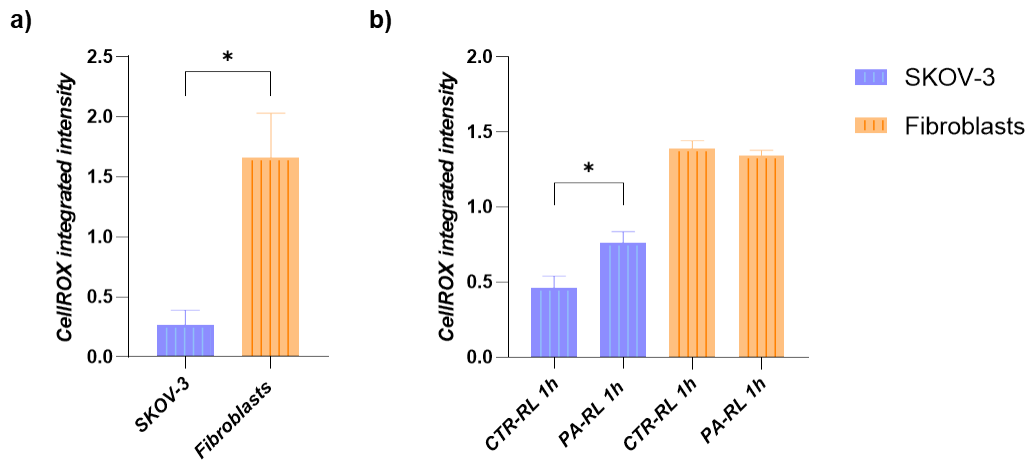


Figure 22. ROS levels in primary fibroblasts and SKOV-3 cell line. Measurement was done using the CellROX red fluorescent probe after a 1h incubation untreated (a) and following PA-RL 1:16 treatment (b). * p -value <0.05

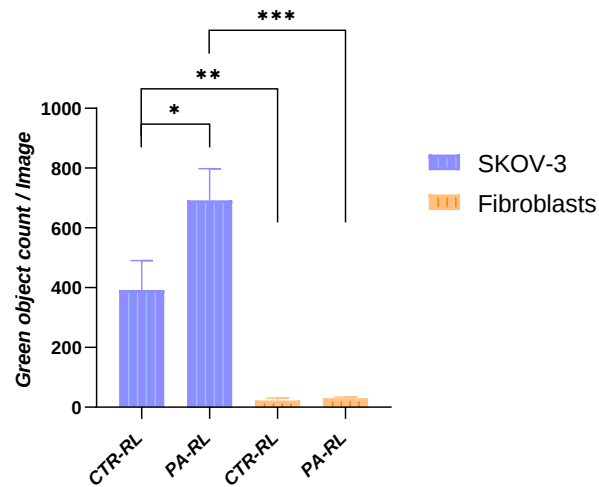


Figure 23. Apoptosis levels in SKOV-3 and primary fibroblasts. Measurements were done with the Incucyte® Caspase-3/7 Dye for Apoptosis. * p -value <0.05 ; ** p -value <0.01 ; *** p -value <0.001

6.6 Creation of an ovarian cancer samples collection

From 2018 to present I was involved first-hand in collecting 172 ovarian cancer tissues. Our collection was initially established in 2012 at the Operating Unit of Medical Genetics, S. Orsola-Malpighi Hospital of Bologna contextually to the study MiPEO (Mitochondria involvement in the endometrial and ovarian tumors' progression mechanisms) approved by the Independent Ethics Committee of the S. Orsola-Malpighi Hospital (107/2011/U/Tess). Inclusion and exclusion criteria defined at the beginning allowed to obtain a disease-oriented collection, aimed at exploring samples biology. Biological samples from EOC patients have been harvested regularly from surgical rooms of our hospital, anonymously labelled and directly processed or stored in a long-term prospect for multiple purposes. Through a coordinated group work, we were able to obtain a proper collection where biological samples have been taken care of in terms of sterile handling, adequate transportation and storage, precise and reproducible aliquoting and freezing, in addition to a proper identification system and registration of clinical data. Generally, our collection has been the source of biological samples utilized in several publications, all aiming to deepen our knowledge about EOC pathobiology. Furthermore, over the past few years, this collection gave life to a series of research projects, ethical committees, national and international collaborations involving multidisciplinary experience of gynecological surgeons, geneticists, biologists and engineers.

Regarding this PhD project, several HGSOC tissues and body fluids included in our collection were processed in order to establish suitable patient's derived models essential to assess PA-RL selectively in a more complex biological system.

6.7 Primary EOC cells from ascites grown in 3D maintain the *TP53* driver mutation, unlike ascites in 2D cultures

Regarding our purpose to scale-up the project and in order to assess PA-RL effects in a biological background closer to the clinical reality, we set out to fine-tune EOC primary models.

The choice was to start from the ascites, contextually to the collaboration with the Operating Unit of Gynecologic Oncology and thanks to the biological samples gradually collected. Given the large heterogeneity of resident ascites cells, also due to the individual patients' specificities, a standardized method to establish primary cell cultures from this source has not been defined to date.

The first attempt to establish primary cell cultures from the freshly-obtained ascitic fluid was in 2D. Primary cultures were obtained from 6 patients, all chemo-therapy naïve diagnosed with HGSOE, who underwent tumor resection and drainage of ascites. For each analyzed ascites, after it was cleaned from erythrocytes, the obtained cells were seeded in three different culture media in order to assess which growth medium was optimal for the isolation and propagation of cancer cells. The chosen media were DMEM HG, MCDB/M199 (50:50) and RPMI-1640 medium, of which the first two were supplemented with 10% of heat-inactivated fetal bovine serum (FBS) and suggested in literature, whereas the latter contained 20% of FBS.

With all media we managed to obtain a good growth rate, with a confluence between 90% and 100% after 5-6 days after culture (Figure 24).

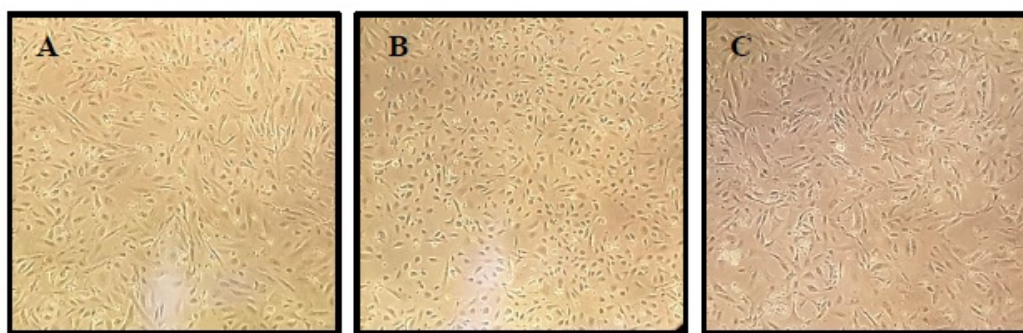


Figure 24. Cellular morphology of primary EOC cells obtained from ascites, in 2D (10X). (A) DMEM HG supplemented with 10% FBS, 2 mM L-glutamine (1% L-glu), 100 U/mL penicillin and 100 µg/mL streptomycin (1% P/S); (B) MCDB/M199 (50:50) medium, supplemented with 10% FBS and 1% P/S (C) RPMI-1640 medium supplemented with 20% FBS, 1% L-glu, 1% P/S.

Primary cultures showed epithelial cell characteristics, such as the typical epithelial cobblestone morphology, up to the passage 1. However, starting from the passage-2, cells shifted towards a fibroblast-like morphology and acquired a slower growth rate (Figure 25).

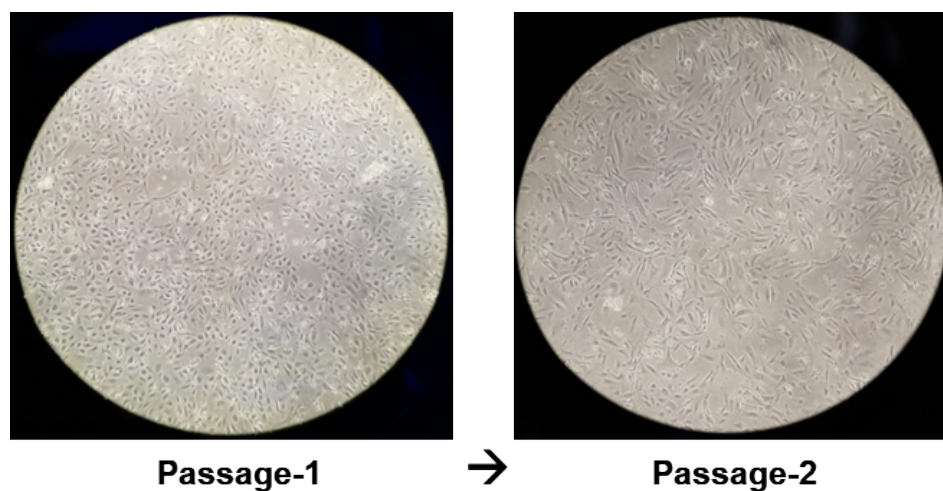


Figure 25. Microscopy pictures of 2D primary cultures arising from harvesting the patients ascitic fluid at the first two passages (20X).

Table 3. TP53 mutations identified in six chemo-therapy naïve HGSOc tumors

Patient no.	Gene exon	Somatic TP53 mutation	Base change	Aminoacidic change	Mutation type	Prediction (Seshat/ClinVar)	Cancer Hotspot
1	7	c.731G>A (p.G244D)	GGC→GAC	Gly→Asp	Missense	Damaging	yes
2	7	c.524G>A (p.R175H)	CGC→CAC	Arg→His	Missense	Partial damaging	yes
3	6	c.574C>T (p.Q192*)	CAG→TAG	Gln→Stop	Nonsense	Damaging	yes
4	Intronic mutation	c.782+1G>T	--	--	Splice_Site	Partial damaging in Li-Fraumeni syndrome	no
5	Intronic mutation	c.672+1G>T	--	--	Splice_Site	Damaging in Hereditary cancer-predisposing syndrome	no
6	6	c.586C>T (p.R196*)	CGA→TGA	Arg→Stop	Nonsense	Damaging	yes

Thus, with the aim to characterize all cultures obtained, assessing their epithelial phenotype and tumoral profile, TP53 mutational state, a gene reported as frequently mutated in HGSOc (96%), was analyzed. Firstly, five original tumor samples from which cultures were successfully established were analyzed by comparison with their respective healthy tissues, in order to identify somatic TP53 driver mutations in the original tumor samples (Table 3). Almost all somatic mutations found were predicted to be damaging or likely damaging and two of them (c.782+1G>T and c.672+1G>T) were reported in

literature to be associated with the Li-Fraumeni syndrome, an inherited disorder that is associated with an elevated risk of certain cancers¹⁴⁹.

The *TP53* gene is usually mutated in a two-hit mechanism, with a missense mutation in one allele followed by loss of the remaining WT *TP53* allele causing a condition of loss of heterozygosity (LOH). The frequency of *TP53* LOH increases significantly as cancer progresses, implying a strong selective pressure for *TP53* LOH incidence as tumors develop¹⁵⁰.

By the study of a polymorphism shared by all the analyzed samples (c.215C>G, Ex.4a) it was possible to ascertain the loss of one WT *TP53* allele in the primary tumor as compared with the healthy tissue (Figure 26a). Thus, the somatic missense mutation c.731G>A found only in the primary tumor suggested a case of LOH, determining the condition of hemizygoty of the *TP53* mutation. On the contrary, the loss of one WT *TP53* allele did not occur in both ascites samples, suggesting the lack of cancer cells during the passage-1 (Figure 26b).

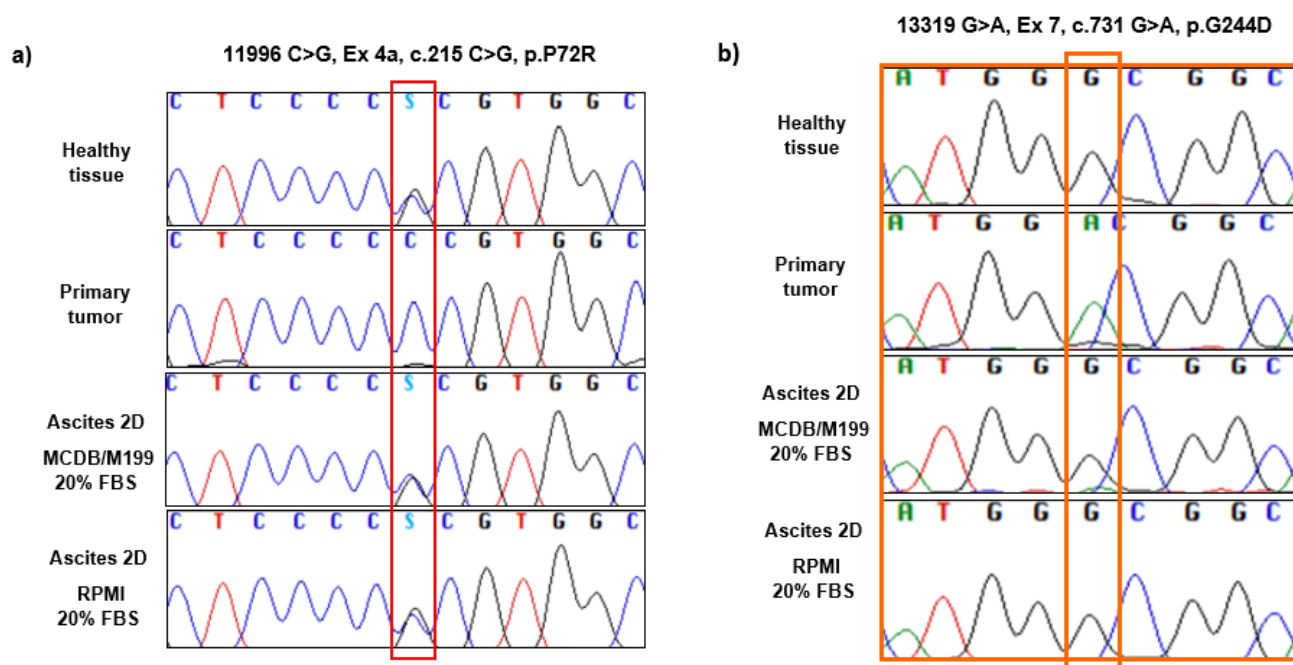


Figure 26. Electropherograms showing the *TP53* polymorphism (a) mutation (b) found in a chemo-therapy naïve HGSOC tumor. The mutation was lost when attempting to culture the ascitic fluid in 2D.

The same result was also seen in other patients. In detail, in the case of Patients no. 2, 5 and 6, the primary tumors were characterized by the presence of mutations in *TP53*. Patient 2 harbored a heterozygous missense mutation c.524G>A (Figure 27a) while Patient 6 harbored a nonsense mutation

c.586C>T (Figure 27c). Patient 5 on the other hand had a mutation in a hemizygous state c.672+1G>T (Figure 27b). Following the same pattern, the ascites from these patients also lost the *TP53* mutations when cultured in 2D after just a couple of passages and regardless the culture media utilized.

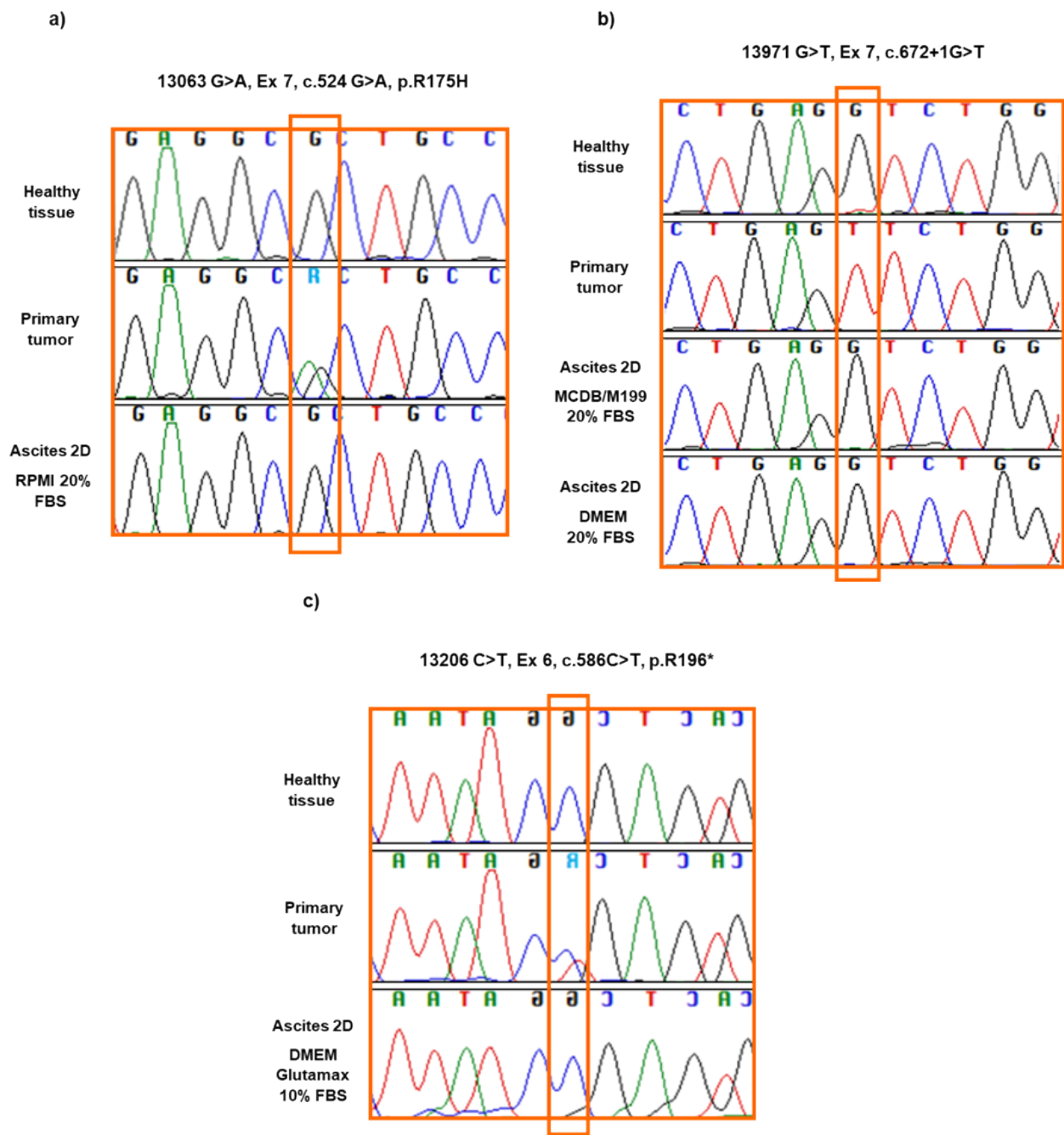


Figure 27. Electropherograms showing the *TP53* mutations found in three chemo-therapy naïve HGSOc tumors. All mutations were lost when attempting to culture the ascitic fluid in 2D.

Suspended ovarian cancer cells floating in ascites tend to aggregate and compact to form dense spheroids. These structures are proposed to undergo EMT and to contain a large population of quiescent cells, so promoting the metastatic process and contributing to chemoresistance^{151,152}.

We hence tried to set up protocols to isolate tumor spheroids from ascites and guarantee their integrity and propagation, in order to obtain a suitable EOC preclinical model.

In fresh ascites seeded in suspension, we observed a wide range of cell clusters, ranging between 20 and 100 cells/spheroid. These spheroids presented a slow rate of proliferation, with a duplication rate of around 20 days from the first seeding (Figure 28).

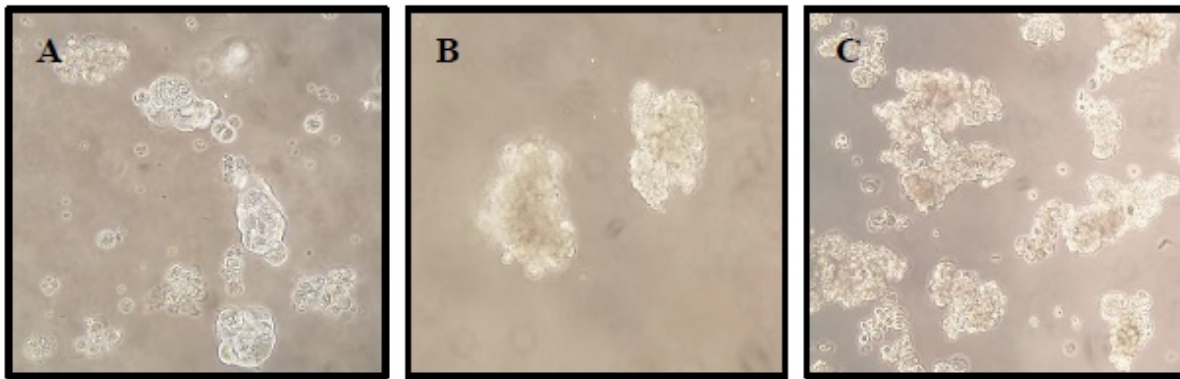


Figure 28. Cellular morphology of spheroids obtained from ascites grown in non-adherent conditions (10x). A. DMEM HG supplemented with 10% FBS, 4mM L-glutamine, 1% P/S, w/o sodium pyruvate. B. MCDB/M199 (50:50) 10% FBS, 1% P/S. C. RPMI1640 20% FBS, 1% L-glutamine, 1% P/S.

Sanger sequencing of the *TP53* gene performed for ascitic spheroids obtained from one HGSOc patient confirmed the maintenance of the mutation detected in the primary tumor at passage-1. Regarding the 2D cell cultures, we searched for the *TP53* mutation after two days of culturing time, before moving to passage 1, and we found that it was already reduced at 40-50% (Figure 29).

In the case of 3D samples, the type of medium was shown not to influence the retention of the mutations, suggesting that spheroids were enriched for cancer cells.

13971 G>T, intronic, c.782+1G>T

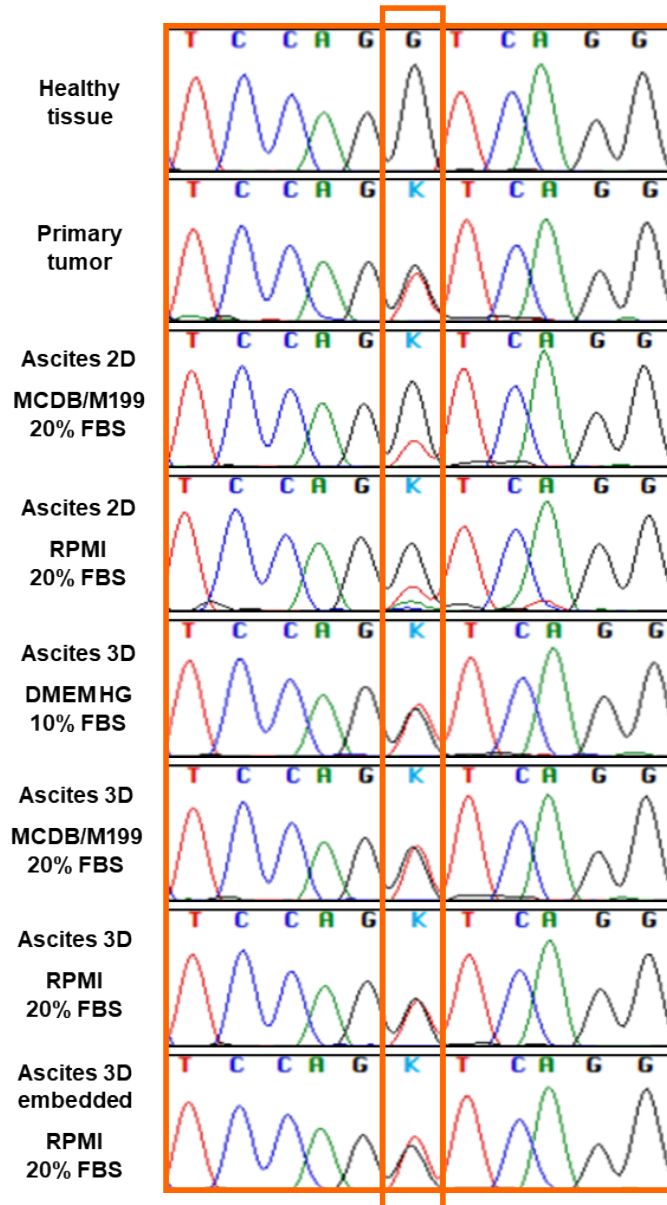


Figure 29. Electropherograms showing the TP53 mutations found in one chemo-therapy naïve HGSOc tumor. All mutations were lost when attempting to culture the ascitic fluid in 2D.

With the aim to improve ascites spheroids derivation rate, possibly speeding-up their growth rate, we tested a particular medium supplemented with compounds shown to support EOC cell growth, already used to derive other types of tumor organoids: N-Acetylcysteine, Nicotinamide, FGF, EGF, Hydrocortisone, B27¹⁵³. In general, it was possible to appreciate the growth of complex structures, floating in the medium alone or aggregated, whose cystic structure may be indicative for spheroid formation (Figure 30).

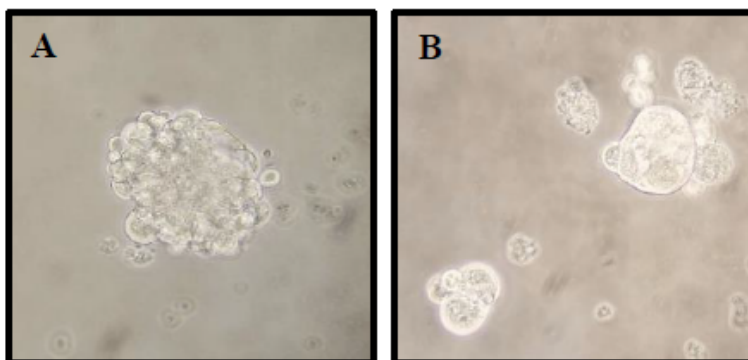


Figure 30. Cellular morphology of primary spheroids obtained from ascites grown in non-adherent conditions (A. 20x, B. 10x). A. DMEM/F12 supplemented with 1% L-glutamine, 1% P/S, 500mM N-Acetylcysteine, 1M Nicotinamide, 100ug/mL FGF, 500ug/mL EGF, 250ug/mL Hydrocortisone, B27 (1x). B. Same medium as in A. but w/o B27 supplement.

This approach allowed to increase possibilities to obtain alive 3D spheroids from fresh ascites put in culture in commonly used plastic flasks. Unfortunately, we were not able to maintain the cultures for more than 2-3 passages and to obtain a real advantage in terms of duplication rate, in times compatible with our experimental needs.

Other approaches tested for spheroids isolation, starting from fresh ascites, demanded the use of plastic supports such as 96-wells flat plates and ultra-low attachment plates previously coated or embedded with Matrigel Matrix alone or in combination with collagen (Figure 31).

Spheroids generated starting from one single ascitic fluid were harvested after 10 days of culture. Similarly, to the aggregates grown in suspension, these spheroids showed to maintain the *TP53* mutation detected in the corresponding primary tumor, as shown in Figure 31 (Ascites 3D embedded

– RPMI 20% FBS). Unfortunately, the 3D structures in question died and disintegrated before they could be propagated.

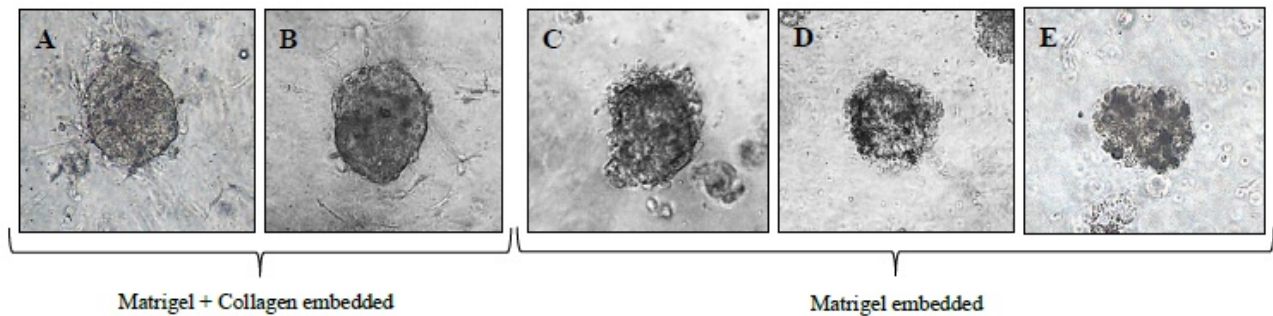


Figure 31. 3D structures obtained from ascites embedded in Matrigel Matrix + Collagen or Matrigel Matrix alone. (A,C) Seeding in 96-wells flat bottom plate. Medium used: complete Ovarian Epithelial Cell Medium (OEpiCM) 20% FBS, 1% L-glutamine (B, D). Seeding in 96-wells flat bottom plate. Medium used: RPMI-1640 20% FBS, 1% L-glutamine, 1%P/S. E. Seeding in 96-wells ultra-low attachment plate in RPMI-1640 20% FBS, 1% L-glutamine, 1%P/S.

6.8 Set up of a reproducible perfused-EOC *ex vivo* model

Previous studies have shown the efficiency of perfusion-based cultures to establish cancer *ex-vivo* 3D models appearing as uniform tissue-like structures able to preserve their viability, proliferation rate as well as both tumor cells and autologous TME, in the context of a dynamic and controlled microenvironment^{73,154}.

In order to overcome the limitations to obtain stable primary cultures starting from ascites, the perfusion-based bioreactor U-CUP (currently distributed by CELLEC Biotek AG) was employed to generate a reproducible EOC 3D *ex vivo* model culturing excised primary ovarian tumors and matched, or not-matched peritoneal metastases, obtained from patients with a diagnosis of HGSOE. The model set up in terms of early settings for culture was performed at the Department of Biomedicine - University Hospital Basel (Switzerland), contextually to a collaboration with the Ovarian Cancer Research and Tissue Engineering laboratories.

The study workflow consisted of a first set of experiments based on processing both fresh primary (n=1) and omental tumors (n=2), not-matched, with the aim to identify the best culture media to

preserve the tissue in U-CUP up to seven days of culture (Figure 32, point 1), based on a time point previously used to generate a primary perfused culture of breast cancer¹³⁵.

Four random tumor pieces, just cut from a biopsy harvested from the surgical room, were placed between two perfusable collagen sponge discs in a “sandwich-like” configuration and thus processed using four different culture media normally usable in the laboratory: DMEM/F12, a widely used basal medium for sustaining a controlled growth of a wide range of mammalian cells; RPMI-1640 medium and M199 that are denser of vitamins suitable to promote mesothelial cells growth; Keratinocyte medium recommended to preserve stroma cells and probably potentiating cancer cells growth in the tissue.

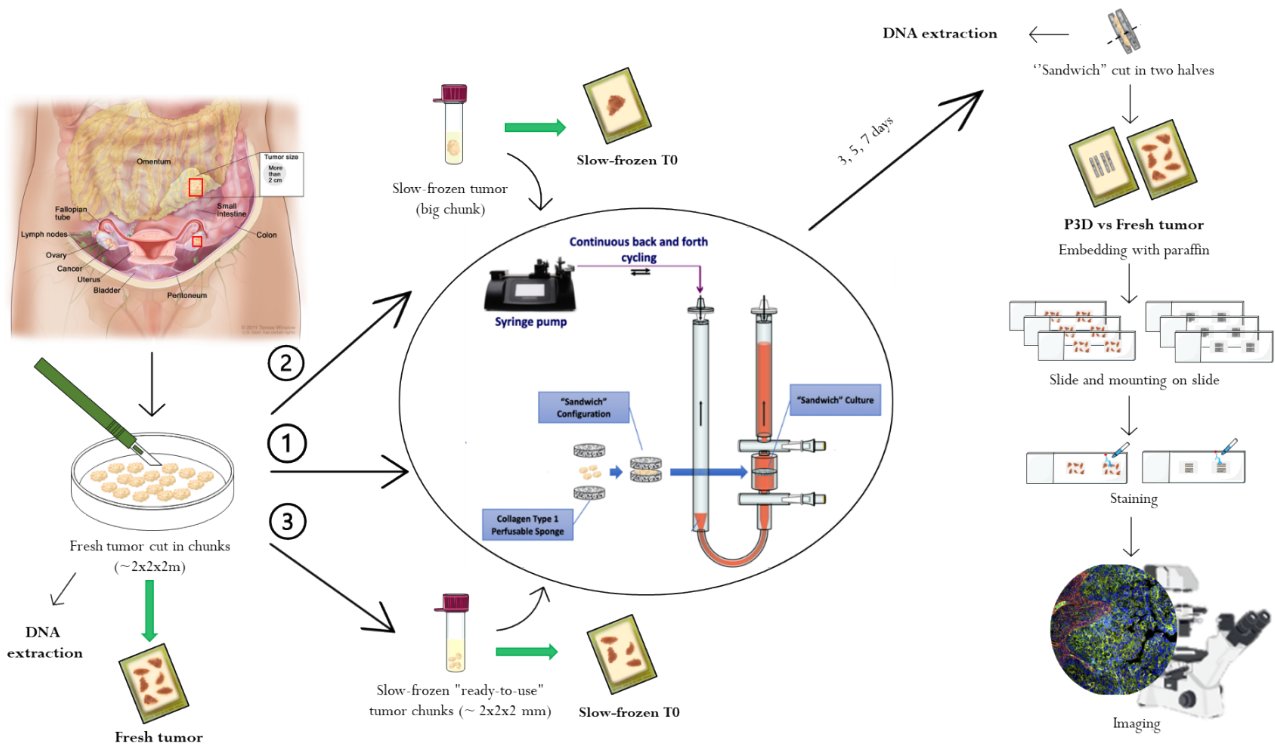


Figure 32. Schematic representation of the experimental workflow. 1) Fresh 2) Slow-frozen as big chunks and 3) Slow-frozen as “ready-to-use” small chunks, all HGSOCS, primary or metastatic, are used to be embedded in paraffin, processed for DNA extraction and processed for the perfusion-based culture in U-CUP. After 3,5, or 7 days of culture the “sandwich” containing the tumor is cut into two halves to be processed for DNA extraction and embedded in paraffin. 4µm sections are cut and stained for H&E and IF. Slow-frozen T0 (immediately after thawing); P3D (perfused-3D).

After seven days of culture, all fresh tumors were entire, viable and ascribable to the original specimens, as confirmed by the inspection of an experienced pathologist. Tumors cultured in

DMEM/F12 and RPMI-1640 showed higher percentages of cancer cells characterized by the typical HGSOc papillary and glandular architecture, instead of tumors cultured in M199 and Keratinocyte media. In general, tumor compartment was preserved especially on the edges of the perfused-3D tumors (P3Ds) generated after seven days (P3D7ds), under these culture conditions (Figure 33). The percentage of success rate was around 66%.

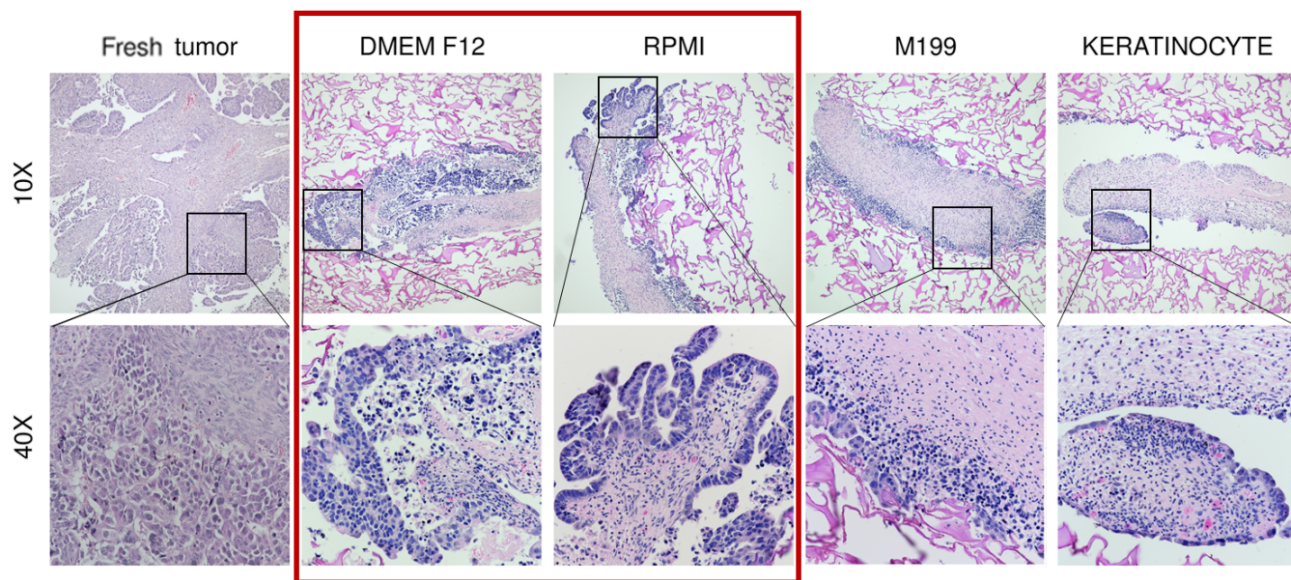


Figure 33. Representative H&E staining of fresh HGSOcs cultured under perfusion with various media. 10x and 40x microscope magnifications are shown.

In the era of the personalized medicine, the possibility to use slow-frozen tumor samples as valid pre-clinical models would allow to delve into mechanisms responsible for the sensitivity of that particular tumor to an innovative treatment, in a time and space-independent manner. Hence, our next main goal was to resuscitate slow-frozen tumor tissue fragments under perfusion-flow culture. We assembled a series of bioreactors using previously slow-frozen HGSOcs in the configuration of big chunks (~1 cm³) (Figure 32, point 2). The patient cohort of this second set of experiments consisted of two primary tumors and seven omental metastases obtained from seven patients. This cohort included chemotherapy naïve (n=6) patients as well as patients treated with first line chemotherapy (n=1) or affected by relapse (n=2).

Tumor tissues cut and fixed immediately after thawing, namely *slow-frozen T0*, appeared as considerably different from the respective fresh tumors, in terms of histologic appearance and overall

tissue integrity. This resulted, after seven days of perfused culture, in a set of disaggregated and not really viable slow-frozen P3D7ds (SF P3D7ds), whose overall cellularity was severely reduced when tissues were perfused using DMEM/F12 or matched ascites (Figure 34). Only in one case out of five, additional cultures were performed with more complex media which allowed to obtain viable P3Ds, similar enough to the *slow-frozen T0*. In detail, the AdvDMEM/F12, characterized by reduced serum supplementation and capable of supporting superior cellular proliferation and maximum cell density showed the preservation of the tumor compartment, although stroma was mainly necrotic. Alternatively, the serum-free Ovarian TumorMACS™ Medium, optimized for the culturing and expansion of tumor cells from primary and xenotransplanted ovarian tumors, showed viable stroma at the expenses of the tumoral compartment. Anyway, both media were worth taking into consideration for additional tests.

Considered the reduced percentages of success rate in obtaining SF P3Ds of good quality starting from big chunks of frozen tumors (~10-15%), they were abandoned in the further experiments.

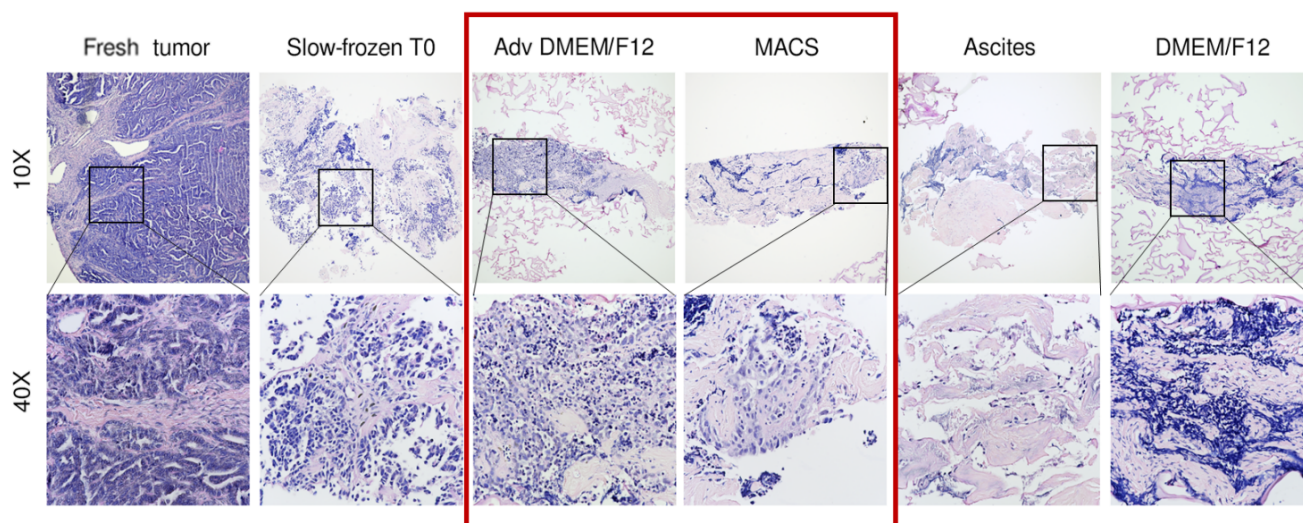


Figure 34. Representative H&E staining of slow-frozen HGSOCs (big chunks) cultured under perfusion with various media. 10x and 40x microscope magnifications are shown.

At this point we wondered if the outcome of the long-term perfusion-based ovarian tumors cultures could depend on the original specimens' state, in terms of integrity and TME viability. Thus, some changes were brought to the slow-frozen tumors perfusion-based cultures workflow, by preparing the

samples in a configuration of “ready-to-use” little chunks, with a volume of $\sim 2 \text{ mm}^3$ (Figure 32, point 3). Indeed, we envisioned that fresh-frozen tumors in the form of small chunks could better retain their structure and tissue compartments when thawed.

Therefore, fresh tumors arriving from the surgical room were cut in small pieces and random pieces were slow-frozen in static conditions, using a cryopreservative medium. These pieces were thawed just before being processed in the bioreactor.

Only for the first experiment performed using this tumor configuration, freezing and thawing in perfusion were tested to allow the cryopreservative medium to perfuse and subsequently be cleared from the tissue at a constant flow rate. Indeed, it was supposed that infusion and removal of the cryopreservative medium from a 3D tissue-like structure could favor its better preservation.

Thanks to this procedure, a high grade of similarity between the *slow-frozen T0* and the original fresh ovary tumor, in terms of structure and heterogeneity of cellular components, was estimated for the first time. Regarding the freezing/thawing modality, the perfusion was not essential to better preserve the tissue’s spatial organization and cell composition. Moreover, the two SF P3D7ds obtained culturing for seven days the slow-frozen primary tumor treated as above appeared intact and well structured, preserving typical clusters of ovarian epithelial cells (Figure 35).

On the basis of these results, only “ready-to-use” slow-frozen tumors in the configuration of little chunks have been used for further experiments.

Further tests were performed using both fresh and slow-frozen tumors with the aim to improve the P3Ds derivation rate. Given the satisfying outcome previously obtained when testing AdvDMEM/F12, it has been repropounded in an enriched version since it was supplemented with compounds and growth factors previously reported to support EOC cell growth as well as other types of tumor 3D structures.

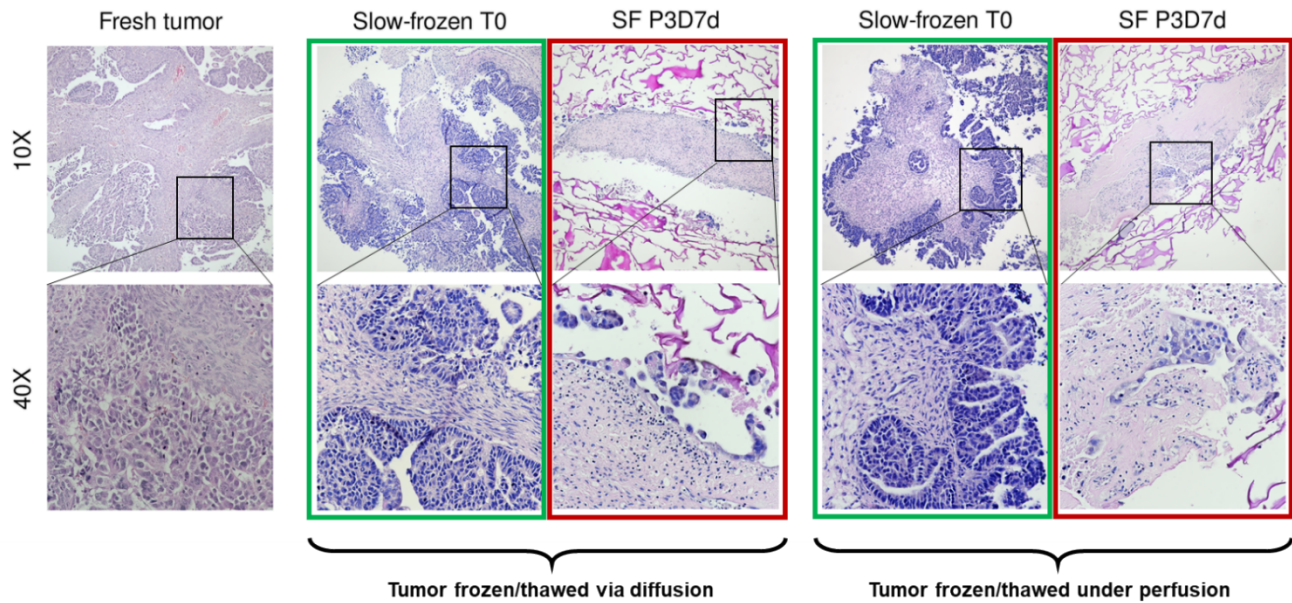


Figure 35. H&E staining of slow-frozen primary HGSOC cultured after freezing/thawing via diffusion and after freezing/thawing under perfusion. 10x and 40x microscope magnifications are shown.

Both fresh (n=2) and slow-frozen (n=1) primary HGSOCs, in addition to fresh metastatic omental tumors (n=2) were cultured for seven days; the AdvDMEM/F12 supplemented (AdvDMEM/F12++++) was compared with the serum-free Ovarian TumorMACS™ Medium. According to a trained pathologist, all P3D7ds were viable, well-structured and they showed to retain all cellular compartments. Nonetheless, a more evident proliferating rate and reduced necrosis are features of P3D7ds cultured in AdvDMEM/F12++++ (Figure 36). In detail, two out of three perfused cultures in TumorMACS™ Medium presented completely necrosis, while AdvDMEM/F12++++ allowed to obtain more viable tissues, with around 20% of viable tumor and only 20% of necrosis, in total.

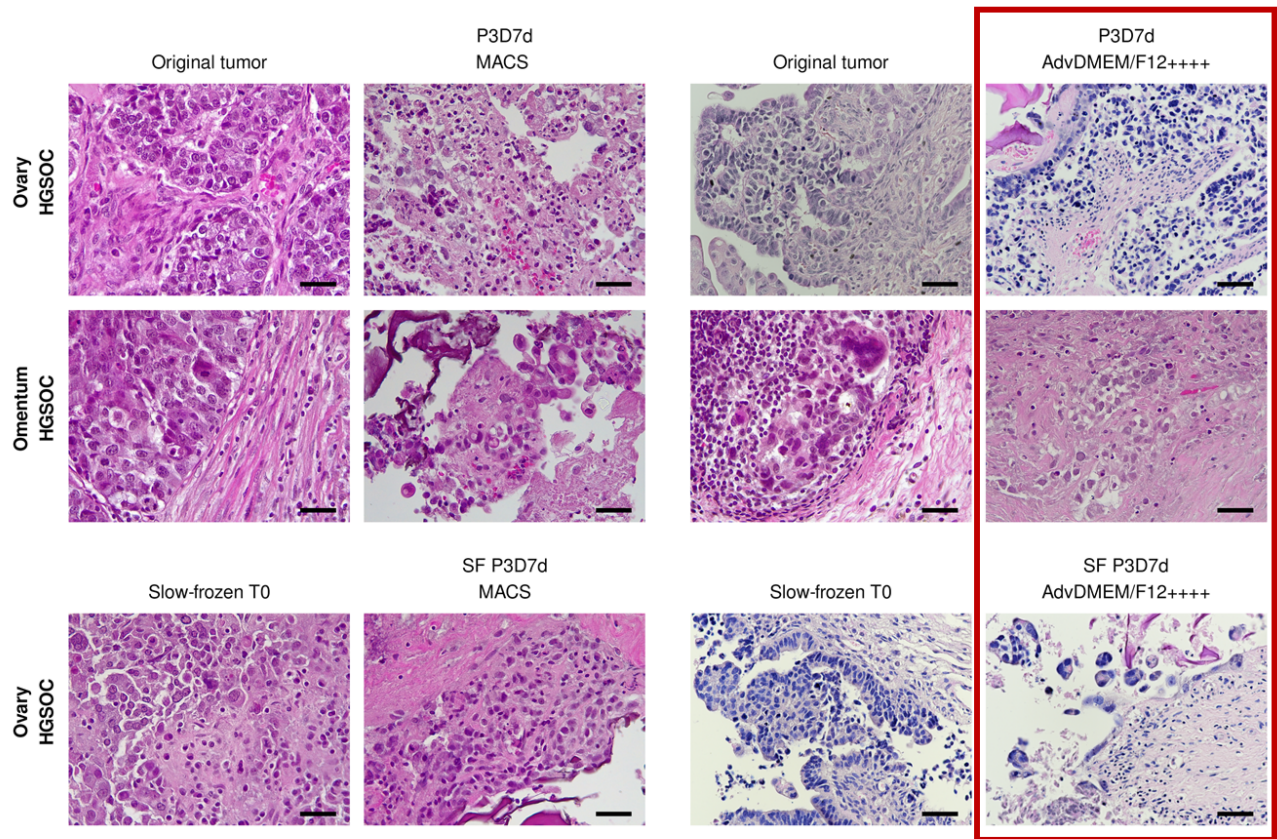


Figure 36. H&E staining fresh and slow-frozen HGSOCs cultured in perfusion for seven days. Representative images of primary and metastatic tumors are shown. 40x microscope magnifications are shown.

This advantage led us to prefer this latter medium for perfusion-based cultures for investigating different time points (3-5-7 days) as well as media changes (MCs), with the final aim to establish the preservation benefit provided by the perfusion system.

A fresh primary tumor cultured in AdvDMEM/F12++++ for three days and with one full media change showed to be viable, preserving both the epithelial compartment with cancer cells (30% of viable tumor) and stroma, according to a trained pathologist. Immediately after thawing, the tumor specimen appeared as well-preserved (10% of viable tumor), allowing to obtain a viable and metabolically active slow-frozen P3D3d (SF P3D3d), faithfully resembling the original tumor with 10% of viable tumor (Figure 37). The only visible necrosis was ascribable to the proliferation, due to the presence of viable cancer cells all around, as observed also in the fresh tumor.

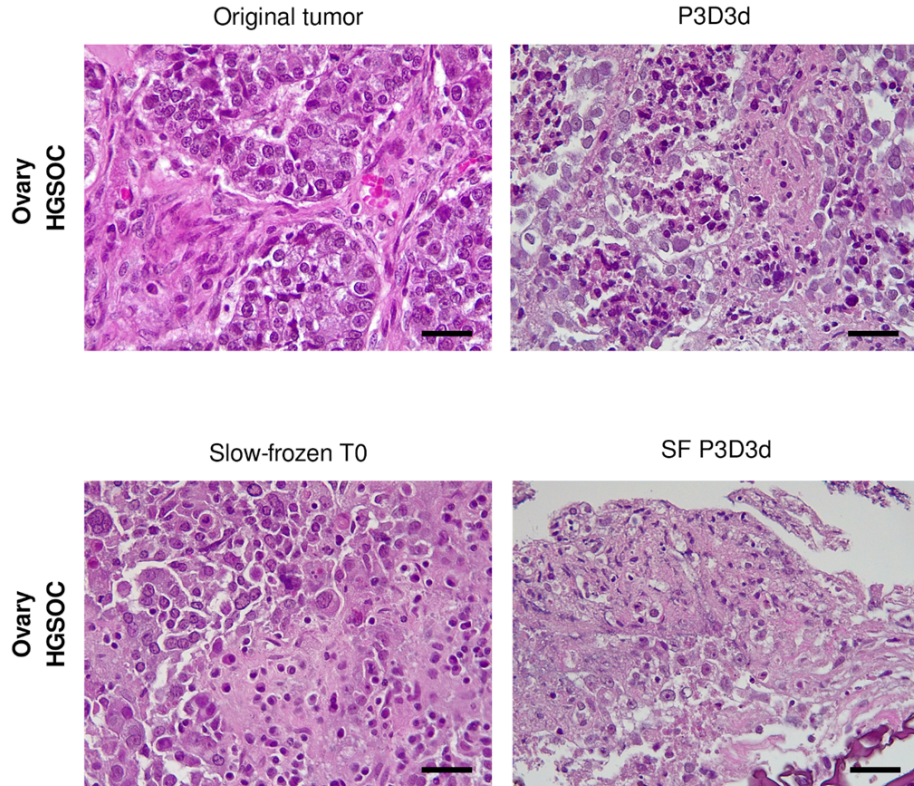


Figure 37. H&E staining of a fresh and slow-frozen primary HGSOc cultured in perfusion for three days in AdvDMEM/F12++++. 40x microscope magnifications are shown.

With the aim of fine-tuning cultures of both fresh and slow-frozen HGSOc samples in AdvDMEM/F12++++, I verified the impact of medium changes on long-term P3Ds. At this step, one secondary objective was to assess the suitability of perfusion-based cultures to better resemble the original tumor, with respect to the static cultures, as previously proven using U-CUP bioreactors to obtain colorectal cancer and breast cancer *ex-vivo* 3D models¹⁵⁵.

Fresh tumors resected from ovaries (n=2) and omental metastases (n=2) were maintained in culture for five days with one medium change. All perfused samples showed the maintenance and integrity of all tissue compartments, with a media of 30% of viable tumor. Moreover, one P3D5d ovary resulted full of vessels and showed proliferating mesenchymal cells, as suggested by a trained

pathologist. When analyzing tumoral pieces cultured in static condition we observed that while the tumoral compartment seemed well preserved (~30% viable), the stromal sector was compromised (~10% viable).

One of the previous omental metastases was used to also set-up a five days culture experiment starting from slow frozen chunks. The fragments cultured in static condition resulted in complete tissue loss and disintegration with a scarce quality, due to the almost complete visible necrosis (Figure 38). On the contrary, the slow frozen P3D5d (SF P3D5ds) maintained the same percentage of viable tumor as the original sample (10%). Moreover, typical calcifications specific for chemotherapy induced

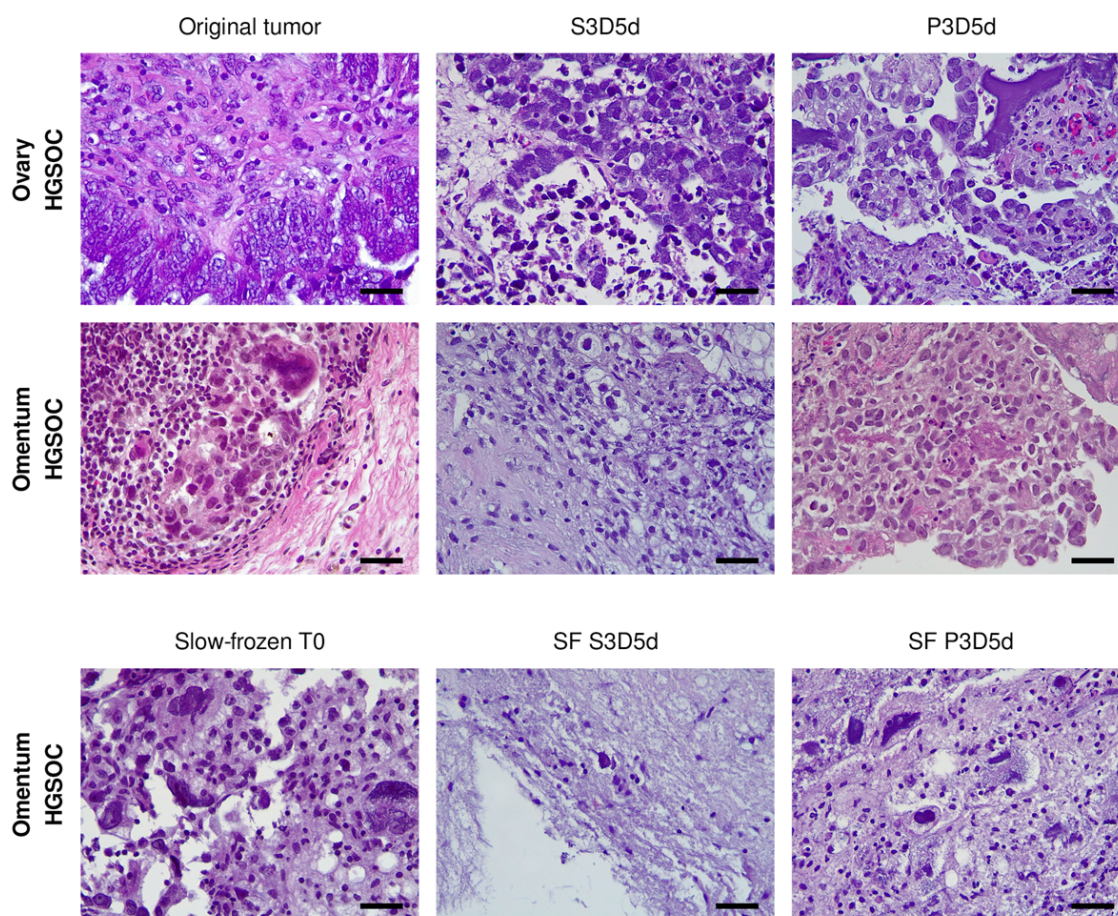


Figure 38. H&E staining of fresh and slow-frozen HGSOcs cultured in perfusion for five days in AdvDMEM/F12++++. Representative images of primary and metastatic tumors are shown. 40x microscope magnifications are shown.

damage were also identified, recapitulating the typical characteristics of tumors responsive to chemotherapy.

Perfusion-based cultures up to one week, with two AdvDMEM/F12++++ medium changes, were the most investigated. Indeed, cultures using fresh primary tumors (n=3), in addition to fresh metastatic tumors localized on the omentum (n=4) and on the diaphragmatic dome (n=1) provided an overview about the specific response to this culture approach. P3D7ds tumoral component ranged from 10% to 70%, with evidence of necrosis in some samples. Overall, models resembled the original tumors in terms of cell differentiation, structure, quality and active proliferation. Static 3D7ds' tumor sections, although still viable after long-term cultures (~30% of viable tumor), showed a greater abundance of necrosis than their P3D7ds counterparts. Also, the heterogeneity of EOC TME was not recapitulated and the stroma was compromised, especially in the SF P7Ds (Figure 39).

Of note, some experiments with slow frozen which used tumoral samples originating from patients undergoing chemotherapy yielded unsatisfactory results since the biopsies had mostly fibrotic tissue with little to no tumoral cells. Again, the pieces cultured in static conditions were precarious.

These results cumulatively indicated that, in comparison to static cultures, short and long-term cultures of both primary and metastatic HGSOCs pieces under perfusion retains the heterogeneity of EOC cellular components to a much greater extent. Cultures in perfusion up to five or seven days seemed to be the best compromise to obtain a viable and structured EOC 3D *ex vivo* model, sufficiently resembling the starting tumor tissue (regardless it is up-front or post-neoadjuvant chemotherapy). Furthermore, slow-frozen tumors in the configuration of “ready-to-use” small chunks appeared as appropriate to generate P3Ds similar to the original HGSOCs, regardless of their primary or metastatic origin.

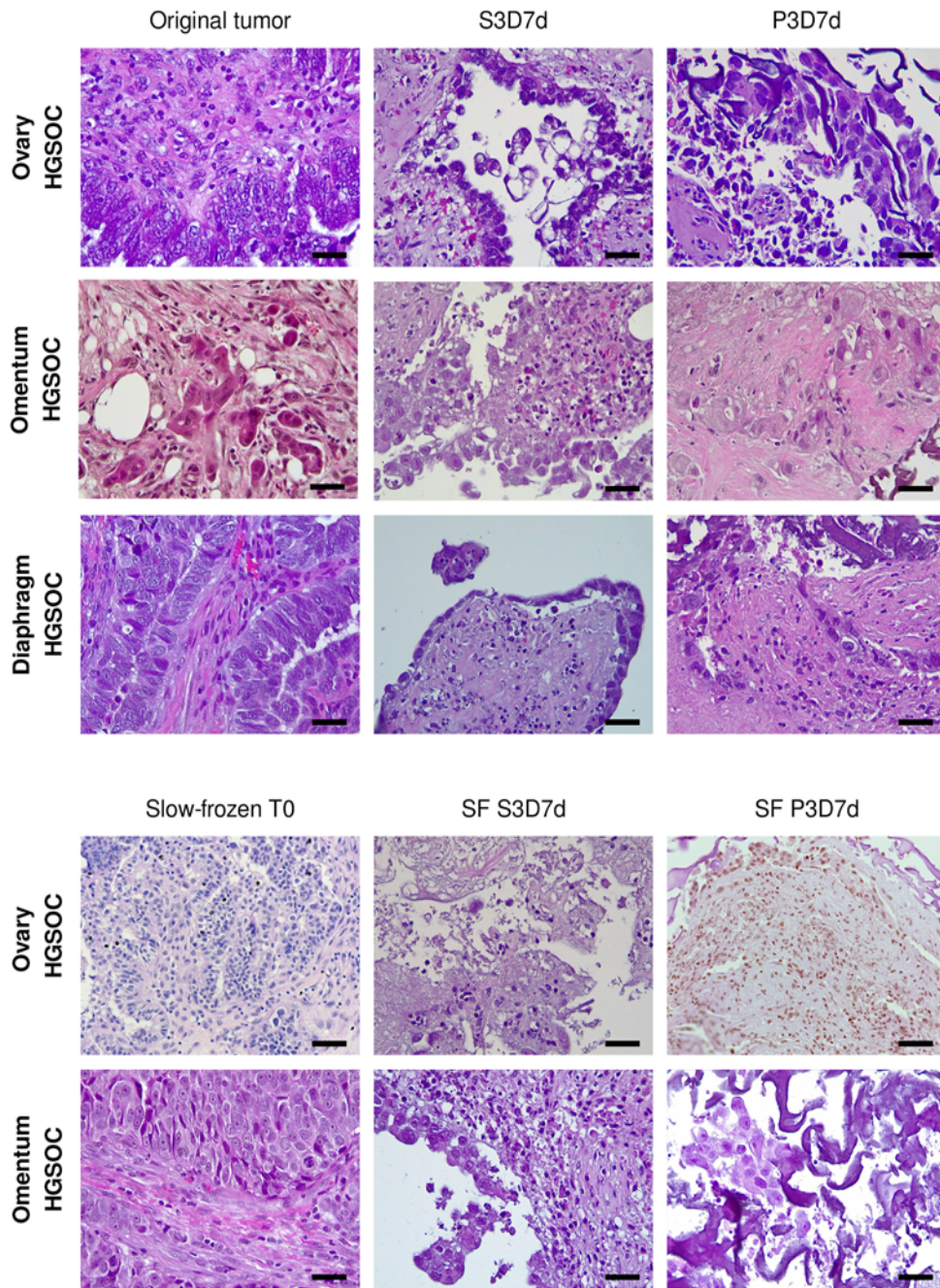


Figure 39. H&E staining of fresh and slow-frozen HGSOCS cultured in perfusion for seven days in AdvDMEM/F12+++. Representative images of primary and metastatic tumors are shown. 40x microscope magnifications are shown.

6.9 Perfused fresh and slow-frozen EOC 3Ds recapitulate the original TME

Perfusion-based bioreactor U-CUP is emerging, over the past few years, as suitable for the maintenance of tumor types not easily cultured *in vitro*. In addition to the structural resemblance to the original specimens and to the tissue quality, an ideal 3D model should be able to preserve as much as possible the TME heterogeneity.

Tissues cell composition has been analyzed upon specific IF staining for epithelial cells (E-cadherin), stromal cells (Vimentin), immune cells (CD45) and endothelial cells (CD31).

Thus, P3Ds and SF P3D7s obtained under seven days of culture in AdvDMEM/F12++++ have been compared to the respective original tumors to assess cell compartments preservation under perfusion. An illustrative set of IF images showed that fresh P3D7ds recapitulate the original TME (Figure 40).

In detail, cultures under perfusion were characterized by a partial reduction of the epithelial component with respect to the respective fresh tissues but showed the maintenance of the endothelial compartment (Figure 41).

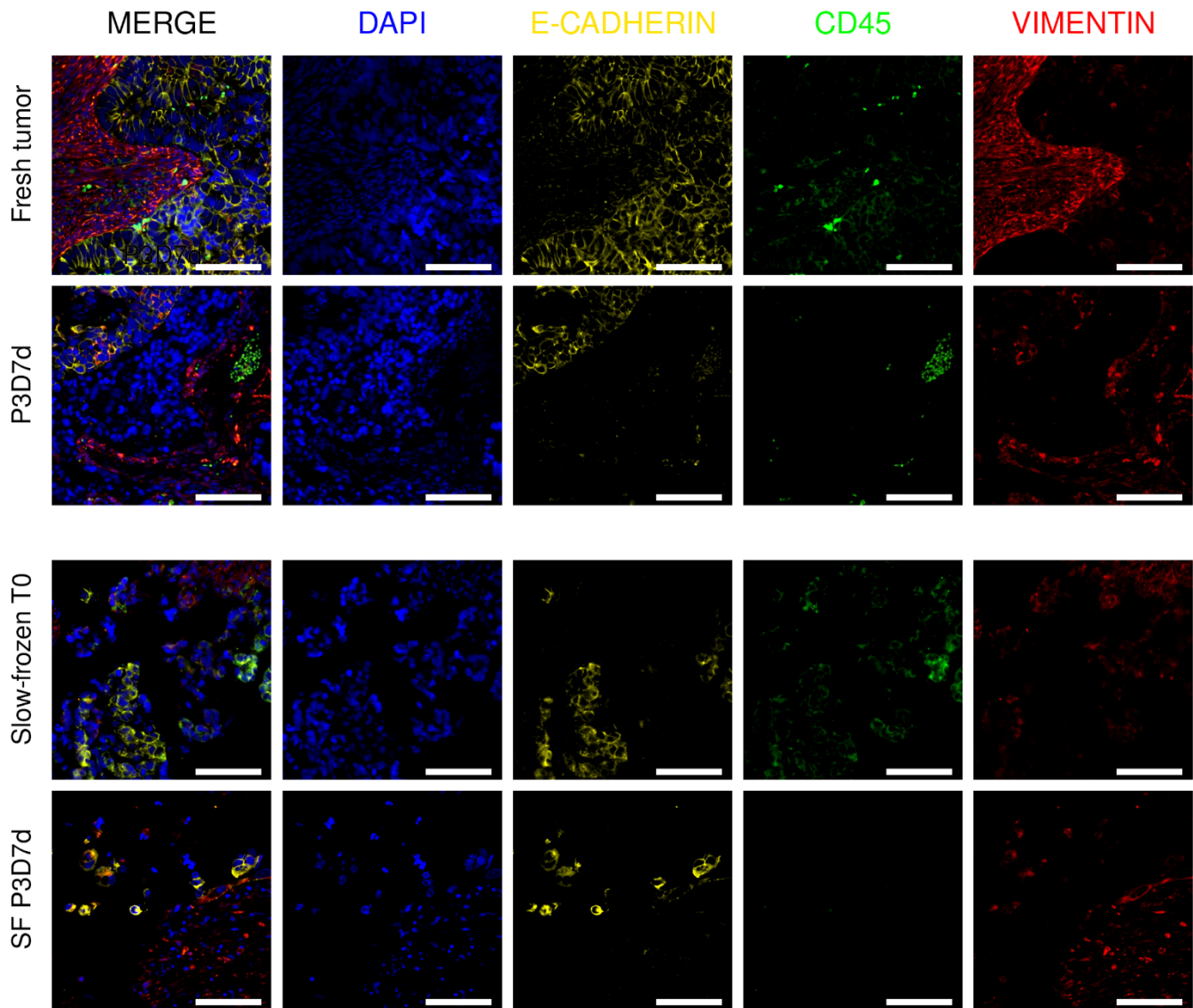


Figure 40. Representative IF staining for TME compartments of fresh and slow frozen HGSOCS cultured in perfusion for seven days in AdvDMEM/F12++++. 20x microscope magnifications are shown.

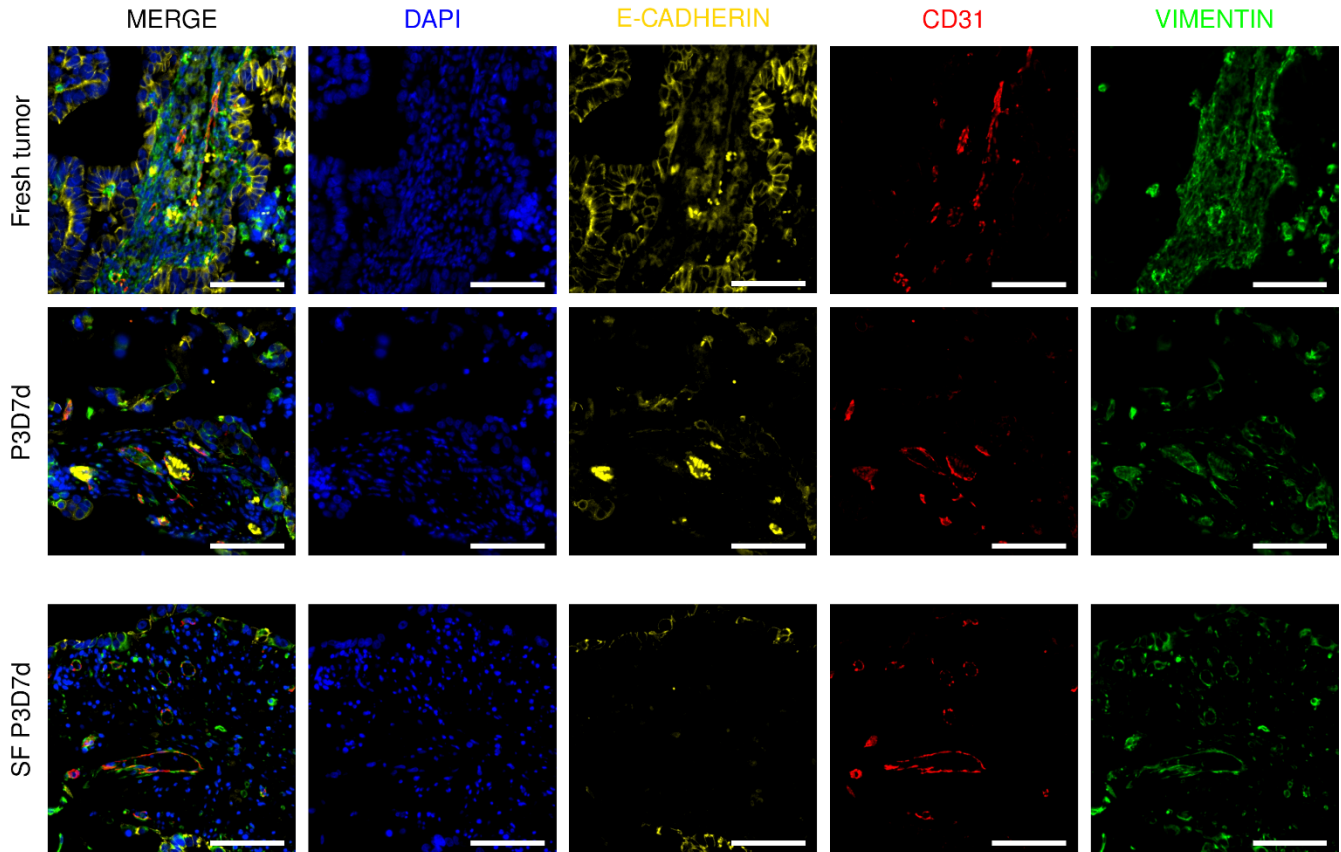


Figure 41. Representative IF staining for endothelial compartment of fresh and slow frozen HGSOCs cultured in perfusion for seven days in AdvDMEM/F12++++. 20x microscope magnifications are shown.

To further examine cell viability inside cultured tissues, we evaluated the presence of proliferating epithelial cells through Ki67 labeling (Figure 42). We found that both fresh and slow-frozen samples maintained the proliferative cells. Thus, perfused fresh and slow-frozen EOC 3Ds preserve viable and proliferative epithelial cells.

A further labeling using an antibody anti-cC3 (Cleaved caspase-3) was performed to assess if epithelial cells were dying through apoptotic death (Figure 43).

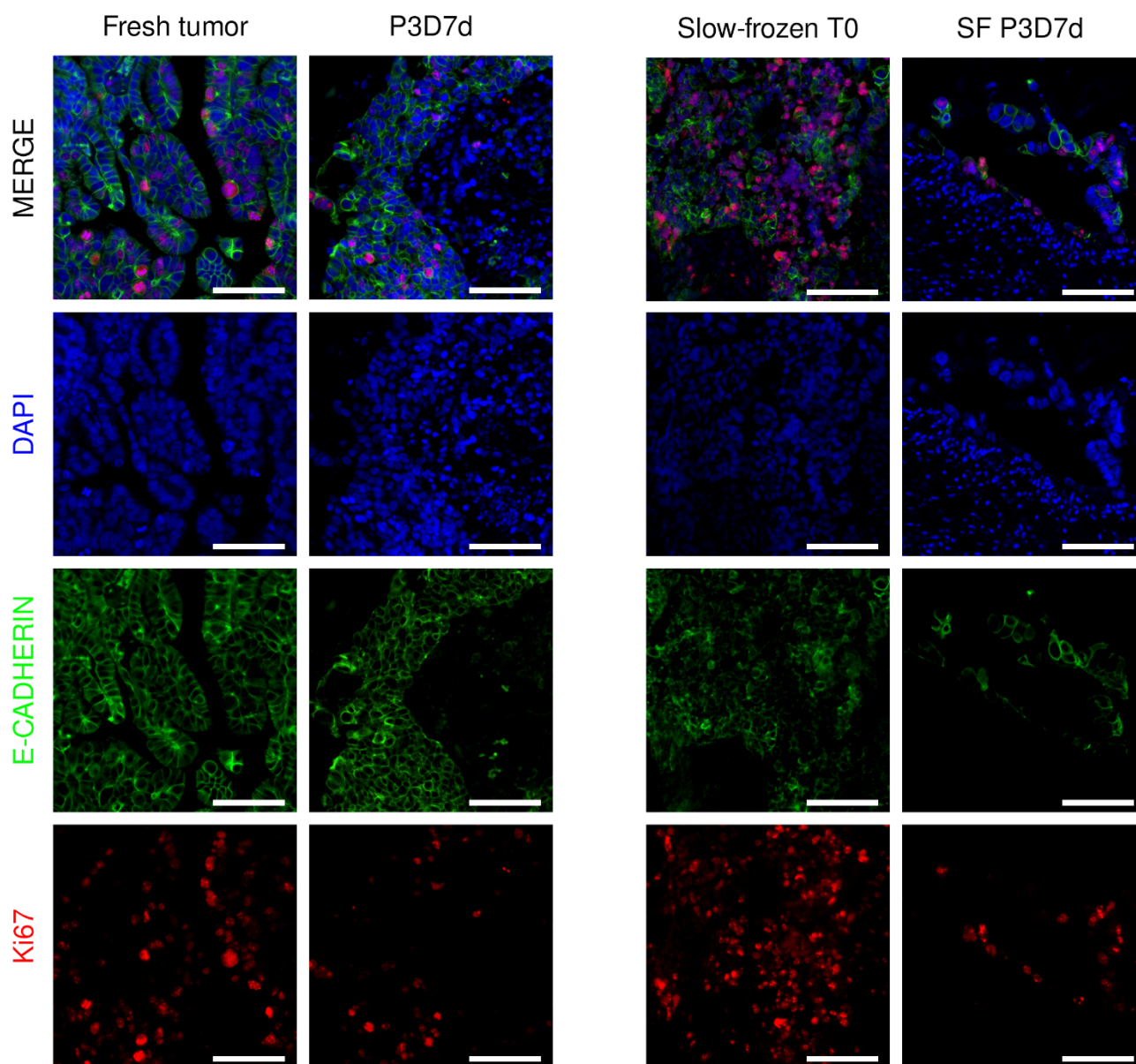


Figure 42. Representative IF staining for proliferative epithelial cells of fresh and slow frozen HGSOCS cultured in perfusion for seven days in AdvDMEM/F12++++. 20x microscope magnifications are shown.

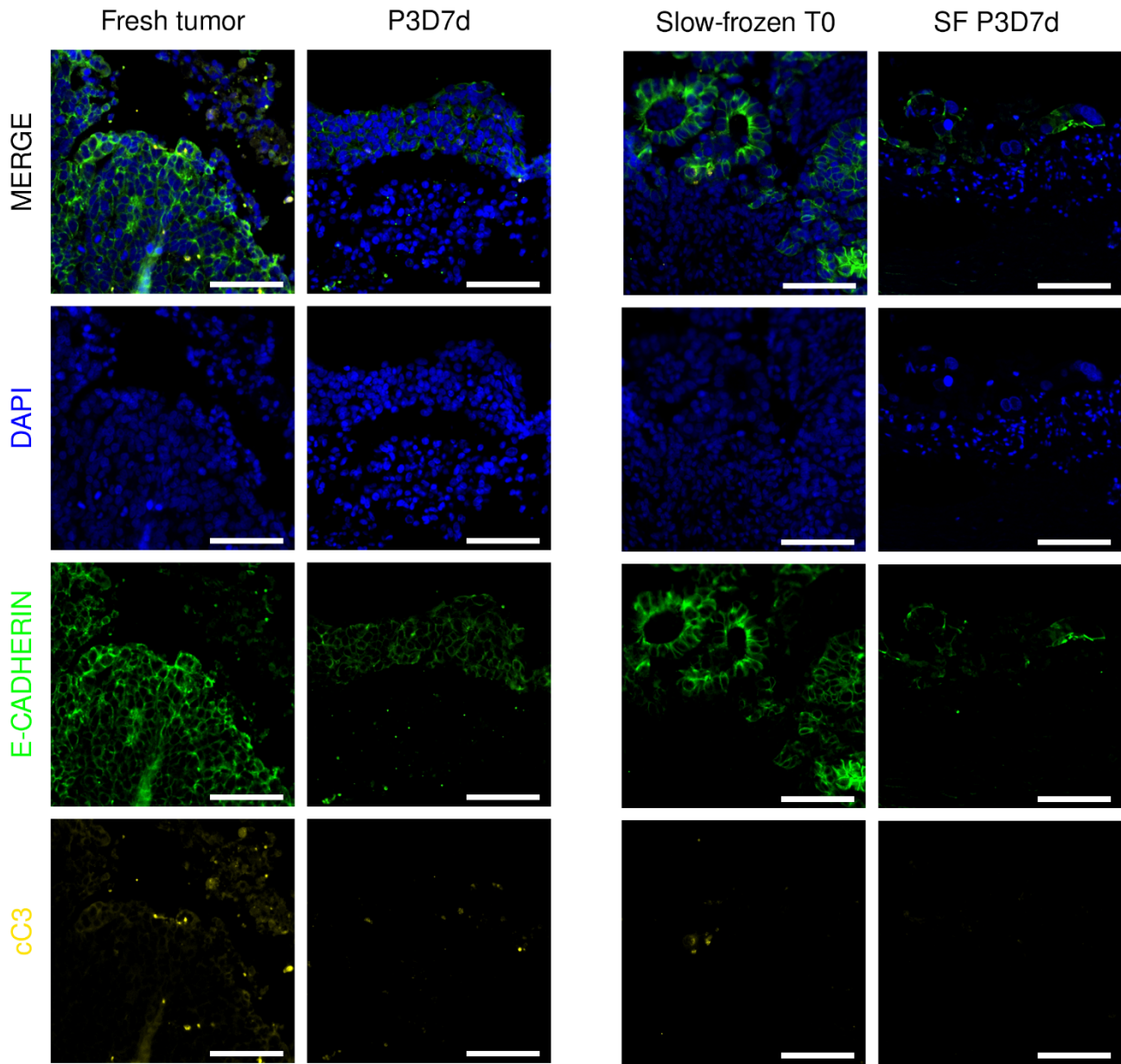


Figure 43. Representative IF staining for apoptotic rates of fresh and slow frozen HGSOCs cultured in perfusion for seven days in AdvDMEM/F12++++. 20x microscope magnifications are shown.

As expected, no marked difference between sample types was observed, thus further strengthening the advantages of the U-CUP model. Overall, both proliferation and apoptotic rates of P3Ds were comparable to those found in fresh tissues.

Thus, bioreactor cultures appear to be suitable for 3D cultures of *ex vivo* tumoral OC samples.

6.10 EOC perfused-3Ds mimic the original tumors from a molecular point of view

The authentication process of our perfusion-based 3D *ex vivo* models considered a further investigation focused on confirming the similarity between HGSOEs obtained from patients and the matching tumors growing into the scaffolds from the genetic point of view.

In detail, some P3Ds established from short- and long-term cultures were sequenced for a small panel of genes typically mutated in HGSOE. We were particularly interested in the state of the tumor suppressor *TP53*, given its high grade of mutation in EOC, III-IV stage (over 96%)²⁶.

Next Generation Sequencing (NGS) was performed on fresh tumors excised from five patients, of which both primary and metastases, and their respective P3Ds obtained both from fresh and slow-frozen original specimens. The analysis showed retention of each somatic *TP53* driver mutation in all the EOC 3D *ex vivo* models tested. According to the number of *TP53* alleles in fresh tumors, abundance of cancer cells varied between one sample and another in a range from about 30% up to having almost all neoplastic cells in the analyzed specimens. The technical validation of the NGS multi-gene panel implemented here revealed that this approach has an error rate of $\pm 5\%$ in detecting variant allele frequency (VAF). In general, *TP53* somatic single nucleotide variants (S-SNVs) with VAF higher than 10% were considered as true mutations. A total of four S-SNVs were detected in *TP53*, of which two missense and two frameshift mutations caused by deletions (Table 4, Figure 44).

According to VAF percentages of the mutant *TP53*, mutated cells tended to halve in P3Ds obtained from fresh primary tumors (P), while they were more abundant in the corresponding slow-frozen P3Ds, especially at three days and/or seven days of culture with two media changes. This means that, in P3Ds obtained from metastatic tumors (M), cancer cells with mutations seemed to be almost completely preserved both starting from fresh and slow-frozen tissues and especially in AdvDMEM F12++++ after seven days of culture, with two media changes.

According to the VAF% of patient no.2, cancer cells bringing additional somatic mutations in *PIK3CA* and *RET* were more abundant in cultures derived from the SF primary tumor, whereas they diminished in SF P3Ds from metastatic tumor. Another patient had a wild-type *TP53* but harboured the percentage of cancer cells with *KRAS* and *SMAD4* mutations in the slow-frozen P3D; the VAFs of mutant *RET* in this patient did not exclude they were germline mutations (Figure 44).

Together, these results suggest that P3Ds obtained starting from both fresh and slow-frozen tissue can maintain the abundance of the *TP53* mutated cancer cells as compared to the starting tumors.

Patient no.	Original cancer tissue	P3Ds	Culture medium (n. of medium changes)	TP53	KRAS	PIK3CA	RET	SMAD4
1	P	/	/	49				
	P (F)	P3D7d	AdvDMEM/F12++++ (2 MCs)	25				
	P (SF)	SF P3D7d	AdvDMEM/F12++++ (2 MCs)	35				
2	P	/	/	45		9	10	
	P (F)	P3D3d	AdvDMEM/F12++++ (no MC)	22		6	7	
	M	/	/	32		24		
	M (F)	P3D7d	AdvDMEM/F12++++ (2 MCs)	47		29		
	P (SF)	SF P3D3d	AdvDMEM/F12++++ (no MC)	51		9	11	
	M (SF)	SF P3D7d	AdvDMEM/F12++++ (2 MCs)	58		9	11	
	M (SF)	SF P3D7d	AdvDMEM/F12++++ (no MC)	14		12	11	
3	M	/	/		12		58	10
	M (F)	P3D7d	AdvDMEM/F12++++ (2 MCs)		11		53	10
	M (SF)	SF P3D7d	AdvDMEM/F12++++ (2 MCs)		16		53	15
4	M	/	/	75				
	M (F)	P3D7d	AdvDMEM/F12++++ (2 MCs)	64				
	M (F)	P3D5d	AdvDMEM/F12++++ (1 MC)	51				
	M (F)	P3D7d	AdvDMEM/F12++++ (no MC)	55				
	P	/	/	14				
	P (F)	P3D7d	AdvDMEM/F12++++ (2 MCs)	57				
	P (F)	P3D5d	AdvDMEM/F12++++ (1 MC)	63				
5	P	/	AdvDMEM/F12++++ (no MC)	53				
	P (F)	P3D7d	AdvDMEM/F12++++ (no MC)	50				
	P (SF)	SF P3D7d	AdvDMEM/F12++++ (no MC)	44				



0 VAF(%) 100

Figure 44. Mutational status of HGSOC specimens cultured in U-CUP. P: primary OC; M: metastasis; F: fresh tumor; SF: slow-frozen tumor; MC: media change

Table 4. Mutations identified in the HGSOCS cultured in U-CUP.

Patient no.	Gene exon/Nucleotidic change/Aminoacidic Change				
	<i>TP53</i>	<i>KRAS</i>	<i>PIK3CA</i>	<i>RET</i>	<i>SMAD4</i>
1	E4 c.157delT p.Trp53GlyfsTer70				
2	E7 c.745A>G p.Arg249Gly		c.3140A>G Gp.His1047Arg	p.Arg813GlyfsTer56	
3	WT	c.35G>A p.Gly12Asp		p.Ala513Gly	p.Leu540Arg
4	E5 c.542G>C p.Arg181Pro				
5	E4 c.326_330delTCCGT p.Phe109Serfs Ter38				

6.11 PA-RL effects on a perfusion-based 3D HGSOC *ex vivo* model

The fact that the established P3Ds mimic the original HGSOCS also from a genetic point of view provides a useful tool to screen conventional drugs, but above all, innovative treatments. This is the case of PA-RL, that could represent a novel and highly selective therapy to eradicate intraperitoneally disseminated EOC. We, hence, evaluated the possibility to exploit bioreactor-based cultures to test the responsiveness to PA-RL in primary and metastatic HGSOC tissues (Figure 45).

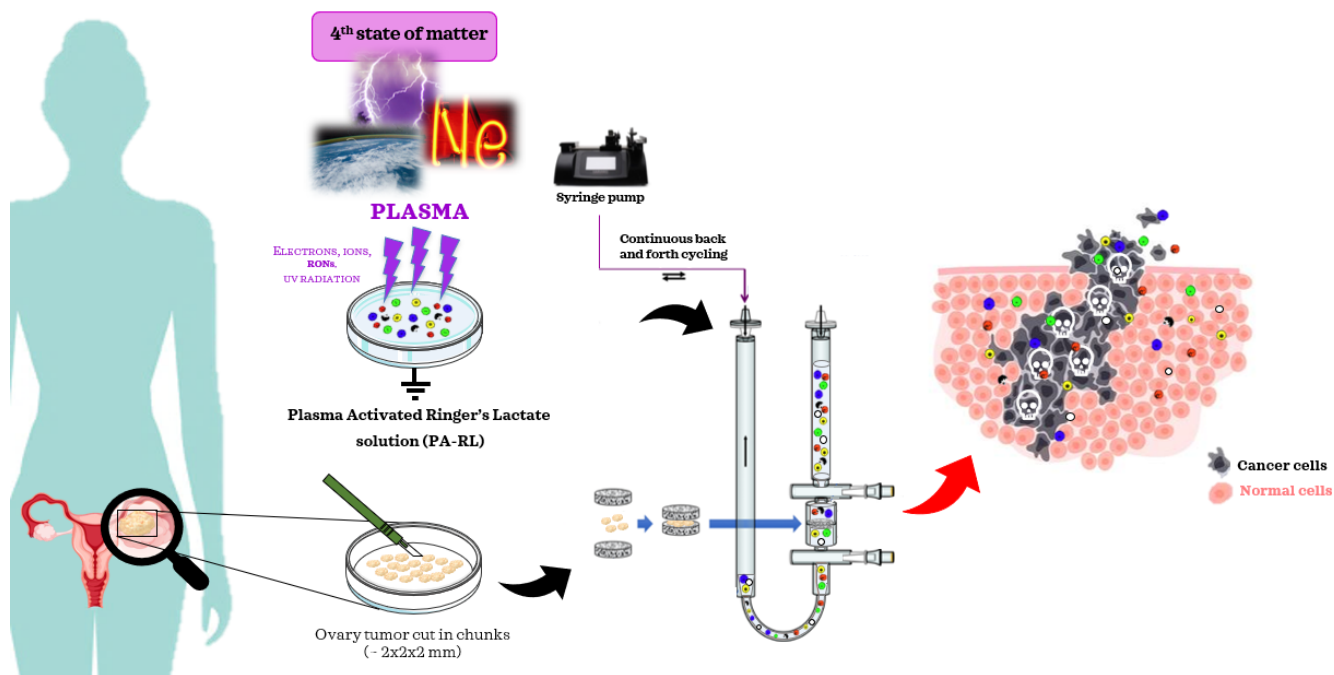


Figure 45. Schematic representation of the proposed use of PA-RL in a perfusion-based culture system.

The PA-RL screening phase has been preceded by the chemical characterization of the two main components of the “sandwich” placed in the U-CUP perfusion chamber. EFTE nylon meshes and collagen sponge discs are in close contact with the tumor chunks, so their possible structural and surface properties modifications under PA-RL infusion need to be taken into account. Surface treatment of polymers using non-thermal plasmas has been intensively investigated recently¹⁵⁶. In detail, plasma modification of biomedical polymers causes a change of their surface properties to improve biocompatibility without affecting bulk qualities^{38,157}.

Nylon meshes and collagen type I discs (Avitene™ Ultrafoam™) were put in contact with both CTR-RL and PA-RL 1:2 for two hours, after which they were left to completely dry.

The Fourier transform infrared spectroscopy analysis (FT-IR) allowed to obtain two spectra, where both PA-RL treated meshes and collagen were compared to their respective CTR-RL and to samples not treated at all. These FT-IR spectra were related to already known ETFE and collagen spectra, with the aim to confirm their entity. In the case of the ETFE meshes, peaks of treated samples had the same wavelengths as compared to not treated samples. Furthermore, peaks showed more or less the same intensity, suggesting that the ETFE did not convey the wet or dry state (Figure 46).

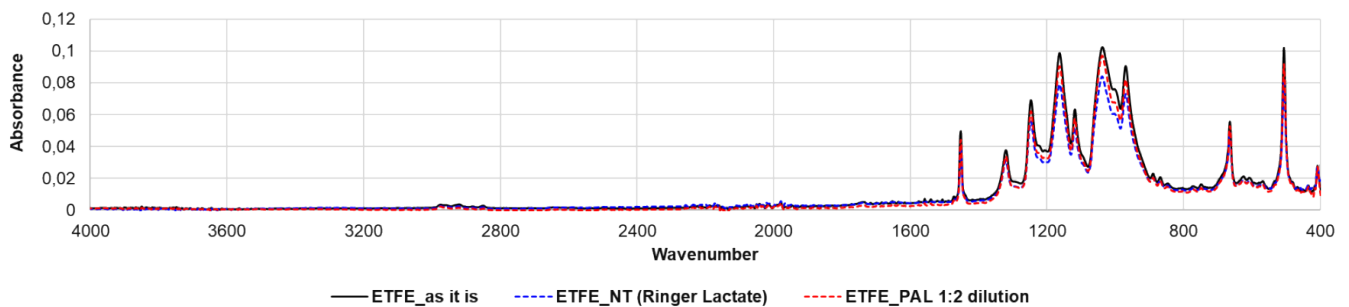


Figure 46. FTIR spectrum of ETFE. Experiment and analysis performed by Dr. Alina Bisag (DIN-Unibo).

Also, the PA-RL treated collagen discs' spectrum is comparable to the one of not treated samples. Peaks intensity is variable and dependent on collagen sponges' consistency when they are not treated or hydrated and dried (Figure 47).

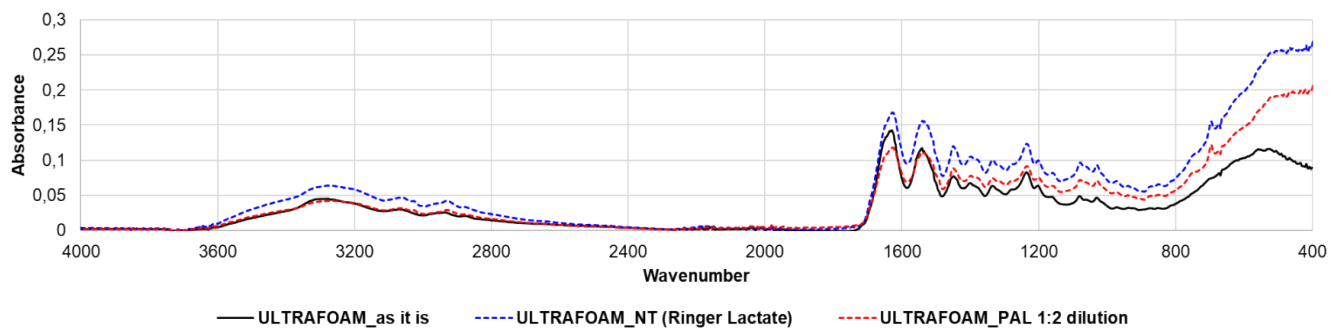


Figure 47. FT-IR spectrum of collagen type I discs (Avitene™ Ultrafoam™). Experiment and analysis performed by Dr. Alina Bisag (DIN-Unibo).

In general, the overlapping of the FT-IR spectra relative to PA-RL treated samples and their respective not treated samples entail that PA-RL does not influence the superficial chemistry neither of the EFTE meshes nor the collagen discs.

A first attempt to test PA-RL was performed on fragments of a fresh chemotherapy naïve metastatic tumor excised from the diaphragm dome, kept in culture in U-CUP for seven days. Two PA-RL dilutions were tested: PA-RL 1:4 and PA-RL 1:16, that are respectively the less and the most diluted solutions previously tested *in vitro* on both EOC cancer and non-cancer epithelial cells and fibroblasts.

Tumor chunks just assembled in the sandwich-like configuration underwent perfusion with both the aforementioned treatments and RL, as control condition (CTR RL), for two hours. After that, a quick washing of PA-RL and RL leftover inside the bioreactors preceded the injection of fresh AdvDMEM/F12++++. Medium changes were carried out twice over a week. P3D7ds harvested at the end of the culture were processed and stained in order to assess tissue structure preservation after contact with CTR RL. Moreover, we envisioned to dissect PA-RL overall impact on both the epithelial and stromal cell compartments, with the perspective to define experimental conditions needed to appreciate PA-RL selectivity in HGSOc *ex vivo* 3D models.

According to the evaluation of a trained pathologist, CTR RL condition showed a good tissue, with both tumoral (10%) and TME components being well retained and viable. Tissue treated with PA-RL 1:4 was well structured, composed, above all, of mesenchymal cells and vessels. However, it seemed to contain clusters of cancer cells which presented specific changes characteristic of cell death. On the contrary, stromal tissue did not show such signs (Figure 48).

The P3D7d treated with PA-RL 1:16 showed a complete viable stromal compartment, with quite few necrosis areas all around the tissue. Anyway, there was no visible tumor in this sample.

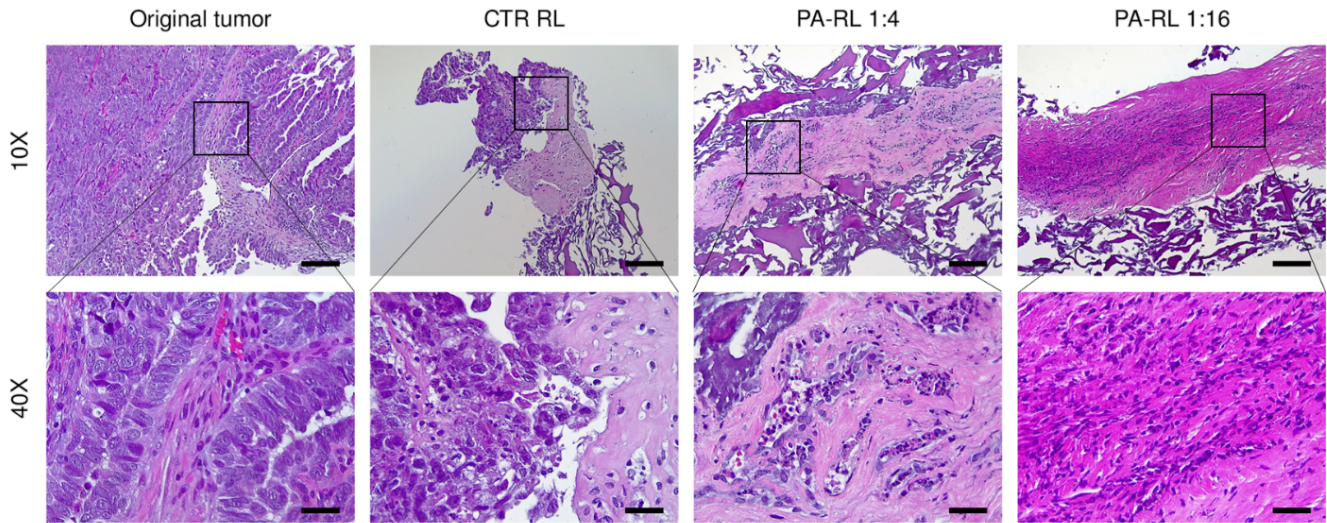


Figure 48. H&E staining of a fresh diaphragmatic metastasis of HGSOC cultured in perfusion for seven days in AdvDMEM/F12++++ after being perfused for 2 hours with CTR-RL, PA-RL 1:4 and PA-RL 1:16. 10x and 40x microscope magnifications are shown.

PA-RL treatment was performed on two additional peritoneal metastases derived from HGSOC. One of the two P3D7s, obtained starting from a diaphragm dome specimen was not valid for subsequent analysis. Notably, individual samples analysis revealed heterogeneous responses to PA-RL treatment.

In particular, the second established P3D7d badly endured the most aggressive PA-RL concentration, given the overall cellularity level. Tumor cultured in CTR RL presented 20-30% of viable tumor in addition to a few necrosis. Clear signs of tissue disintegration and death concerned both stroma (50% viable) and tumor compartment (>10% viable) under treatment with 1:4 PA-RL dilution. The latter appeared as almost completely targeted; indeed, only a few single cancer cells were still viable and interacting with the scaffold collagen fibers. The P3D7d treated with PA-RL 1:16 showed in part better preserved stroma and in part diffused tumor apoptosis, with still around 15-20% of viable tumor that had infiltrated into the scaffold surviving to the treatment (Figure 49).

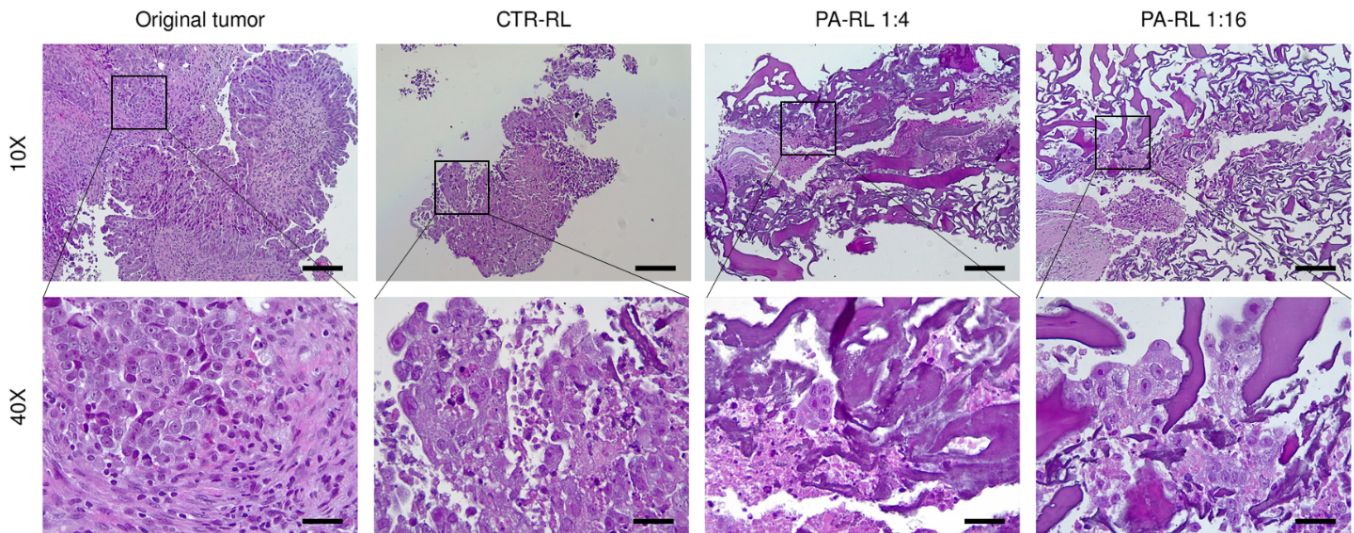


Figure 49. H&E staining of a fresh omental metastasis of HGSOc cultured in perfusion for seven days in AdvDMEM/F12++++ after being perfused for 2 hours with CTR-RL, PA-RL 1:4 and PA-RL 1:16. 10x and 40x microscope magnifications are shown.

Preliminary results on PA-RL treatments against 3D *ex-vivo* HGSOc metastatic specimens seem to assess 1:4 PA-RL dilution had a damaging effect against tumor, without relevant damage neither to the stroma nor to TME components such as vessels or macrophages (according to the evaluation of a trained pathologist). The 1:16 PA-RL dilution was even better for the stroma preservation. In this case, the overall necrosis was reduced, in exchange of regions with higher percentages of live tumor. These results were comparable with those of our second experiment.

7. DISCUSSION and CONCLUSIONS

Over the past 15 years, the application of CAP in oncology has been investigated in depth¹³². In particular, the indirect plasma irradiation of liquid substrates potentially administrable to humans is the first step in view of possibly applying PALs as novel anti-cancer treatments. PALs could be used either in combination with standard therapies, or even as an alternative treatment in case of tumor resistance to the classical chemotherapeutic approaches. The feasibility of PALs usage in a clinical setting requires that their production does not imply the use of a technical gas and most importantly, that they can be made in large volumes, necessary for example in the case of an intraperitoneal administration.

In this thesis, we show for the first time the usage of a multiwire plasma source, sustained by the *AlmaPULSE* generator, in treating Ringer's lactate solution, using environmental air as working gas. Ignition of the plasma generating device in a sealed chamber not only allowed to finely control the gas phase chemical composition, but also to guarantee a homogeneous treatment of a considerable liquid volume. This strategy enables this approach to be easily scalable, thus overcoming the aforementioned limitations. The novelty of this approach lies in the use of this system to treat the Ringer's Lactate solution thus obtaining PA-RL previously tested against tumors characterized by dissemination in body cavities, both *in vitro* and *in vivo*.

PA-RL production procedure was standardized, establishing the optimal conditions to prepare it. The electrical characterization of plasma confirmed the generation of microdischarges whose power values increased in a controlled and directly proportional manner to the amplitude of the applied voltage.

To delve into the mechanisms by which plasma interacts with living systems, the chemistry of plasma-liquids interaction is definitely of help. Indeed, the exposure of liquid substrates to high voltage electrical discharges leads to the production of RONS, that are initially generated in the air phase and then diffused into the liquid. Given the pivotal role of plasma-treated liquids' chemical composition in their downstream overall effect, PA-RL was characterized in terms of radical concentrations. H_2O_2 , the major anti-tumor factor in plasma-activated solutions, is generated in gas phase in the course of plasma irradiation, to be then dissolved in the liquid. H_2O_2 concentration increased depending on the irradiation interval (10 minutes), as confirmed also by Yang Liu et al., 2021. After a 2h incubation, H_2O_2 levels decreased, in favor of NO_2 concentration that was unchanged. Thus, the optimal condition

appears to be an air composition, implying that plasma-generating conditions in the atmosphere would be acceptable^{89,90,95}.

NO production in non-equilibrium plasma is possible thanks to the production of a high number of vibrationally excited N_2 molecules. In the case of a plasma discharge operating in ambient air, vibrationally excited N_2 molecules emit light at a wavelength of around 400 nm¹⁴². High-speed filter images confirmed the presence of excited N_2 molecules in the air phase, thus justifying the origin of NO_2^- detected in the PA-RL.

Unlike cell culture medium, Ringer's lactate solution does not contain a buffer that could keep the pH constant under plasma treatment¹⁵⁸. By measuring the pH values of the plasma-treated RL solution after 10 minutes of irradiation, the pure PA-RL showed an acid pH of 5.36, compared to the pH of 6.15 of the untreated solution (CTR-RL). The reduction in pH values has been ascribed to production of hydrogen ions (H^+) in addition to the acid generation of nitrite or nitrate. On the other hand, pH values of plasma-irradiated lactated solutions raise simultaneously with higher sodium lactate concentration. This tendency is confirmed in our PA-RL dilutions, where the pH values ranging from 4- to 16-fold dilutions are closer to the CTR-RL one. Our choice to go on using 1:4, 1:8 and 1:16 PA-RL dilutions depended on avoiding possible pH influence on PA-RL antitumor potential to be assessed on EOC and non-cancer cell lines.

Tanaka et al (Sci Rep, 2016) dissected, for the first time, PA-RL effects against the EOC cancer cell line SKOV-3, discovering that they are effectively killed by Ringer's solutions containing lactate and acetic acid¹¹⁹. With respect to our experiments, SKOV-3 viability after 24h from the end of the treatment was around 20%, with significant difference using 1:4 (cell viability 17,9%) or 1:16 (cell viability 25,6%) of PA-RL dilutions. Procedural differences in factors as, for example, the RL solution treatment time, the cancer cells exposure time and the gas phase, could justify the minimal discordance with results obtained from Tanaka et al. using the same PA-RL dilutions (% of cell viability lower than 20%). Indeed, different plasma sources provide markedly different radical concentrations and hence cell-killing characteristics⁹⁰. Of note, we demonstrated that PA-RL generated in environmental air exerts cytotoxic effect on two EOC cell lines with genetic features similar to HGSOC in a time- and dose-dependent manner, up to 72 hours after treatment.

We did question if PA-RL-induced cell injury may depend on H_2O_2 and NO_2^- or on the pH change caused by RL solution. Although RL solution composition is simple, since it is made by four components, not much is known about components derived from the interaction between plasma and

its only one anti-tumor component, the L-sodium lactate. At 72 hours time point, the less concentrated PA-RL showed to significantly reduce viability of both cell lines compared to H₂O₂ and NO₂⁻ concentrations and to a pH value as previously measured in this dilution. This result fits with the hypothesis that additional components are responsible for the selective killing of cancer cells by PA-RL¹⁵⁹. Recently, advanced technologies as the NMR and the direct infusion-electrospray ionization (ESI) with tandem mass spectrometry analyses allowed to estimate PA-RL components, identifying the 2,3-dimethyltartrate as the responsible for the selective cytotoxicity on cancer cells.

For the first time, both EOC populations and two non-cancer cell lines, among which a non-cancer epithelial cell line of ovarian origin, were subjected to treatment with PA-RL dilutions in order to define a selective window of the treatment. The same PA-RL dilutions previously tested on cancer cells showed to induce almost the same effect on both the ovarian healthy counterpart and primary fibroblasts mimicking the mesenchymal compartment. Specifically, their viability decrease was clearly detectable starting from 48 hours after treatment, reaching levels around 60% when 72 hours passed from the PA-RL 1:16 treatment ending. Despite the different sensitivity displayed by SKOV-3 and OV-90 to PA-RL 1:16 at 72 hours (% of cell viability: 5% vs 22% respectively), all non-cancer cell lines were significantly more viable, making this PA-RL dilution the selective window we were searching for. Our choice to monitor cell models up to 3 days after treatment, at least, mirrored the need to observe possible damaging consequences on healthy cells. Further analysis on PA-RL-treated cells viability would be useful to verify the long-term healthy cell's reaction to the treatment, that may reveal a cytostatic effect or, conversely, a negligible effect on their proliferation.

The topic of selectivity has always been a relevant one in the context of anticancer therapies discovery. In detail, numerous research lines focused on highlighting molecular differences between cancerous and normal cells on which to design a focused strategy. One such divergence has been demonstrated in cancer cell's ability to handle high oxidative stress as a result of their active metabolic status¹²⁰, high proliferation rate and all the microenvironment conditions contributing to a tumor mass growth^{121,160}. We aimed to explain the response of our models to the boost of RONS provided by PA-RL treatment focusing on their antioxidant response, which may underlie their diverse sensitivity to PA-RL. SOD-1 levels, as one of the most active antioxidant enzymes, showed to be higher in both cancer cell lines than in fibroblasts. It must be noted that, although not statistically significant, OV-90 showed a trend of increase of SOD-1 levels with respect to SKOV-3 which could be explained by the high oxidative metabolic profile observed in OV90, also responsible for a chemo-resistant profile, as

described by Gentric G et al.¹⁶¹. The enzymatic milieu is responsible for reactive species detoxification, and it may be that cancer cells trigger this salvage mechanism because they suffer from oxidative stress. Higher basal SOD-1 levels would justify lower ROS levels in the untreated SKOV-3 cells, compared to fibroblasts.

At the moment of PA-RL 1:16 treatment we questioned if the selective cytotoxic effect endured by cancer cells may be due to the large amount of ROS generated in the liquid substrate. As expected, immediately after the two hours of contact with PA-RL, cancer cells significantly increased their intrinsic ROS concentration, unlike fibroblasts. Indeed, only fibroblasts showed a statistically significant increment in SOD-1 expression, whereas enzyme levels remain unaltered in cancer cells implying that the antioxidant response has likely reached a limit threshold beyond which enzyme levels cannot be increased. Although not statistically significant, fibroblasts showed an increase in SOD-1 levels also in response to RL solution alone, with a comparable fold increase as with PA-RL. On the one hand, this could imply that RL solution acts synergistically with PA-RL in eliciting upregulation of SOD-1 enzyme; on the other hand, the casual hit responsible for such this enzyme increase is negligible, given the activation of a mechanism that seem to still protect against RONS.

Fibroblast's ability to adapt to the oxidative burst by increasing SOD-1 levels is confirmed by their considerably lower levels of apoptosis with respect to cancer cells, where the combination of ROS increasing and SOD-1 decreasing, after treatment, revealed as lethal.

Although our attempt to delineate the possible mechanism underlying the different sensitivity of our cell models to PA-RL is just preliminary, the results we obtained seemed to disagree with the assumption that, in glioblastoma cells, the plasma-activated lactated Ringer's solution (PAL) would induce apoptosis through a mechanism that excludes intracellular ROS increasing¹²³. In this case, both antioxidant genes such as *CAT*, *SOD2* and *GPX1* and stress-inducible genes such as *GADD45* were not upregulated by PA-RL. Opposite, PAL was proven to have ROS-mediated antitumor effects, via inducing apoptosis in pancreatic cancer cells¹⁴¹. To our knowledge, our study is the first one to show that PA-RL selective cytotoxicity of EOC cancer cells could be oxidative stress dependent¹³⁸.

The different response of our EOC cancer cells to PA-RL treatment begs the question about possible mechanisms that could affect the extent of the cytotoxic response to the treatment. Since the main mediator of PA-RL biological effects is H₂O₂ it is possible that this treatment carries out its selective cytotoxicity by targeting the redox homeostasis.

Literature describes alterations in the redox homeostasis mechanism including the liver kinase B1 (LKB1)-AMP-activated protein kinase (AMPK) axis that has been established as crucial for redox equilibrium, avoiding cell death in the event of glucose starvation¹⁶². Due to LKB1 mutations in non-small cell lung cancer (NSCLC) cells, AMPK cannot be adequately activated by glucose deprivation, resulting in ROS accumulation, which oxidize and inhibit AMPK finally leading to cell death¹⁶³. Therefore, cancer cells deficient in this pathway are more susceptible to the oxidative stress.

With respect to the ovarian cancer, the activity the LKB1-AMPK pathway has been demonstrated to be increased in quiescent EOC spheroids, supporting their formation and survival under energy stress, such as nutrient deprivation and hypoxia¹⁶⁴⁻¹⁶⁶ and thus EOC metastatic potential and platinum resistance, largely in an AMPK-independent manner. Thus, LKB1 status results as predictive of tumor response to several chemotherapeutic regimens, as platinum¹⁶⁷.

Another antioxidant defense mechanism involved in ovarian cancer progression is mediated by the glutathione peroxidase 3 (GPx3) expression, necessary for defense against exogenous sources of H₂O₂. Unlike all the other antioxidant molecules, it is the only enzyme whose high expression is negatively associated with patient overall survival, while low expression disadvantages EOC spheroids clonogenic survival in patient-derived ascites fluid¹⁶⁸.

In view of our results, treatment of liquids by means of cold atmospheric pressure plasma, because of their RONS concentration, may respond to the need for innovative treatments against ovarian cancer to be used in association with standard therapies, which often fail likely because of its high biological complexity and heterogeneous nature^{79,169}.

In this regard, there is the urgent need to find pre-clinical models able to faithfully resemble the original tumor, thus improving our understanding of the HGSOC pathobiology and mechanism responsible for the failure of the current therapies as well as the success of cutting-edge anti-cancer treatments.

HGSOC dissemination inside the peritoneal cavity is associated with accumulation of ascitic fluid in the peritoneal cavity, a sign of advanced disease and poor prognosis. The ascites acts as a unique TME and has been proposed as a valuable and readily available source of tumor material and information on EOC biology¹⁷⁰.

This second part of this thesis aimed to scale-up the investigation about PA-RL effect against ovarian cancer by using more suitable EOC primary models. A series of fresh ascites acquired from

patients diagnosed with HGSOC and undergoing debulking surgery allowed to obtain primary 2D cultures, reaching first confluence in less days than one week and depicting typical epithelial cobblestone morphology, in addition to multicellular aggregates spheroids floating without attachment. After 24 hours most spheroids eventually attached, transforming from 3D structure to flattened cellular clusters made by layers of adherent cells. In agreement with two previously published protocols^{81,171}, cells in adhesion had high proliferative capacity, on average, but suffered gradual loss of the epithelial characteristics in favor of a more fibroblasts-like morphology. Confluent monolayers of spindle-shaped cells were shown to overtake epithelial cell cultures and this phenomenon was confirmed by genetic characterization which showed that ascites-derived 2D cell populations lost the *TP53* mutations specific of their tumor of origin in just a few passages regardless of the culture media used. The aforementioned protocols drew the same conclusions, by characterizing the 2D cell cultures through the expression of typical epithelial or mesenchymal markers. Indeed, reduced expression of the epithelial marker E-cadherin, in favor of the mesenchymal N-cadherin and vimentin was evidenced in spindle-shaped cells⁸¹.

These results collectively suggest that adherent culture conditions are not the best ones to isolate cancer cells from ascites and that the large heterogeneity of resident ascites cells prevented the definition of a standardized method to successfully establish primary EOC cell cultures mirroring the original patients' tumors. Elsewhere, 2D cultures were already labelled as unable to highlight features HGSOC-related, including maintenance of individual patient specificities¹⁷².

The discovery of novel technologies to reliably collect the cell populations contributing to tumor growth is a main priority¹⁷². In this regard, 3D cultures have lately emerged as a powerful approach to recreate key aspects of the original tumor and to propagate *in vitro* cell populations that adequately represent the complexity of tumors¹⁷³. Cellular structures as spheroids are widely considered to better simulate the cell-cell, cell-matrix interactions, metabolic gradients, cellular survival, and differentiation of malignant cells within the solid tumor than traditional monolayer cultures¹⁷⁴.

Tumoral spheroids floating in the two ascitic fluids were successfully isolated in non-adherent culture conditions. Of note, two spheroid populations maintained the *TP53* genetic alterations found in their respective primary tumors, in contrast to 2D cultured cells from the same ascites. The same outcome was reached by characterizing the genetic profile of EOC 3D structures we generated by seeding the ascites into ultra-low attachment plates pre-treated with Matrigel, combined or not with

collagen. The *TP53* mutational profile retention in 3D cultures confirms the maintenance of epithelial cancer cells inside them, whose behavior is probably highly metastatic.

The major drawback of this attempt to establish primary EOC *in vitro* models is the impossibility to maintain and propagate the tumorous portion in the ascites. Furthermore, the genetic characterization with respect to the *TP53* gene state is not exhaustive to define the evolutionary history of these cells in the patient.

Whole-genome sequencing method allowed to detect high levels of intra-tumor heterogeneity in both primary tumor and tumor spheroids and their different phylogenetic origins, thus they derive from two different ancestral tumor clones. This evidence implies that not all the primary clones disseminate into the ascites¹⁵¹. In this regard, a series of studies on malignant ascites proven its inter-patient variability, influencing each patient' respond to a particular therapy. For example, a different LKB1 protein expression in EOC clones derived from ascites was previously reported¹⁶⁷, supporting the hypothesis which is why clones activate diverse stress response pathways in response to hypoxic, acidic and oxidative stresses. Hence, the urgent need to characterize the subpopulations of ascites-derived cells contextually to the cancer stage, and patient response to chemotherapy, in order to estimate the efficacy of new treatments against EOC spheroids and to find molecular signatures within subpopulations with diagnostic and prognostic value¹⁷⁵.

Challenges in managing tumor spheroids are the high variability in size, density and homogeneity, all parameters profoundly affecting their response to drugs, as well the lack of vasculature. Indeed, they require special care in handling, given their tendency to easily disintegrate^{72,176}. In the same way, the automation of scaffold-based spheroids cultures was previously considered challenging as matrixes such as Matrigel are temperature sensitive.

All the mentioned drawbacks in using ascites-derived spheroid and the difficulties I run into in propagating EOC cells in non-adherent culture conditions convinced us to focus on fine-tuning an alternative approach to generate appropriate EOC preclinical model.

The third and last part of this thesis focused on the attempt to establish a perfusion-based 3D EOC *ex vivo* model able to mirror the tissue of origin and to preserve the unique ovarian TME. Screening of novel antitumor compounds imposes to assess their ability to target cancer cells proliferation, inducing cytotoxicity in a biological system closer to the *in vivo* reality¹⁷⁷. In this regard, 2D and 3D systems differentially impact on cancer cells response to drugs¹⁷⁶ and both of them can

mimic only in part *in vivo* TME conditions. Cell-to-cell and cell-ECM interactions affect drug sensitivity and it has been proven, for example, in the case of co-cultures of tumor spheroids with stromal cells submitted to treatments testing¹⁵⁵.

This finding emphasizes the relevance of including TME in a pre-clinical model, as a key factor that influences the response to drugs¹⁷⁸. Although organotypic 3D models significantly reduce the time and expense of drug development, animal models will still be required for confirming *in-vivo* drug toxicity until more advanced whole organ culture systems are available. The system herein described promised, for the first time, to exploit advantages of the perfusion-based culture with the aim to generate a faithful model of HGSOc, obviating the use of PDXs and potentiating organotypic models in resembling human tumor.

The preliminary data obtained from culturing both fresh primary and metastatic HGSOcs in the U-CUP perfusion-based bioreactor agree with evidence showed very recently by other two studies that took advantage of perfusion and “sandwich-like” format of tumor to preserve its structural characteristics and viability¹⁵³. According to the histopathological analysis, ovarian cancer tissue is well preserved in terms of tissue cellularity and the original tumor architecture is maintained, up to seven days of culture. The whole tumor tissue was viable, including cancer cells and mesenchymal stromal cells. P3D7ds were derived with a success rate of 66%. The advantage of the U-CUP system is on one hand due to the constant perfusion which allows for a better long-term survival of the tumoral tissue, and to the type I collagen scaffold on the other. Because the major component of human ECM is indeed made up of this type of collagen (approx. 90%), using such a base structure in the U-CUP bioreactor enhances the cell-fiber interaction offering an optimal support for proliferation and migration¹⁵⁵.

Given the originality of this approach to study HGSOc, standard culture media were used for the first tests. After initial experiments however, the AdvDMEM/F12 medium was chosen to evaluate, for the first time, the possibility to resuscitate slow-frozen tumoral tissue fragments under perfusion-flow culture. The success of this approach represents an adequate solution to a widespread major problem: the fact that surgical rooms and research laboratories are often far apart which limits the immediate usage of fresh raw material to generate 3D models for studies¹⁷⁹. Moreover, it could be intriguing the opportunity to exploit the use of tumor specimens harvested from the same patient at different moments of her clinical history, to be used to gain better insight into complex mechanisms responsible for ovarian cancer spread and chemoresistance, in time-independent manner^{88,179}.

Experiments performed using slow-frozen HGSOs highlighted the importance of the original specimens' state, in terms of integrity preservation, to successfully keep it alive up to seven days after thawing. Indeed, slow-frozen tumors of around 1cm³ of volume appeared disaggregated, full of necrosis and thus different from their respective fresh tumors. We hypothesize that the failure of these proofs is not ascribable to the culture media tested, considered the fair quality of P3D7ds cultured using more sophisticated media (AdvDMEM/F12 and serum-free Ovarian TumorMACS™ Medium), but rather to the inaccurate cryopreservation of these tissues. The cryoprotective agents (FBS + 10% Me₂SO) transport throughout the tissue in static conditions is supposed to be dependent upon the dimensions of the tissue, because their insufficient amount, or even complete lack in the core of the tissue, could lead to damage during cryopreservation. In fact, due to all these problems our success rate, when using 1cm³ slow-frozen tumors was indeed very low, of around 20%⁸⁸.

In this regard, perfusion-bioreactor based cryopreservation was demonstrated to increase viability of slow-frozen 3D tissue-like constructs as compared to the static diffusion-based method¹⁷⁹. These data made us suppose we could have applied the same conditions to slow-frozen tumors, which were frozen in little chunks, with a volume of ~2mm³, to be immediately placed in the bioreactor after thawing.

The first experiment performed using “ready-to-use” little chunks aimed to assess the potential qualitative advantage obtainable through freezing and thawing tissues by adding and removing the cryoprotective agents under perfused flow. Actually, little tumor chunks immediately after thawing (*slow-frozen T0*) showed preservation of the general structure and heterogeneity of cellular components when compared to the fresh primary tumor. Typical HGSO papillary and glandular cluster of cancer cells were also well preserved. In this case, the perfusion-based cryopreservation was not an essential condition neither to better preserve the slow-frozen T0 chunks nor to increase derivation rates of their respective P3D7ds. The tumor volume is supposed to be the unavoidable condition to derive 3D *ex vivo* models starting from frozen tumors.

After seeing that the 3D *ex-vivo* experimental model settings previously published can be applied to EOC tumors as well, we primarily focused on the improvement of the P3Ds derivation rate by upgrading the media used with supplements that favor the growth of EOC organoids as shown by Kopper et al.¹⁶⁹. In fact, this culturing method allowed us to not only obtain reproducible results in short-term culture (3 days), but also the extension for up to 7 days without compromising any of the tumoral compartments and overall viability. These successful results were obtained from both fresh

primary and metastatic HGSOCs as well as their derived slow-frozen samples. This is not the first time that an *ex-vivo* ovarian tissue is maintained vital in long term culture. In fact, it has been shown previously that culturing tumoral tissue in agitation is possible for up to 30 days¹⁸⁰. We chose to limit our experiments to one week of culture as our primary goal is to develop a model compatible with large scale drug screenings which can have a translational impact in a clinical setting. By choosing a reduced culture timeframe, the model cultured in U-CUP could be fast enough to reveal tumoral sensitivity to any proposed therapy for each patient, prior to the initiation of chemotherapy cycles.

Another interesting paper is represented by the work of Marrella et al. 2021, in which they examine the advantages of a perfused environment using 3D models obtained from SKOV-3 cell lines¹⁸¹. While this approach represents a useful tool for drug screening, it lacks the unique EOC TME, which is a well-known modifier of drug response. On the other side, a few studies tackle the subject of TME generating 3D EOC organotypic models where ovarian cancer cells constitute a co-culture together with primary omental fibroblasts and mesothelial cells⁸⁵. While these models are one-step closer to the *in-vivo* context, they are rather simplistic as they lack essential primary features as vasculature and ECM components⁸⁵.

In agreement with other studies that determined the genetic correlation between 3D models and corresponding tumors¹⁸², NGS analysis confirmed the maintenance, in our P3Ds, of the genetic profile of the original tissue, in all tested specimens. This encouraging result was obtained not only in the case of the primary tumor but also in the omental metastases. Interestingly, metastases seemed to be more stable in terms of genetic similarity to the original tissue, also after thawing and up to 7 days of culture. On the contrary, it is possible that the stromal component of the primary tumor localized on the ovaries is better represented with respect to the metastases. This is reflected in the variation of the mutation percentages between samples.

These results brought us to envision the possible use of this technology for treatment testing. In the era of personalized treatment, the evidence that the P3Ds maintain the genetic profile of the original tumor is of fundamental importance. In fact, a lot of targeted therapies are nowadays focused on molecular markers harbored by neoplasia. The fact that the EOC P3Ds mimic the original tumors also from a molecular point of view, provides a useful tool for drug testing, for example to investigate how the tumors respond to the treatment. Moreover, this model could be useful to monitor the eventual appearance of resistance mutations, in a dynamic *ex vivo* system.

Plasma-activated liquid treatments seem promising as a new therapeutic strategy to be used in combination with standard therapies given their ability to act locally against cancer cells, preserving healthy tissue and thus common chemotherapy side effects. The biggest challenge in developing this potential targeting agent is to test it on a research model capable of mimicking the complex nature of ovarian cancer. The successful results we obtained from the establishment of perfused-3D EOC *ex-vivo* models with preserved TME paved the way for testing PA-RL efficacy in a context closer to the clinical practice, since the major interest in proposing this new treatment is the possibility to preserve the epithelium and the connective tissue localized around peritoneal tumoral lesions. Despite a recent study demonstrated that the intraperitoneal PA-RL washing may prolong the overall survival in an ovarian cancer xenograft¹⁸³, the path to arrive to a phase of clinical trials for PA-RL testing is still long and strenuous as further evidence for its safety are required.

To the best of our knowledge, this is the first attempt to screen PA-RL treatment on *ex-vivo* EOC tumors in the advanced stage. In this system we envisioned to study PA-RL selectivity, so it could act locally on ovarian tumor inducing cancer cell death with reduced damage on the surrounding healthy cells.

For two of three HGSOCS, the P3Ds were recovered from the bioreactor after 7 days of culture starting from the end of 2 hours of treatment with both PA-RL 1:14 and 1:16. Pathological evaluation on the *ex-vivo* models derived from this preliminary study defined tissues that met CTR-RL as intact and viable. Unfortunately, a clear selective PA-RL-induced damaging effect on tumor compartment could not be confirmed, because of the presence of still few viable cancer cells and damaged stroma in one sample under PA-RL 1:4. Of note, both tumors treated with PA-RL 1:16 showed abundance of preserved stroma after 7 days. The power of this dilution in destroying cancer cells is in doubt, given their higher abundance in one sample, compared to the PA-RL 1:4 model, and their complete absence in the other.

A limitation of our perfusion-based culture approach is the ovarian intra-tumor heterogeneity, so chunks with no cancer, stroma and/or immune cells could be assembled in the bioreactor turning out to be different from the original specimen. In such a case, one is unable to appreciate the real effects induced by any type of treatment.

A clear selective PA-RL-induced damaging effect on tumor cultured in 3D could not be confirmed, because of the limited number of samples analyzed in this preliminary phase. Anyway, it seems that the dose is critical and that further testing is required to fully demonstrate it.

In conclusion, although further research is needed to fully reveal the potential of the U-CUP system for the establishment of EOC perfusion-based 3D models, our work demonstrated the maintenance of viability, proliferation as well as preservation of the tumoral cells and autologous TME in *ex-vivo* tumor samples from patients.

Overall, our perfusion-based 3D EOC *ex vivo* model represents an innovative tool to deepen and refine the study of the complex ovarian cellular microenvironments, in a context of inter- and intra-tumor heterogeneity between primary site and metastasis.

Moreover, our encouraging preliminary results regarding PA-RL treatment on *ex-vivo* tumor specimens show that this approach can be particularly useful in exploring a tumors' response to therapy, and thus moving a step forward on the path towards personalized medicine in OC.

8. REFERENCES

1. National Cancer Institute. Surveillance, Epidemiology, and End Results Program. Cancer stat facts: ovarian cancer. Available at: <https://seer.cancer.gov/statfacts/html/ovary.html>. (Accessed 30 December 2021).
2. Ovarian Cancer Research Alliance. Statistics. Available at: <https://ocrahope.org/patients/about-ovarian-cancer/statistics/>. (Accessed 30 December 2018).
3. Cannistra, S. A. Cancer of the ovary. *N. Engl. J. Med.* **351**, 2519–2529 (2004).
4. Lheureux, S., Braunstein, M. & Oza, A. M. Epithelial ovarian cancer: Evolution of management in the era of precision medicine. *CA. Cancer J. Clin.* **69**, 280–304 (2019).
5. Kim, J. *et al.* Cell Origins of High-Grade Serous Ovarian Cancer. *Cancers* **10**, 433 (2018).
6. Matz, M. *et al.* The histology of ovarian cancer: worldwide distribution and implications for international survival comparisons (CONCORD-2). *Gynecol. Oncol.* **144**, 405–413 (2017).
7. Bast, R. C., Hennessy, B. & Mills, G. B. The biology of ovarian cancer: new opportunities for translation. *Nat. Rev. Cancer* **9**, 415–428 (2009).
8. Labidi-Galy, S. I. *et al.* High grade serous ovarian carcinomas originate in the fallopian tube. *Nat. Commun.* **8**, 1093 (2017).
9. Terada, K. Y., Ahn, H. J. & Kessel, B. Differences in risk for type 1 and type 2 ovarian cancer in a large cancer screening trial. *J. Gynecol. Oncol.* **27**, e25 (2016).
10. Mallen, A. *et al.* Surgical prevention strategies in ovarian cancer. *Gynecol. Oncol.* **151**, 166–175 (2018).
11. Prat, J. & Mutch, D. G. Pathology of cancers of the female genital tract including molecular pathology. *Int. J. Gynaecol. Obstet. Off. Organ Int. Fed. Gynaecol. Obstet.* **143 Suppl 2**, 93–108 (2018).

12. Lisio, M.-A., Fu, L., Goyeneche, A., Gao, Z. & Telleria, C. High-Grade Serous Ovarian Cancer: Basic Sciences, Clinical and Therapeutic Standpoints. *Int. J. Mol. Sci.* **20**, 952 (2019).
13. Kim, H. S. & Song, Y. S. International Federation of Gynecology and Obstetrics (FIGO) staging system revised: what should be considered critically for gynecologic cancer? *J. Gynecol. Oncol.* **20**, 135–136 (2009).
14. Bischof, K. *et al.* Influence of p53 Isoform Expression on Survival in High-Grade Serous Ovarian Cancers. *Sci. Rep.* **9**, 5244 (2019).
15. Lheureux, S., Gourley, C., Vergote, I. & Oza, A. M. Epithelial ovarian cancer. *Lancet Lond. Engl.* **393**, 1240–1253 (2019).
16. De Leo, A. *et al.* What Is New on Ovarian Carcinoma: Integrated Morphologic and Molecular Analysis Following the New 2020 World Health Organization Classification of Female Genital Tumors. *Diagnostics* **11**, 697 (2021).
17. Fagotti, A. *et al.* Prospective validation of a laparoscopic predictive model for optimal cytoreduction in advanced ovarian carcinoma. *Am. J. Obstet. Gynecol.* **199**, 642.e1–6 (2008).
18. WHO Classification of Tumours Editorial Board. *Female Genital Tumours: WHO Classification of Tumours, 5th ed.; IARC: Lyon, France, 2020; Volume 4.*
19. Ellenson, L. H. *et al.* *WHO Classification of Tumours of Female Reproductive Organs.* 41 (IARC, 2014).
20. Macpherson, A. M., Barry, S. C., Ricciardelli, C. & Oehler, M. K. Epithelial Ovarian Cancer and the Immune System: Biology, Interactions, Challenges and Potential Advances for Immunotherapy. *J. Clin. Med.* **9**, 2967 (2020).

21. Bergsten, T. M., Burdette, J. E. & Dean, M. Fallopian tube initiation of high grade serous ovarian cancer and ovarian metastasis: Mechanisms and therapeutic implications. *Cancer Lett.* **476**, 152–160 (2020).
22. Alsop, K. *et al.* BRCA Mutation Frequency and Patterns of Treatment Response in BRCA Mutation–Positive Women With Ovarian Cancer: A Report From the Australian Ovarian Cancer Study Group. *J. Clin. Oncol.* **30**, 2654–2663 (2012).
23. Soslow, R. A. *et al.* Morphologic patterns associated with BRCA1 and BRCA2 genotype in ovarian carcinoma. *Mod. Pathol. Off. J. U. S. Can. Acad. Pathol. Inc* **25**, 625–636 (2012).
24. Bell, D. *et al.* Integrated genomic analyses of ovarian carcinoma. *Nature* **474**, 609–615 (2011).
25. TP53 oncomorphic mutations predict resistance to platinum- and taxane-based standard chemotherapy in patients diagnosed with advanced serous ovarian carcinoma. <https://www.spandidos-publications.com/10.3892/ijo.2014.2747>.
26. Vang, R. *et al.* Molecular Alterations of TP53 are a Defining Feature of Ovarian High-Grade Serous Carcinoma: A Rereview of Cases Lacking TP53 Mutations in The Cancer Genome Atlas Ovarian Study. *Int. J. Gynecol. Pathol. Off. J. Int. Soc. Gynecol. Pathol.* **35**, 48–55 (2016).
27. Ren, Y. A. *et al.* Mutant p53 Promotes Epithelial Ovarian Cancer by Regulating Tumor Differentiation, Metastasis, and Responsiveness to Steroid Hormones. *Cancer Res.* **76**, 2206–2218 (2016).
28. Ma, X. The omentum, a niche for premetastatic ovarian cancer. *J. Exp. Med.* **217**, e20192312 (2020).
29. Ji, Z. *et al.* Deregulation of Lipid Metabolism: The Critical Factors in Ovarian Cancer. *Front. Oncol.* **10**, 593017 (2020).

30. Lengyel, E. Ovarian cancer development and metastasis. *Am. J. Pathol.* **177**, 1053–1064 (2010).
31. Feng, W., Dean, D. C., Hornicek, F. J., Shi, H. & Duan, Z. Exosomes promote pre-metastatic niche formation in ovarian cancer. *Mol. Cancer* **18**, 124 (2019).
32. Zhang, B. *et al.* Revisiting ovarian cancer microenvironment: a friend or a foe? *Protein Cell* **9**, 674–692 (2018).
33. Ford, C. E., Werner, B., Hacker, N. F. & Warton, K. The untapped potential of ascites in ovarian cancer research and treatment. *Br. J. Cancer* **123**, 9–16 (2020).
34. Kuroki, L. & Guntupalli, S. R. Treatment of epithelial ovarian cancer. *BMJ* **371**, m3773 (2020).
35. Chandra, A. *et al.* Ovarian cancer: Current status and strategies for improving therapeutic outcomes. *Cancer Med.* **8**, 7018–7031 (2019).
36. Elattar, A., Bryant, A., Winter-Roach, B. A., Hatem, M. & Naik, R. Optimal primary surgical treatment for advanced epithelial ovarian cancer. *Cochrane Database Syst. Rev.* CD007565 (2011) doi:10.1002/14651858.CD007565.pub2.
37. Mutch, D. G. Surgical management of ovarian cancer. *Semin. Oncol.* **29**, 3–8 (2002).
38. Terraneo, N., Jacob, F., Dubrovskaja, A. & Grünberg, J. Novel Therapeutic Strategies for Ovarian Cancer Stem Cells. *Front. Oncol.* **10**, (2020).
39. Wright, A. A. *et al.* Use and Effectiveness of Intraperitoneal Chemotherapy for Treatment of Ovarian Cancer. *J. Clin. Oncol. Off. J. Am. Soc. Clin. Oncol.* **33**, 2841–2847 (2015).
40. Esselen, K. M. *et al.* Patterns of recurrence in advanced epithelial ovarian, fallopian tube and peritoneal cancers treated with intraperitoneal chemotherapy. *Gynecol. Oncol.* **127**, 51–54 (2012).
41. Kigawa, J. New strategy for overcoming resistance to chemotherapy of ovarian cancer. *Yonago Acta Med.* **56**, 43–50 (2013).

42. Piccart, M. J. *et al.* Randomized intergroup trial of cisplatin-paclitaxel versus cisplatin-cyclophosphamide in women with advanced epithelial ovarian cancer: three-year results. *J. Natl. Cancer Inst.* **92**, 699–708 (2000).
43. van Zyl, B., Tang, D. & Bowden, N. A. Biomarkers of platinum resistance in ovarian cancer: what can we use to improve treatment. *Endocr. Relat. Cancer* **25**, R303–R318 (2018).
44. Elies, A. *et al.* The role of neoadjuvant chemotherapy in ovarian cancer. *Expert Rev. Anticancer Ther.* **18**, 555–566 (2018).
45. Sato, S. & Itamochi, H. Neoadjuvant chemotherapy in advanced ovarian cancer: latest results and place in therapy. *Ther. Adv. Med. Oncol.* **6**, 293–304 (2014).
46. Vergote, I. *et al.* Neoadjuvant Chemotherapy or Primary Surgery in Stage IIIC or IV Ovarian Cancer. *N. Engl. J. Med.* **363**, 943–953 (2010).
47. Gao, Y. *et al.* Evaluating the benefits of neoadjuvant chemotherapy for advanced epithelial ovarian cancer: a retrospective study. *J. Ovarian Res.* **12**, 85 (2019).
48. Cowan, R., Chi, D., Kehoe, S., Nankivell, M. & Leary, A. Primary Surgery or Neoadjuvant Chemotherapy in Advanced Ovarian Cancer: The Debate Continues.... *Am. Soc. Clin. Oncol. Educ. Book* 153–162 (2016) doi:10.1200/EDBK_160624.
49. Cooke, S. L. & Brenton, J. D. Evolution of platinum resistance in high-grade serous ovarian cancer. *Lancet Oncol.* **12**, 1169–1174 (2011).
50. van Baal, J. O. A. M. *et al.* Development of Peritoneal Carcinomatosis in Epithelial Ovarian Cancer: A Review. *J. Histochem. Cytochem.* **66**, 67–83 (2018).
51. Stuart, G. C. E. *et al.* 2010 Gynecologic Cancer InterGroup (GCIG) consensus statement on clinical trials in ovarian cancer: report from the Fourth Ovarian Cancer Consensus Conference. *Int. J. Gynecol. Cancer Off. J. Int. Gynecol. Cancer Soc.* **21**, 750–755 (2011).

52. Davis, A., Tinker, A. V. & Friedlander, M. 'Platinum resistant' ovarian cancer: what is it, who to treat and how to measure benefit? *Gynecol. Oncol.* **133**, 624–631 (2014).
53. Kelland, L. The resurgence of platinum-based cancer chemotherapy. *Nat. Rev. Cancer* **7**, 573–584 (2007).
54. Chohanadisai, W. *et al.* Cisplatin Resistant Spheroids Model Clinically Relevant Survival Mechanisms in Ovarian Tumors. *PLOS ONE* **11**, e0151089 (2016).
55. Ishida, S., McCormick, F., Smith-McCune, K. & Hanahan, D. Enhancing tumor-specific uptake of the anticancer drug cisplatin with a copper chelator. *Cancer Cell* **17**, 574–583 (2010).
56. Buß, I. & Jaehde, U. Platinum Complexes. in *Encyclopedia of Cancer* (ed. Schwab, M.) 2358–2363 (Springer, 2009). doi:10.1007/978-3-540-47648-1_4616.
57. Freimund, A. E., Beach, J. A., Christie, E. L. & Bowtell, D. D. L. Mechanisms of Drug Resistance in High-Grade Serous Ovarian Cancer. *Hematol. Oncol. Clin. North Am.* **32**, 983–996 (2018).
58. Haunschild, C. E. & Tewari, K. S. Bevacizumab use in the frontline, maintenance and recurrent settings for ovarian cancer. *Future Oncol. Lond. Engl.* **16**, 225–246 (2020).
59. Garcia, J. *et al.* Bevacizumab (Avastin®) in cancer treatment: A review of 15 years of clinical experience and future outlook. *Cancer Treat. Rev.* **86**, (2020).
60. Pfisterer, J. *et al.* Bevacizumab and platinum-based combinations for recurrent ovarian cancer: a randomised, open-label, phase 3 trial. *Lancet Oncol.* **21**, 699–709 (2020).
61. Sisay, M. & Edessa, D. PARP inhibitors as potential therapeutic agents for various cancers: focus on niraparib and its first global approval for maintenance therapy of gynecologic cancers. *Gynecol. Oncol. Res. Pract.* **4**, 18 (2017).

62. Zhang, J., Kan, Y., Tian, Y., Wang, Z. & Zhang, J. Effects of poly (ADP-ribose) polymerase (PARP) inhibitor on cisplatin resistance & proliferation of the ovarian cancer C13* cells. *Indian J. Med. Res.* **137**, 527–532 (2013).
63. Combination treatment with cisplatin, paclitaxel and olaparib has synergistic and dose reduction potential in ovarian cancer cells. <https://www.spandidos-publications.com/10.3892/etm.2021.10367>.
64. Rynne-Vidal, A. *et al.* Mesothelial-to-mesenchymal transition as a possible therapeutic target in peritoneal metastasis of ovarian cancer. *J. Pathol.* **242**, 140–151 (2017).
65. Jewell, A., McMahon, M. & Khabele, D. Heated Intraperitoneal Chemotherapy in the Management of Advanced Ovarian Cancer. *Cancers* **10**, E296 (2018).
66. Alberts, D. S. *et al.* Intraperitoneal cisplatin plus intravenous cyclophosphamide versus intravenous cisplatin plus intravenous cyclophosphamide for stage III ovarian cancer. *N. Engl. J. Med.* **335**, 1950–1955 (1996).
67. Markman, M. *et al.* Phase III trial of standard-dose intravenous cisplatin plus paclitaxel versus moderately high-dose carboplatin followed by intravenous paclitaxel and intraperitoneal cisplatin in small-volume stage III ovarian carcinoma: an intergroup study of the Gynecologic Oncology Group, Southwestern Oncology Group, and Eastern Cooperative Oncology Group. *J. Clin. Oncol. Off. J. Am. Soc. Clin. Oncol.* **19**, 1001–1007 (2001).
68. Armstrong, D. K. *et al.* Intraperitoneal cisplatin and paclitaxel in ovarian cancer. *N. Engl. J. Med.* **354**, 34–43 (2006).
69. van Driel, W. J. *et al.* Hyperthermic Intraperitoneal Chemotherapy in Ovarian Cancer. *N. Engl. J. Med.* **378**, 230–240 (2018).

70. Ibarrola-Villava, M., Cervantes, A. & Bardelli, A. Preclinical models for precision oncology. *Biochim. Biophys. Acta Rev. Cancer* **1870**, 239–246 (2018).
71. Charwat, V. & Egger, D. The Third Dimension in Cell Culture: From 2D to 3D Culture Formats. in *Cell Culture Technology* (eds. Kasper, C., Charwat, V. & Lavrentieva, A.) 75–90 (Springer International Publishing, 2018). doi:10.1007/978-3-319-74854-2_5.
72. Han, S. J., Kwon, S. & Kim, K. S. Challenges of applying multicellular tumor spheroids in preclinical phase. *Cancer Cell Int.* **21**, 152 (2021).
73. Lengyel, E. *et al.* Epithelial ovarian cancer experimental models. *Oncogene* **33**, 3619–3633 (2014).
74. *Cell Culture Technology*. (Springer International Publishing, 2018). doi:10.1007/978-3-319-74854-2.
75. Clevers, H. Modeling Development and Disease with Organoids. *Cell* **165**, 1586–1597 (2016).
76. Meditz, K. & Rinner, B. Establishment of Tumor Cell Lines: From Primary Tumor Cells to a Tumor Cell Line. in *Cell Culture Technology* (eds. Kasper, C., Charwat, V. & Lavrentieva, A.) 61–73 (Springer International Publishing, 2018). doi:10.1007/978-3-319-74854-2_4.
77. Pauli, C. *et al.* Personalized *In Vitro* and *In Vivo* Cancer Models to Guide Precision Medicine. *Cancer Discov.* **7**, 462–477 (2017).
78. Corrà, C., Novellademunt, L. & Li, V. S. W. A brief history of organoids. *Am. J. Physiol.-Cell Physiol.* **319**, C151–C165 (2020).
79. Maru, Y. & Hippo, Y. Current Status of Patient-Derived Ovarian Cancer Models. *Cells* **8**, E505 (2019).
80. Jiang, W., Xie, S., Liu, Y., Zou, S. & Zhu, X. The Application of Patient-Derived Xenograft Models in Gynecologic Cancers. *J. Cancer* **11**, 5478–5489 (2020).

81. Isolation and phenotypic characterization of tumor cells of patients with a diagnosis of ovarian cancer - PubMed. <https://pubmed.ncbi.nlm.nih.gov/31549393/>.
82. Velletri, T. *et al.* Single cell-derived spheroids capture the self-renewing subpopulations of metastatic ovarian cancer. *Cell Death Differ.* (2021) doi:10.1038/s41418-021-00878-w.
83. Kim, S. *et al.* Evaluating Tumor Evolution via Genomic Profiling of Individual Tumor Spheroids in a Malignant Ascites. *Sci. Rep.* **8**, 12724 (2018).
84. Frontiers | Application of Ovarian Cancer Organoids in Precision Medicine: Key Challenges and Current Opportunities | Cell and Developmental Biology. <https://www.frontiersin.org/articles/10.3389/fcell.2021.701429/full>.
85. Watters, K. M., Bajwa, P. & Kenny, H. A. Organotypic 3D Models of the Ovarian Cancer Tumor Microenvironment. *Cancers* **10**, 265 (2018).
86. Peters, P. N., Schryver, E. M., Lengyel, E. & Kenny, H. Modeling the Early Steps of Ovarian Cancer Dissemination in an Organotypic Culture of the Human Peritoneal Cavity. *J. Vis. Exp. JoVE* e53541 (2015) doi:10.3791/53541.
87. Li, S.-S. *et al.* Modeling Ovarian Cancer Multicellular Spheroid Behavior in a Dynamic 3D Peritoneal Microdevice. *J. Vis. Exp. JoVE* (2017) doi:10.3791/55337.
88. Walsh, A. J., Cook, R. S., Sanders, M. E., Arteaga, C. L. & Skala, M. C. Drug response in organoids generated from frozen primary tumor tissues. *Sci. Rep.* **6**, 18889 (2016).
89. Haertel, B., von Woedtke, T., Weltmann, K.-D. & Lindequist, U. Non-Thermal Atmospheric-Pressure Plasma Possible Application in Wound Healing. *Biomol. Ther.* **22**, 477–490 (2014).
90. Choi, E. H., Uhm, H. S. & Kaushik, N. K. Plasma bioscience and its application to medicine. *AAPPS Bull.* **31**, 10 (2021).

91. von Woedtke, Th., Metelmann, H.-R. & Weltmann, K.-D. Clinical Plasma Medicine: State and Perspectives of *in Vivo* Application of Cold Atmospheric Plasma. *Contrib. Plasma Phys.* **54**, 104–117 (2014).
92. Stapelmann, K. *et al.* Utilization of Low-Pressure Plasma to Inactivate Bacterial Spores on Stainless Steel Screws. *Astrobiology* **13**, 597–606 (2013).
93. Isbary, G. *et al.* Successful and safe use of 2 min cold atmospheric argon plasma in chronic wounds: results of a randomized controlled trial. *Br. J. Dermatol.* **167**, 404–410 (2012).
94. Devasenapathy, N. *et al.* Efficacy and safety of convalescent plasma for severe COVID-19 based on evidence in other severe respiratory viral infections: a systematic review and meta-analysis. *CMAJ Can. Med. Assoc. J. J. Assoc. Medicale Can.* **192**, E745–E755 (2020).
95. Plasma-generated reactive oxygen and nitrogen species can lead to closure, locking and constriction of the *Dionaea muscipula* Ellis trap | Journal of The Royal Society Interface. <https://royalsocietypublishing.org/doi/10.1098/rsif.2018.0713>.
96. Yan, D., Sherman, J. H. & Keidar, M. The Application of the Cold Atmospheric Plasma-Activated Solutions in Cancer Treatment. *Anticancer Agents Med. Chem.* **18**, 769–775 (2018).
97. Yan, D., Sherman, J. H. & Keidar, M. Cold atmospheric plasma, a novel promising anti-cancer treatment modality. *Oncotarget* **8**, 15977–15995 (2017).
98. Korolev, Yu. D. Low-current discharge plasma jets in a gas flow. Application of plasma jets. *Russ. J. Gen. Chem.* **85**, 1311–1325 (2015).
99. Iseki, S. *et al.* Selective killing of ovarian cancer cells through induction of apoptosis by nonequilibrium atmospheric pressure plasma. *Appl. Phys. Lett.* **100**, 113702 (2012).

100. Ja Kim, S., Min Joh, H. & Chung, T. H. Production of intracellular reactive oxygen species and change of cell viability induced by atmospheric pressure plasma in normal and cancer cells. *Appl. Phys. Lett.* **103**, 153705 (2013).
101. Non-Thermal Atmospheric Pressure Plasma Preferentially Induces Apoptosis in p53-Mutated Cancer Cells by Activating ROS Stress-Response Pathways. <https://journals.plos.org/plosone/article?id=10.1371/journal.pone.0091947>.
102. Kalghatgi, S. *et al.* Effects of Non-Thermal Plasma on Mammalian Cells. *PLOS ONE* **6**, e16270 (2011).
103. Vandamme, M. *et al.* Response of Human Glioma U87 Xenografted on Mice to Non Thermal Plasma Treatment. *Plasma Med.* **1**, 27–43 (2011).
104. Guerrero-Preston, R. *et al.* Cold atmospheric plasma treatment selectively targets head and neck squamous cell carcinoma cells. *Int. J. Mol. Med.* **34**, 941–946 (2014).
105. Arndt, S. *et al.* Cold atmospheric plasma, a new strategy to induce senescence in melanoma cells. *Exp. Dermatol.* **22**, 284–289 (2013).
106. Yan, D. *et al.* Controlling plasma stimulated media in cancer treatment application. *Appl. Phys. Lett.* **105**, 224101 (2014).
107. Vandamme, M. *et al.* ROS implication in a new antitumor strategy based on non-thermal plasma. *Int. J. Cancer* **130**, 2185–2194 (2012).
108. Van der Speeten, K., Lemoine, L. & Sugarbaker, P. Overview of the optimal perioperative intraperitoneal chemotherapy regimens used in current clinical practice. *Pleura Peritoneum* **2**, 63–72 (2017).

109. Pokryvailo, A., Wolf, M., Yankelevich, Y., Abramzon, E. & Welleman, A. A Compact High-Power Pulsed Corona Source for Treatment of Pollutants in Heterogeneous Media. in *2005 IEEE Pulsed Power Conference* 1188–1191 (2005). doi:10.1109/PPC.2005.300550.
110. Grabowski, L., Veldhuizen, E., Pemen, A. & Rutgers, W. Corona Above Water Reactor for Systematic Study of Aqueous Phenol Degradation. *Plasma Chem. Plasma Process.* **26**, 3–17 (2006).
111. Schiorlin, M., Marotta, E., Ren, X., Rea, M. & Paradisi, C. Advanced Oxidation Process for Degradation of Aqueous Phenol in a Dielectric Barrier Discharge Reactor. *Plasma Process. Polym.* **10**, 867–875 (2011).
112. Magureanu, M., Bradu, C., Piroi, D., Mandache, N. B. & Parvulescu, V. Pulsed Corona Discharge for Degradation of Methylene Blue in Water. *Plasma Chem. Plasma Process.* **33**, (2012).
113. Ceriani, E. *et al.* A versatile prototype plasma reactor for water treatment supporting different discharge regimes. *J. Phys. Appl. Phys.* **51**, 274001 (2018).
114. Dobrynin, D., Fridman, G., Friedman, G. & Fridman, A. Physical and biological mechanisms of direct plasma interaction with living tissue. *New J. Phys.* **11**, 115020 (2009).
115. Cheng, X. *et al.* The Effect of Tuning Cold Plasma Composition on Glioblastoma Cell Viability. *PLOS ONE* **9**, e98652 (2014).
116. Wende, K. *et al.* Identification of the biologically active liquid chemistry induced by a nonthermal atmospheric pressure plasma jet. *Biointerphases* **10**, 029518 (2015).
117. Tanaka, H. & Hori, M. Medical applications of non-thermal atmospheric pressure plasma. *J. Clin. Biochem. Nutr.* **60**, 29–32 (2017).
118. Machala, Z. *et al.* Formation of ROS and RNS in Water Electro-Sprayed through Transient Spark Discharge in Air and their Bactericidal Effects. *Plasma Process. Polym.* **10**, 649–659 (2013).

119. Tanaka, H. *et al.* Non-thermal atmospheric pressure plasma activates lactate in Ringer's solution for anti-tumor effects. *Sci. Rep.* **6**, 36282 (2016).
120. Schumacker, P. T. Reactive oxygen species in cancer cells: live by the sword, die by the sword. *Cancer Cell* **10**, 175–176 (2006).
121. Trachootham, D., Alexandre, J. & Huang, P. Targeting cancer cells by ROS-mediated mechanisms: a radical therapeutic approach? *Nat. Rev. Drug Discov.* **8**, 579–591 (2009).
122. Kajiyama, H. *et al.* Future perspective of strategic non-thermal plasma therapy for cancer treatment. *J. Clin. Biochem. Nutr.* **60**, 33–38 (2017).
123. Tanaka, H. *et al.* Plasma-Activated Medium Selectively Kills Glioblastoma Brain Tumor Cells by Down-Regulating a Survival Signaling Molecule, AKT Kinase. *Plasma Med.* **1**, (2011).
124. Chang, J. W. *et al.* Non-thermal atmospheric pressure plasma induces apoptosis in oral cavity squamous cell carcinoma: Involvement of DNA-damage-triggering sub-G(1) arrest via the ATM/p53 pathway. *Arch. Biochem. Biophys.* **545**, 133–140 (2014).
125. Ishaq, M. *et al.* Atmospheric gas plasma-induced ROS production activates TNF-ASK1 pathway for the induction of melanoma cancer cell apoptosis. *Mol. Biol. Cell* **25**, 1523–1531 (2014).
126. Ruwan Kumara, M. H. S. *et al.* Non-thermal gas plasma-induced endoplasmic reticulum stress mediates apoptosis in human colon cancer cells. *Oncol. Rep.* **36**, 2268–2274 (2016).
127. Bauer, G. Increasing the endogenous NO level causes catalase inactivation and reactivation of intercellular apoptosis signaling specifically in tumor cells. *Redox Biol.* **6**, 353–371 (2015).
128. Shi, L. *et al.* Non-thermal plasma induces a stress response in mesothelioma cells resulting in increased endocytosis, lysosome biogenesis and autophagy. *Free Radic. Biol. Med.* **108**, 904–917 (2017).

129. Furuta, T., Shi, L. & Toyokuni, S. Non-thermal plasma as a simple ferroptosis inducer in cancer cells: A possible role of ferritin. *Pathol. Int.* **68**, 442–443 (2018).
130. Ishikawa, K. *et al.* Non-thermal plasma-activated lactate solution kills U251SP glioblastoma cells in an innate reductive manner with altered metabolism. *Arch. Biochem. Biophys.* **688**, 108414 (2020).
131. Attri, P., Park, J. H., Ali, A. & Choi, E. H. How Does Plasma Activated Media Treatment Differ From Direct Cold Plasma Treatment? *Anticancer Agents Med. Chem.* **18**, 805–814 (2018).
132. Li, Y., Tang, T., Lee, H. & Song, K. Cold Atmospheric Pressure Plasma-Activated Medium Induces Selective Cell Death in Human Hepatocellular Carcinoma Cells Independently of Singlet Oxygen, Hydrogen Peroxide, Nitric Oxide and Nitrite/Nitrate. *Int. J. Mol. Sci.* **22**, 5548 (2021).
133. Mohades, S., Laroussi, M., Sears, J., Barekzi, N. & Razavi, H. Evaluation of the effects of a plasma activated medium on cancer cells. *Phys. Plasmas* **22**, 122001 (2015).
134. Dai, X., Bazaka, K., Thompson, E. W. & Ostrikov, K. K. Cold Atmospheric Plasma: A Promising Controller of Cancer Cell States. *Cancers* **12**, E3360 (2020).
135. Wang, M. *et al.* Cold atmospheric plasma for selectively ablating metastatic breast cancer cells. *PloS One* **8**, e73741 (2013).
136. Utsumi, F. *et al.* Variable susceptibility of ovarian cancer cells to non-thermal plasma-activated medium. *Oncol. Rep.* **35**, 3169–3177 (2016).
137. Nakamura, K. *et al.* Novel Intraperitoneal Treatment With Non-Thermal Plasma-Activated Medium Inhibits Metastatic Potential of Ovarian Cancer Cells. *Sci. Rep.* **7**, 6085 (2017).
138. Azzariti, A. *et al.* Plasma-activated medium triggers cell death and the presentation of immune activating danger signals in melanoma and pancreatic cancer cells. *Sci. Rep.* **9**, 4099 (2019).

150. Ghaleb, A., Padellan, M. & Marchenko, N. Mutant p53 drives the loss of heterozygosity by the upregulation of Nek2 in breast cancer cells. *Breast Cancer Res.* **22**, 133 (2020).
151. Kipps, E., Tan, D. S. P. & Kaye, S. B. Meeting the challenge of ascites in ovarian cancer: new avenues for therapy and research. *Nat. Rev. Cancer* **13**, 273–282 (2013).
152. Dar, S. *et al.* Bioenergetic Adaptations in Chemoresistant Ovarian Cancer Cells. *Sci. Rep.* **7**, 8760 (2017).
153. Manfredonia, C. *et al.* Maintenance of Primary Human Colorectal Cancer Microenvironment Using a Perfusion Bioreactor-Based 3D Culture System. *Adv. Biosyst.* **3**, 1800300 (2019).
154. Aref, A. R. *et al.* 3D microfluidic *ex vivo* culture of organotypic tumor spheroids to model immune checkpoint blockade. *Lab. Chip* **18**, 3129–3143 (2018).
155. Redmond, J., McCarthy, H., Buchanan, P., Levingstone, T. J. & Dunne, N. J. Advances in biofabrication techniques for collagen-based 3D *in vitro* culture models for breast cancer research. *Mater. Sci. Eng. C Mater. Biol. Appl.* **122**, 111944 (2021).
156. Chan, C.-M., Ko, T.-M. & Hiraoka, H. Polymer surface modification by plasmas and photons. *Surf. Sci. Rep.* **24**, 1–54 (1996).
157. Chu, P. K., Chen, J. Y., Wang, L. P. & Huang, N. Plasma-surface modification of biomaterials. *Mater. Sci. Eng. R Rep.* **36**, 143–206 (2002).
158. Nakamura, K. *et al.* Adjusted multiple gases in the plasma flow induce differential antitumor potentials of plasma-activated solutions. *Plasma Process. Polym.* **17**, 1900259 (2020).
159. Kurake, N. *et al.* Cell survival of glioblastoma grown in medium containing hydrogen peroxide and/or nitrite, or in plasma-activated medium. *Arch. Biochem. Biophys.* **605**, 102–108 (2016).
160. DeBerardinis, R. J. & Chandel, N. S. Fundamentals of cancer metabolism. *Sci. Adv.* **2**, e1600200 (2016).

161. Gentric, G. *et al.* PML-Regulated Mitochondrial Metabolism Enhances Chemosensitivity in Human Ovarian Cancers. *Cell Metab.* **29**, 156–156 (2019).
162. Ren, Y. & Shen, H.-M. Critical role of AMPK in redox regulation under glucose starvation. *Redox Biol.* **25**, 101154 (2019).
163. Ciccarese, F., Zulato, E. & Indraccolo, S. LKB1/AMPK Pathway and Drug Response in Cancer: A Therapeutic Perspective. *Oxid. Med. Cell. Longev.* **2019**, 1–16 (2019).
164. Hardie, D. G., Ross, F. A. & Hawley, S. A. AMPK: a nutrient and energy sensor that maintains energy homeostasis. *Nat. Rev. Mol. Cell Biol.* **13**, 251–262 (2012).
165. LSR promotes epithelial ovarian cancer cell survival under energy stress through the LKB1-AMPK pathway | Elsevier Enhanced Reader.
<https://reader.elsevier.com/reader/sd/pii/S0006291X20322610?token=FD13D7F0A445F066A3CC405A95B9674F624A2EE314EE246B338B7A1B16FF079DB0BBFF591E8AC64EFA555CC2208F5731&originRegion=eu-west-1&originCreation=20220514233723>
doi:10.1016/j.bbrc.2020.12.079.
166. Intact LKB1 activity is required for survival of dormant ovarian cancer spheroids - PubMed.
<https://pubmed.ncbi.nlm.nih.gov/26068970/>.
167. Buensuceso, A., Ramos-Valdes, Y., DiMattia, G. E. & Shepherd, T. G. AMPK-Independent LKB1 Activity Is Required for Efficient Epithelial Ovarian Cancer Metastasis. *Mol. Cancer Res. MCR* **18**, 488–500 (2020).
168. Worley, B. L. *et al.* GPx3 supports ovarian cancer progression by manipulating the extracellular redox environment. *Redox Biol.* **25**, (2019).
169. Kopper, O. *et al.* An organoid platform for ovarian cancer captures intra- and interpatient heterogeneity. *Nat. Med.* **25**, 838–849 (2019).

170. Carter, E. P., Roozitalab, R., Gibson, S. V. & Grose, R. P. Tumour microenvironment 3D-modelling: simplicity to complexity and back again. *Trends Cancer* **7**, 1033–1046 (2021).
171. Latifi, A. *et al.* Isolation and characterization of tumor cells from the ascites of ovarian cancer patients: molecular phenotype of chemoresistant ovarian tumors. *PLoS One* **7**, e46858 (2012).
172. Single cell derived organoids capture the self-renewing subpopulations of metastatic ovarian cancer | bioRxiv. <https://www.biorxiv.org/content/10.1101/484121v1>.
173. Drost, J. & Clevers, H. Organoids in cancer research. *Nat. Rev. Cancer* **18**, 407–418 (2018).
174. Proliferative activity and tumorigenic conversion: impact on cellular metabolism in 3-D culture. <https://journals.physiology.org/doi/epdf/10.1152/ajpcell.2000.278.4.C765>
doi:10.1152/ajpcell.2000.278.4.C765.
175. Getting to know ovarian cancer ascites: opportunities for targeted therapy-based translational research - PubMed. <https://pubmed.ncbi.nlm.nih.gov/24093089/>.
176. Herrmann, D. *et al.* Three-dimensional cancer models mimic cell–matrix interactions in the tumour microenvironment. *Carcinogenesis* **35**, 1671–1679 (2014).
177. Hirt, C. *et al.* Bioreactor-engineered cancer tissue-like structures mimic phenotypes, gene expression profiles and drug resistance patterns observed ‘*in vivo*’. *Biomaterials* **62**, 138–146 (2015).
178. Nath, S. & Devi, G. R. Three-dimensional culture systems in cancer research: Focus on tumor spheroid model. *Pharmacol. Ther.* **163**, 94–108 (2016).
179. He, A. *et al.* Cryopreservation of Viable Human Tissues: Renewable Resource for Viable Tissue, Cell Lines, and Organoid Development. *Biopreservation Biobanking* **18**, 222–227 (2020).
180. Abreu, S. *et al.* Patient-derived ovarian cancer explants: preserved viability and histopathological features in long-term agitation-based cultures. *Sci. Rep.* **10**, 19462 (2020).

181. Marrella, A. *et al.* 3D fluid-dynamic ovarian cancer model resembling systemic drug administration for efficacy assay. *ALTEX* **38**, 82–94 (2021).
182. Maru, Y., Tanaka, N., Itami, M. & Hippo, Y. Efficient use of patient-derived organoids as a preclinical model for gynecologic tumors. *Gynecol. Oncol.* **154**, 189–198 (2019).
183. Nakamura, K. *et al.* Preclinical Verification of the Efficacy and Safety of Aqueous Plasma for Ovarian Cancer Therapy. *Cancers* **13**, 1141 (2021)